VOL.107 NO.GT4. APRIL 1981

JOURNAL OF THE GEOTECHNICAL ENGINEERING DIVISION

PROCEEDINGS OF
THE AMERICAN SOCIETY
OF CIVIL ENGINEERS

VOL. 107 NO. GT4. APRIL 1981

JOURNAL OF THE GEOTECHNICAL ENGINEERING DIVISION

PROCEEDINGS OF THE AMERICAN SOCIETY OF CIVIL ENGINEERS

Copyright© 1981 by
American Society
of Civil Engineers
All Rights Reserved
ISSN 0093-6405

AMERICAN SOCIETY OF CIVIL ENGINEERS

BOARD OF DIRECTION

President
Irvan F. Mendenhall

Past President
Joseph S. Ward

President Elect
James R. Sims

Vice Presidents
Robert D. Bay — Lyman R. Gillis
Francis J. Connell — Albert A. Grant

Directors
Martin G. Abegg — Paul R. Munger
Floyd A. Bishop — William R. Neuman
L. Gary Byrd — Leonard S. Oberman
Larry J. Feeser — John D. Parkhurst
John A. Focht, Jr. — Celestino R. Pennoni
Sergio Gonzalez-Karg — Robert B. Rhode
James E. Humphrey, Jr. — S. Russell Stearns
Richard W. Karn — William H. Taylor
Leon D. Luck — Stafford E. Thornton
Arthur R. McDaniel — Robert E. Whiteside
Richard S. Woodruff

EXECUTIVE OFFICERS

Eugene Zwoyer, *Executive Director*
Julie E. Gibouleau, *Assistant to the Executive Director*
Louis L. Meier, *Washington Counsel/Assistant Secretary*
William H. Wisely, *Executive Director Emeritus*
Michael N. Salgo, *Treasurer*
Elmer B. Isaak, *Assistant Treasurer*

STAFF DIRECTORS

Donald A. Buzzell, *Managing Director for Education and Professional Affairs*
Robert A. Crist, Jr., *Managing Director for Publications and Technical Affairs*
Alexander Korwek, *Managing Director for Finance and Administrative Services*
Alexandra Bellow, *Director, Human Resources*
David Dresia, *Director, Publications Production and Marketing*
Barker D. Herr, *Director, Membership*
Richard A. Jeffers, *Controller*
Carl E. Nelson, *Director, Field Services*
Don P. Reynolds, *Director, Policy, Planning and Public Affairs*
Bruce Rickerson, *Director, Legislative Services*
James M. Shea, *Director, Public Communications*
Albert W. Turchick, *Director, Technical Services*
George K. Wadlin, *Director, Education Services*
R. Lawrence Whipple, *Director, Engineering Management Services*

COMMITTEE ON PUBLICATIONS

Stafford E. Thornton, *Chairman*
Martin G. Abegg — Richard W. Karn
John A. Focht, Jr. — Paul R. Munger
William R. Neuman

GEOTECHNICAL ENGINEERING DIVISION

Executive Committee
Robert Schuster, *Chairman*
Ernest T. Selig, *Vice Chairman*
William F. Swiger — Harvey E. Wahls
Robert T. Darragh, Jr., *Secretary*
Elio D'Appolonia, *Management Group E Contact Member*

Publications Committee
William F. Marcuson III, ***Chairman***
O. B. Andersland — Fred H. Kulhawy
Warren J. Baker — C. C. Ladd
Don C. Banks — Poul V. Lade
James M. Bell — Leonard J. Langfelder
Chandra S. Brahama — Felipe A. Len-Rios
John T. Christian — Gholamreza Mesri
G. W. Clough — Donald J. Murphy
Tuncer B. Edil — S. V. Nathan
Herbert H. Einstein — Thom L. Neff
Arley G. Franklin — Michael W. O'Neill
D. H. Gray — Jean H. Prevost
Bobby Hardin — Adel Saada
Cornelius J. Higgins — Surendra K. Saxena
William H. Highter — Robert L. Schiffman
Robert D. Holtz — Woodland G. Schockley
Izzat M. Idriss — Marshall L. Silver
L. H. Irwin — Glen S. Tarbox
Reuben H. Karol — G. R. Thiers
H. Y. Ko — D. D. Treadwell
William D. Kovacs — Charles R. Ullrich
Leland M. Kraft — J. Lawrence Von Thun
Raymond J. Krizek — R. N. Yong
E. T. Selig, *Exec. Comm. Contact Member*

PUBLICATION SERVICES DEPARTMENT

David Dresia, *Director, Publications Production and Marketing*

Technical and Professional Publications

Richard R. Torrens, *Manager*
Joseph P. Cerami, *Chief Copy Editor*
Linda Ellington, *Copy Editor*
Thea C. Feldman, *Copy Editor*
Meryl Mandle, *Copy Editor*
Joshua R. Spieler, *Copy Editor*
Shiela Menaker, *Production Co-ordinator*
Richard C. Scheblein, *Draftsman*

Information Services

Elan Garonzik, *Editor*

PERMISSION TO PHOTOCOPY JOURNAL PAPERS

Permission to photocopy for personal or internal reference beyond the limits in Sections 107 and 108 of the U.S. Copyright Law is granted by the American Society of Civil Engineers for libraries and other users registered with the Copyright Clearance Center, 21 Congress Street, Salem, Mass. 01970, provided the appropriate fee is paid to the CCC for all articles bearing the CCC code. Requests for special permission or bulk copying should be addressed to the Manager of Technical and Professional Publications, American Society of Civil Engineers.

CONTENTS

There Were Giants on the Earth in Those Days
by George F. Sowers 383

Effect of Wetting and Drying on Shear Strength
by Mehter Mohamed Allam and Asuri Sridharan 421

Measurement of Porosity in Natural Sand Deposits
by S. A. Denekamp and Y. Tsur-Lavie 439

Stochastic FEM in Settlement Predictions
by Gregory B. Baecher and Thomas S. Ingra 449

Ignition Test for Soil Organic-Content Measurement
by Abdul-Amir W. N. Al-Khafaji and Orlando B. Andersland 465

Centrifuge Modeling of Coal Waste Embankments
by Mosaid M. Al-Hussaini, Deborah J. Goodings, Andrew N. Schofield, and Frank C. Townsend 481

Earthquake-Induced Liquefaction Near Lake Amatitlan, Guatemala
by H. Bolton Seed, Ignacio Arango, Clarence K. Chan, Alberto Gomez-Masso, and Rebecca Grant Ascoli 501

This Journal is published monthly by the American Society of Civil Engineers. Publications office is at 345 East 47th Street, New York, N.Y. 10017. Address all ASCE correspondence to the Editorial and General Offices at 345 East 47th Street, New York, N.Y. 10017. Allow six weeks for change of address to become effective. Subscription price to members is $16.00. Nonmember subscriptions available; prices obtainable on request. Second-class postage paid at New York, N.Y. and at additional mailing offices. GT.

The Society is not responsible for any statement made or opinion expressed in its publications.

TECHNICAL NOTES

Proc. Paper 16156

Acoustic Emission Monitoring of Seepage
by Robert M. Koerner, W. Martin McCabe, and Luis F. Baldivieso 521

DISCUSSION

Proc. Paper 16150

Dam Failure in Benefit/Cost Analyses,* by Gregory Baecher, Marie-Elisabeth Paté, and Richard De Neufville (Jan., 1980).
by Francis G. McLean 529
by Ralph B. Peck 531
closure 532

Cracking, Leakage, and Erosion of Earth Dam Materials,* by Erik I. Hjeldnes, and Bhagwat V. K. Lavania (Feb., 1980).
by Marvin R. Pyles 533
closure 535

INFORMATION RETRIEVAL

The key words, abstract, and reference "cards" for each article in this Journal represent part of the ASCE participation in the EJC information retrieval plan. The retrieval data are placed herein so that each can be cut out, placed on a 3 × 5 card and given an accession number for the user's file. The accession number is then entered on key word cards so that the user can subsequently match key words to choose the articles he wishes. Details of this program were given in an August, 1962 article in CIVIL ENGINEERING, reprints of which are available on request to ASCE headquarters.

*Discussion period closed for this paper. Any other discussion received during this discussion period will be published in subsequent Journals.

16190 THERE WERE GIANTS ON THE EARTH IN THOSE DAYS

KEY WORDS: Adobe; **Archaeology; Construction methods;** Drainage; **Geotechnical engineering; Historic sites; History;** Masonry; Mounds (archaeology); Piles; Roads; **Sociological factors**

ABSTRACT: There are numerous examples of noteworthy pre-Columbian geotechnology in the Americas. These include earth mounds, stone temple pyramids, pile foundations, roads, retaining walls, terraces, irrigation structures, and small dams. They exhibit well-conceived designs and organized construction. Some investigators speculate that these sophisticated works reflect unrecorded technology from the Old World or possibly extra-terrestial intervention. However, the responsibility can be found in both indigeneous, ingeneous responses to local social and economic problems as well as well-organized community efforts. The lack of a formal system of logic, mathematical computation, and written communication inhibited the development and interaction of the embryonic technologies. Their decay was completed by the European conquest.

REFERENCE: Sowers, George F., "There Were Giants on the Earth in Those Days," *Journal of the Geotechnical Engineering Division,* ASCE, Vol. 107, No. GT4, **Proc. Paper 16190**, April, 1981, pp. 383-419

16178 WETTING AND DRYING ON SHEAR STRENGTH

KEY WORDS: **Climatic changes;** Cohesion; Drying; Friction; **Shear strength; Soil mechanics; Strength;** Stress-strain curves; **Time factors; Triaxial tests;** Wetting

ABSTRACT: Climatic changes, such as repeated wetting and drying over geological ages, lead to the degeneration of the parent rock to form soil. Simultaneously these actions can also cause some aggregation of soil particles and the production of bonds, called desiccation bonds, which impart an intrinsic effective stress to the soil. This intrinsic effective stress can influence the shear strength behavior of soils subjected to such climatic actions. When a soil is subjected to repeated wetting and drying in the laboratory, an intrinsic effective stress is imparted to it which results in greater shear strength and in a stiffer stress-strain response. This intrinsic effective stress may be attributed to chemical bonds.

REFERENCE: Allam, Mehter Mohamed, and Sridharan, Asuri, "Effect of Wetting and Drying on Shear Strength," *Journal of the Geotechnical Engineering Division,* ASCE, Vol. 107, No. GT4, **Proc. Paper 16178**, April, 1981, pp. 421-438

16173 POROSITY IN NATURAL SAND DEPOSITS

KEY WORDS: Dry density; **Dunes; Hardening; Impregnation;** Laboratory tests; Peel tests; **Porosity; Relative density;** Relative density determination; **Sand;** Undisturbed samples; Wet density

ABSTRACT: The proposed technique enables porosity measurement to be made on undisturbed samples taken from sand deposits. It is based on the impregnation and hardening of sand in the field and the preparation of small cube samples which are tested in the laboratory. The method proved successful in both dry and wet sand. Its application is demonstrated in the study of porosity variations in a dune. The internal structure of the dune was studied by means of replicas or "peels" which reveal in detail the layering of the dune sand. A definite relationship was established between porosity and relative density of the sand and its internal structure and mode of deposition. Very high densities were found in sand deposited by accretion on the dune's back. Relative densities in accretion deposits approach and even exceed 100 percent.

REFERENCE: Denekamp, S. A., and Tsur-Lavie, Y., "Measurement of Porosity in Natural Sand Desposits," *Journal of the Geotechnical Engineering Division,* ASCE, Vol. 107, No. GT4, **Proc. Paper 16173**, April, 1981, pp. 439-447

16179 STOCHASTIC FEM IN SETTLEMENT PREDICTIONS

KEY WORDS: **Deformation; Finite element method; Footings;** Foundation design; **Foundations; Probability theory;** Settlement analysis; Settlement measurement; **Settlement (structural);** Stochastic processes

ABSTRACT: Stochastic finite element analysis is used to predict uncertainties in total and differential settlement under a large flexible footing. The results are compared with one-dimensional stochastic solutions already in the literature. Differences between the one- and two-dimensional analyses, particularly for differential settlement, are distinct. These differences seem primarily attributable to randomness in the stress field which cannot be included in one-dimensional models, and to mechanistic correlations by common dependence on the realizations of particular random variables. In principle, second-moment techniques can be extended to a broad range of analyses now performed using finite element and finite difference techniques.

REFERENCE: Beacher, Gregory B., and Ingra, Thomas S., "Stochastic FEM In Settlement Predictions," *Journal of the Geotechnical Engineering Division,* ASCE, Vol. 107, No. GT4, **Proc. Paper 16179,** April, 1981, pp. 449-463

16174 SOIL ORGANIC-CONTENT MEASUREMENT

KEY WORDS: Decomposing organic matter; **Decomposition; Ignition tests;** Measurement; Organic particle composites; **Organic soils; Soil dynamics; Soil mechanics;** Soil microorganisms; Soil physical properties

ABSTRACT: Problems with organic soils are often avoided by engineers because of uncertainties in organic-content measurement and lack of information on potential decomposition. High temperatures, used in the ignition test for measurement of the organic fraction, require that a correction be made for loss of surface hydration water from the mineral solids. Model soils, prepared from kaolinite and pulp fiber, and the dehydration curves for these materials have permitted development of a correction factor for use with the ignition test. A review of published data and an error analysis suggest that this correction factor may be suitable for natural organic soils. The ignition test does not distinguish between undecomposed organic matter and microorganisms formed during decomposition; hence, the degree of decomposition has not been available. A relationship—between microorganism cell content, undecomposed organic matter, and the mineral fraction—has been developed which permits computation of the degree of decomposition.

REFERENCE: Al-Kafaji, Abdul-Amir W.N., and Andersland, Orlando B., "Ignition Test for Soil Organic-Content Measurement," *Journal of the Geotechnical Engineering Division,* ASCE, Vol. 107, No. GT4, **Proc. Paper 16174,** April, 1981, pp. 465-479

16180 MODELING OF COAL WASTE EMBANKMENTS

KEY WORDS: **Centrifugation; Coal; Embankments;** Laboratory tests; Model tests; **Seepage;** Shear strength; **Slope stability;** Tailings; **Wastes**

ABSTRACT: Centrifuge model embankments with varying geometries and properties were constructed of coal waste material, accelerated to 100-120, and subjected to various reservoir depths until failure occurred. Complimentary laboratory tests were performed on the waste materials to obtain strength and permeability parameters for analytical calculations to predict observed centrifugal model behavior. Failures occurred in model embankments with 1 Vertical:1.5 Horizontal and 1 Vertical:2 Horizontal slopes when the phreatic surface due to seepage exited on the downstream slope and initiated sloughing at the toe. Positive seepage control, i.e., a toe drain, successfully prevented sloughing and failures. Slope stability analyses agreed well, albeit conservatively, with observed model performance. These models verified existing criteria of minimum safety factor of 1.3 and the necessity of positive seepage control.

REFERENCE: Al-Hussaini, Mosaid M., Goodings, Deborah J., Schofield, Andrew N., and Townsend, Frank C., "Centrifuge Modeling of Coal Waste Embankments," *Journal of the Geotechnical Engineering Division,* ASCE, Vol. 107, No. GT4, **Proc. Paper 16180,** April, 1981, pp. 481-499

16212 EARTHQUAKE-INDUCED LIQUEFACTION

KEY WORDS: Case reports; **Cyclic loads; Earthquakes;** Guatemala; **Liquefaction;** Penetration resistance; Pumice; **Sand; Sandy soils;** Weight (mass)

ABSTRACT: One of the effects of the February 4, 1976, Guatemala earthquake was the extensive liquefaction which occurred at the settlement of La Playa on the northeast shore of Lake Amatitlan. Ground accelerations in the area resulting from the magnitude 7.5 earthquake are estimated to be of the order of 0.12 g to 0.15 g. The characteristics of the sand are investigated, including its standard penetration resistance and its cyclic loading characteristics. Despite the fact that the sand is somewhat lighter in weight than sand deposits which have liquefied in other earthquakes, its liquefaction characteristics are apparently influenced by the same factors as other sand deposits; its overall behavior is consistent with that exhibited by other sands. The high degree of liquefaction at the La Playa site was probably due in large measure to the lightweight nature of the pumiceous sands.

REFERENCE: Seed, H. Bolton, Arango, Ignacio, Chan, Clarence K., Gomez-Masso, Alberto, and Ascoli, Rebecca Grant, "Earthquake-Induced Liquefaction Near Lake Amatitlan, Guatemala," *Journal of the Geotechnical Engineering Division,* ASCE, Vol. 107, No. GT4, **Proc. Paper 16212**, April, 1981, pp. 501-518

U.S. Customary-SI Conversion Factors

In accordance with the October, 1970 action of the ASCE Board of Direction, which stated that all publications of the Society should list all measurements in both U.S. Customary and SI (International System) units, the following list contains conversion factors to enable readers to compute the SI unit values of measurements. A complete guide to the SI system and its use has been published by the American Society for Testing and Materials. Copies of this publication (ASTM E-380) can be purchased from ASCE at a price of $3.00 each; orders must be prepaid.

All authors of *Journal* papers are being asked to prepare their papers in this dual-unit format. To provide preliminary assistance to authors, the following list of conversion factors and guides are recommended by the ASCE Committee on Metrication.

To convert	To	Multiply by
inches (in.)	millimeters (mm)	25.4
feet (ft)	meters (m)	0.305
yards (yd)	meters (m)	0.914
miles (miles)	kilometers (km)	1.61
square inches (sq in.)	square millimeters (mm^2)	645
square feet (sq ft)	square meters (m^2)	0.093
square yards (sq yd)	square meters (m^2)	0.836
square miles (sq miles)	square kilometers (km^2)	2.59
acres (acre)	hectares (ha)	0.405
cubic inches (cu in.)	cubic millimeters (mm^3)	16,400
cubic feet (cu ft)	cubic meters (m^3)	0.028
cubic yards (cu yd)	cubic meters (m^3)	0.765
pounds (lb) mass	kilograms (kg)	0.453
tons (ton) mass	kilograms (kg)	907
pound force (lbf)	newtons (N)	4.45
kilogram force (kgf)	newtons (N)	9.81
pounds per square foot (psf)	pascals (Pa)	47.9
pounds per square inch (psi)	kilopascals (kPa)	6.89
U.S. gallons (gal)	liters (L)	3.79
acre-feet (acre-ft)	cubic meters (m^3)	1,233

JOURNAL OF THE GEOTECHNICAL ENGINEERING DIVISION

THE FIFTEENTH TERZAGHI LECTURE

Presented at the American Society of Civil Engineers Annual Convention and Exposition, Atlanta, Georgia

October 25, 1979

GEORGE F. SOWERS

Introduction of Fifteenth Terzaghi Lecture

By William F. Swiger

George Sowers has always been a civil engineer. As a child he accompanied his father, George B. Sowers, F. ASCE, on inspections of tunnel, foundation, and port construction. His undergraduate education was at Case Institute of Technology; his graduate work was at Harvard where he was a student of Karl Terzaghi and Arthur Casagrande.

George worked as a hydraulic and hydrologic engineer with the United States TVA and served in the United States Navy during WW II.

Since 1947 he has pursued a dual career: teacher and consultant, presently Regents Professor of Civil Engineering at the Georgia Institute of Technology, he pioneered geotechnical engineering education in the southeast. His textbook Introductory Soil Mechanics and Foundations is in its fourth United States edition, plus Spanish, international, and even pirated Taiwan editions. In addition, he has published more than 100 technical publications.

George is a cofounder of Law Engineering, one of the largest geotechnical environmental and materials engineering firms of the United States. He has been a consultant on geotechnical design throughout the United States and in many foreign countries.

He has been President of the Georgia Section ASCE and Chairman of the Geotechnical Engineering Division, ASCE. Presently he is the Vice President for North America of the ISSMFE.

He is married; his wife, Frances, has practiced hydraulic engineering. They have four children, two of whom are geologists.

THERE WERE GIANTS ON THE EARTH IN THOSE DAYS

By George F. Sowers,[1] F. ASCE

SYNOPSIS

Many examples of pre-Columbian earth construction have been uncovered in the Americas. Some reflect well-organized technologies comparable to those of the Old World of the same time period. Earth fills, stone and adobe structures, highways, and water management systems exhibit both well-conceived designs and organized effort for construction.

A few investigators speculate that such sophisticated works represent unrecorded technology transfer from the Old World; some pseudohistorians suggest visits from outer space. However, the evidence demonstrates that indigenous, ingenious responses to local social and economic problems and organized community efforts were responsible. Lack of both a formal logic-mathematics system and written communication inhibited synergistic development of the technologies. They were vulnerable to decay and were virtually obliterated by conquest.

INTRODUCTION

Flying high above the earth, about 370 km south-southeast of Lima, Peru, and crossing a broad, arid valley 50 km from the sea, one can see patterns in the valley floor below. Even the earth resources satellites, 950 km (570 miles) high, can discern straight lines, some several kilometers or miles long. At lower altitudes, the lines become more distinct, up to 50 m wide, in strange criss-cross patterns on the 60 km (35 mile) long, 2 km (nearly a mile) wide braided-plain terrace 500 m (1,600 ft) above sea level.

[1]Regents Prof. of Civ. Engrg., Georgia Inst. of Tech., Atlanta, Ga. 30332; also Sr. Vice Pres., Law Engrg. Testing Co., 2749 Delk Road, S.E., Marietta, Ga. 30067.

Note.—Discussion open until September 1, 1981. To extend the closing date one month, a written request must be filed with the Manager of Technical and Professional Publications, ASCE. Manuscript was submitted for review for possible publication on February 5, 1980. This paper is part of the Journal of the Geotechnical Engineering Division, Proceedings of the American Society of Civil Engineers, ©ASCE, Vol. 107, No. GT4, April, 1981. ISSN 0093-6405/81/0004-0385/$01.00.

There is a cursory resemblance to a runway that one can identify approaching at low altitude, 600 m (2,000 ft) above the surface (Fig. 1). The Swiss science-fiction author, Eric Von Daniken (3), in *Chariots of the Gods,* asks, "What is wrong with the idea that the lines were laid out to say to the gods, 'Land here! Everything has been prepared as you ordered!' . . . What other purpose could they have served?" (Although Von Daniken's ideas are not taken seriously by archeologists, he has an amazingly large audience.)

With a closer look, the illusion of a landing field is dispelled by the criss-cross patterns. Some lines are oriented at random while others radiate from a common center like the points of a compass. Scattered among the straight lines are curves. Some are geometric, but most are cartoon-like outlines of familiar creatures, such as a monkey, a spider, or a hummingbird (Fig. 2). All are about 75 m–100 m across.

FIG. 1.—Nazca Lines of Southwest Peru from 600 m (2,000 ft) above Ground

Still closer, their construction is seen to be simple. The gravel-sized stones of desert pavement are covered with a dark brown coating, i.e., desert varnish (a dark brown, shiny coating of iron oxide and silica brought to the exposed surface of bed rock and gravel by capillarity and deposited by evaporation in a severe desert environment). When the stones are moved aside or overturned, the unexposed surface or light-colored protected sand is exposed. The patterns are merely strips of desert from which the pavement has been moved aside forming little brown ridges that outline the light colored lines and figures. A brief experiment suggests that a person can clear 1 m^2 in 10 min. Even one of the larger lines, 30 m wide and 300 m long, could be constructed in 100 man-days–200 man-days. Archaeologists are still debating the meaning of the lines (12,17). Most are oriented with prominent stars, the moon, or the sun at special times of the year. All probably have a religious significance. Considering

the time that is required for desert varnish to develop, the figures are probably 500 yr–1,500 yr old. This is compatible with archaeological evidence of the pre-Inca civilization that inhabited this valley. It agrees with carbon-14 dating of wood stakes at the ends of the lines that were used to establish alignment by sighting (12).

These lines and figures are not unique. There are figures outlined in the southern California desert that are remarkably similar. High on a mountain ridge in northern Wyoming, there is outlined a lopsided wheel about 22 m (75 ft) diam made of light colored limestone cobbles and small boulders that contrast with the green grass. Because some of the spokes are aligned with sunrise at the vernal equinox, it also appears to have an astronomical significance.

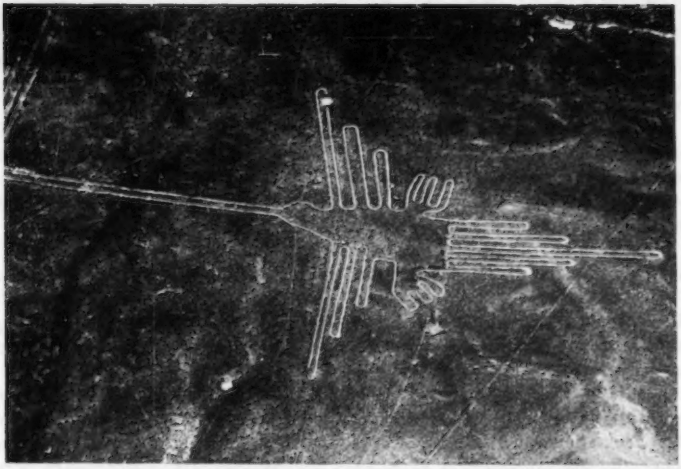

FIG. 2.—Nazca Humming Bird, 100 m (330 ft) Wide

The Indians of a century ago knew that it was sacred but were ignorant of its meaning or of who built it.

Tradition of Western (European) Technology

The development of western (European) technology is reasonably well documented. First, there was the empirical or trial-and-error approach that marked the craftsmen of the Middle East and Egypt. Later, the Greeks added geometry and a formal logic for the behavior of physical objects. The Romans combined these with their genius for organizing and communicating throughout their empire. The Arabs added innovations in mathematics. The scientists and engineers of the Renaissance and Industrial Revolution resurrected these concepts from their suppression during the Dark Ages to establish the framework for engineering as we know it.

The members of the American Society of Civil Engineers are products of that tradition. With this background of empiricism, keen observation, logic, and mathematics, such a genius as Karl Terzaghi was able to conceive imaginative and innovative solutions to problems in soil and rock that had confounded engineers for milleniums. The engineering structures of this century are a testimony to this tradition.

It is sobering, however, to realize that until the twentieth century the largest structure known to western technology was the Pyramid of Cheops, built 4500 years ago. It was conceived and constructed without two of the tools of modern technology: Logic and formal mathematics. One contemporary religious writer suggests that it was built by Gods from other worlds—the Egyptians could not have undertaken such a feat. His idea is not new. The ancient Greeks attributed the large polygonal stones of the walls of Mycenae to the Cyclops—mythical one-eyed giants. Our term "cyclopean masonry," walls of very large boulders, is derived from their tradition. More than 3,000 years ago, Hebrew herdsmen explained monuments of giant stones that they found in the desert by exclaiming, "There were giants on the earth in those days" (8).

The traditions of the pre-Columbian Americas are not well documented. The early Spanish conquistadors found flourishing civilizations in Mexico and Peru, but destroyed many of the native works in a passion for gold and religion (4,10). Remains of some older, dying, or dead civilizations were gutted for building materials or looted by souvenir seekers.

The construction relics are still being uncovered; lost cities are coming to light in the jungles of Yucatan, Central America and the Andes of South America. Their scale is staggering. What was probably the largest structure in the world, the Pyramid of Tepanapa, 1.5 times the volume of the Pyramid of Cheops, is yet to be fully excavated. Countless other structural works on both continents are only now being analyzed by engineers.

It is the purpose of this paper to examine pre-Columbian structures and public works from the civil engineering point of view. It considers their features, their geographic and chronologic development, and presents hypotheses for their conception and construction. It explores whether they were conceived by occult forces, such as visitors from outer space (as suggested by Von Daniken) (3), inspired by lost mariners and early explorers from Europe and Africa who never reported back to the old world, or were the products of independent innovation. Most important, it relates the development and decline of pre-Columbian technology to the evolution of engineering today.

Pits and Heaps

The earliest construction was a hole in the ground, either for disposal of excrement or burial of the dead. Both practices are common (but not universal) thoughout the world. The need may have been sanitation, or possibly the religious idea that both excrement and corpses have magic, malevolent power that must be kept from view. On the other hand, the Mayan farmers of Meso-America and the Creek Indians of the Southeastern United States buried their dead below the floors of their houses so that their spirits could rise and guide the future.

Where hard soil made excavation difficult, heaps of stones substituted for

burial. An eskimo grave in Greenland is a crude cairn of small boulders over hard permafrost.

Both shallow pits and heaps of stones were used for shelter. The early Indians of the Mesa Verde area (Southwest Colorado, about 500 A.D.) found the ground was warmer than the outside air in winter and cooler in summer. They excavated elongated pits about 1 m deep and 3 m–6 m diam; where the soil was loose, the holes were lined with stones. Above ground, low rubble stone or laced twigs formed walls; poles, twigs, and grass formed a roof. Similar pit houses are found along the north coast of Peru, dated about 3000 B.C.

The more advanced Indian civilization of the American Southwest retained the pit house in the kiva, Fig. 3. This is a stonelined pit, about 3 m–5 m diam and 3 m–4 m deep with a roof of logs and earth. The kiva served as a fraternal-clan retreat for the men, isolated from the bustle of daily work. Although the details vary, most included a stone-lined fresh air duct at the base, a draft deflector at the inlet, a raised platform for a fire, and a small hole in the floor that served as a symbolic connection to the depths of the

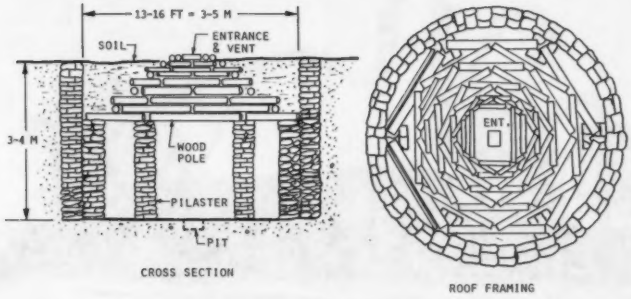

FIG. 3.—Details of Small Kiva, Mesa Verde, Southwest Colorado

earth. Kivas, some below ground, but others above (where the soil is shallow), play a vital part in the life of the Pueblo Indians today.

The Creek Indians also built earth covered ceremonial or clan lodges with provisions for a fire and a small floor hole. These date between 500 A.D. and 1200 A.D.

These excavations possibly reflect the instinctive feeling of security that a child exhibits when he retreats to a corner when under duress, or the dugouts made by older children to escape the adult world. The pit is not limited to primitive societies or children; the United States defense headquarters is far underground in the Colorado mountains.

Mounds

Large heaps of earth and piles of stones were constructed by men in all parts of the world except Australia. Until the twentieth century, they were the largest structures ever built.

Trash heaps are one form. Despite the romantic fantasies of historians, some American Indian tribes merely dumped their trash, garbage, broken pottery, and fecal wastes in irregular piles immediately adjacent to their permanent camps. Refuse mounds up to 4 m (13 ft) high of shells, bones, and broken stone utensils from about 300 B.C. are found along the sea coast in Peru. Similar shell mounds occur along the South Atlantic and Florida Coasts in the United States dating from about 2000 B.C. Some became mounds as high as 6 m (20 ft). Although they are now rich sources for archeologists, they must have bred flies and rodents, and exuded rich odors when in use.

Burial mounds, constructed between 800 B.C. and about 150 A.D. by Woodland Indians, are widely distributed in the Eastern United States. Many are from 3 m–10 m (10 ft–33 ft) high with side slopes typically 30°–35° from the horizontal and have round tops. Most appear to have been built during a relatively short

FIG. 4(*a*).—Etowah Mound, Cartersville, Ga.

time period, representing only a generation or two, based on a comparison of possessions that accompanied the burials and on very limited carbon-14 dating. Long-term use of a site produced a succession of mounds instead of a single, growing burial. Burial mounds are also found in the coastal settlements of South America, dating from about 500 B.C. (11).

Platform Mounds.—Platform mounds for worship ceremonies or bases of temples appeared in the Eastern United States about 700 A.D. Similar structures in Meso-America, such as Tikal in Guatemala, date as early as 500 B.C. (1,2). Platform mounds, built by filling over old pit and wall houses with soil and debris are found on the north and central coast of Peru (11). The debris associated with them dates about 2000 B.C. by carbon-14. The mounds were constructed of local materials with uniformly sloping sides and flat tops. Most were built

in stages over a long period of time, eventually becoming the largest structures of the pre-Columbian era.

The Etowah group, near Cartersville, Ga., 35 miles north-northwest of Atlanta, were built on a low terrace on the right bank of the Etowah River. It consists of three mounds, a village area, and a 1.3 m (4 ft) deep perimeter ditch enclosing a circular area about 450 m (1,500 ft) diam. The smallest mound has been completely excavated. It was constructed in stages between about 700 A.D. and 1200 A.D. and consists of a series of concentric truncated square pyramids with side slopes of 33°–37° with the horizontal. The top was flat and was similar in size for each stage. On each top was a simple wood temple with walls of vertical poles set in sockets in the ground. The bark-stained sockets remain and mark each platform level. At the death of a chief or priest, marking the end of a period of unified leadership, the wood structure was destroyed, and the leader was buried in the mound with weapons, jewels, and vestments. A new platform and temple were then constructed 1 m–3 m (3 ft–10 ft) above

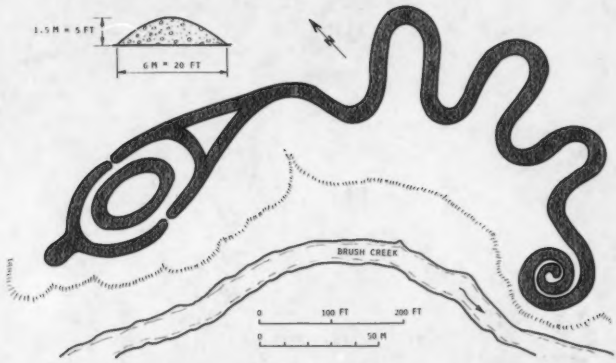

FIG. 4(*b*).—Serpent Mound, Southwest Ohio: Plan

the earlier one. The stages in construction are reflected in different soils and slightly different artifacts.

The largest mound of the Etowah group, Fig. 4(*a*), contains about 110,000 m^3 or 150,000 cu yd of soil. It has not been excavated. There are remains of a wood temple or council house on top. It appears to have been built in the same stage construction as the smallest mound.

Monks Mound of the Cahokia group, adjacent to a small creek about 25 miles east of St. Louis is the largest in the eastern United States. It is nearly 30 m or 90 ft high with 25° side slopes. Soil borings with undisturbed samples show it was built in about 14 stages, commencing about 900 A.D. and ending about 1150 A.D. (16). The stages range in thickness between 1 m (3 ft) and 5 m (17 ft). The total fill volume is about 750,000 m^3 or 1,000,000 cu yd.

Protective Mounds.—A few mounds are in the form of continuous embankments enclosing the remains of villages and ceremonial centers. At "Fort Ancient," near Cincinnati, Ohio, a perimeter mound 6 km (3.5 miles) long encloses a

40 ha (100 acre) segment of bluff overlooking a river. The mound varies from 3 m–5 m (10 ft–16 ft) high with side slopes of 30°–40°. Other fort-like or stockade mounds have been found in the upper Mississippi and Ohio River area.

Effigy Mounds.—A number of mounds are shaped like animals. Most are in southern Wisconsin or northeastern Iowa, although a few are scattered throughout the eastern United States. Most are low, 1 m–3 m (3 ft–10 ft) high, and cover areas 10 m to more than 100 m (33 ft to more than 330 ft) diam. Animals, such as the panther, bear, deer, buffalo, turtle, beaver, and dog predominate, but birds are also found. Most are on bluffs above rivers and are associated with small burial mounds. Those excavated appear to have been built in a single stage. Although there are some associated burials and nearby burial mounds, they appear to be clan symbols or ceremonial structures.

The Serpent Mound of southeastern Ohio, Fig. 4*b* and 4*c* is the largest and

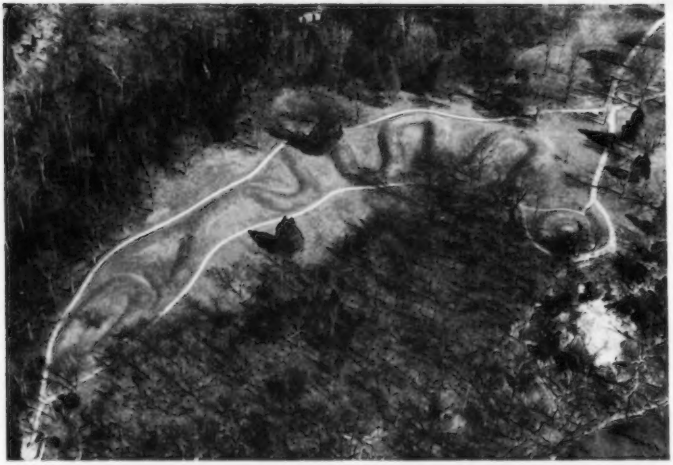

FIG. 4(*c*).—Aerial View of Serpent Mound

best known of the effigy mounds in the United States. It lies on a bluff overlooking a small river. It is made of gravelly clay, following a pattern laid out with a row of stones and ashes after removing the topsoil. The approximate volume is 2,000 m^3 or 2,500 cu yd.

Mound Construction.—Those mounds that have been excavated or core drilled all exhibit evidence of similar construction. They were placed in level layers 2 cm–8 cm or 1 in.–3 in. thick. In some cases the edges of the layers were confined by logs secured by stakes: simple forms. These forms were removed and reset as the work progressed, but occasionally left to rot in place as shown by remains of bark and rotted wood. Side slopes were typically 33°–37° with the horizontal with no obvious correlation between height, soil texture, and slope. Although the sides were usually dressed to a common straight slope,

the only protection was vegetation which developed naturally. The occasional eroded gully was sometimes filled with stones.

The tools for construction have been pieced together from fragments remaining in the mounds. The soil was loosened with a pointed digging stick, hardened by fire. The same sticks were also used for planting corn. I have seen them in use today in remote rural Mexico, Honduras, Peru, and Bolivia. Excavation was by hoes made from shoulder blades of deer lashed to poles. The earth was carried in baskets or leather bags on the backs of the workers, about 20 kg or 45 lb at a time.

Experiments by various investigators, cited by Erasmus (6) suggest that a team of one digger and three basket carriers could excavate 3 m^3 (4 cu yd) and move and place the soil 200 m (650 ft) from the source in one day. At this rate, the largest Etowah mound required about 100,000 man-days and the largest Cahokia mound 1,000,000 man-days. The Incas of South America were required to devote about 90 days/yr to community labor. Reed et al. (16) estimate that the North American Indian may have contributed 40 days. At this rate, Etowah required 2500 man-years and Cahokia 25,000 man-years. Both were built over periods of about 250 years. Thus the required average annual labor force would have been only 10 persons and 100 persons, respectively. Cahokia, however, was built in 14 stages averaging 18 years (probably 14 generations), thus Cahokia required 1,800 man-years/generation. On the same basis Etowah required only 200. The large volumes are not unreasonable for the modest labor forces available, when the religious and secular leaders organized the people for the common effort.

Platforms and Pyramids

In the southeastern United States the earth platform temple base possibly evolved from the burial mound. In Meso-America and Peru the temple base developed independently. The earliest were flat platforms of earth and boulders faced with walls of rubble masonry and topped with flat stones (11). On top were stone monoliths and remains of small buildings that probably were worship related. The earliest appeared about 1800 B.C. in Peru and Mexico.

During later periods, some of the platforms were enlarged by building new walls around them, and then raised in increments of 3 m–5 m (10 ft–16 ft). The platform became a series of terraces or a step pyramid, with very steep sides, and a level top which was the focus of religious rites.

Still later, the platforms were augmented by faces of rubble, adobe brick, and later of trimmed stone, battered at slopes of 60°–70° with the horizontal. These truncated pyramids first appeared about 1800 B.C. in Peru. Their construction climaxed with the Pyramid of the Sun at Pachamac, about 30 km (18 miles) south of Lima, between about 200 A.D. and 1000 A.D. The pyramid is of stones and adobe brick, about 220 m (700 ft) square, flat topped, and about 23 m (75 ft) high.

The largest earth-stone pyramids were constructed in the Valley of Mexico. At Cholula, about 50 km (30 miles) east of Mexico City is the Pyramid of Tepenapa. It is possibly the largest structure built before the 20th century, constructed between 350 A.D. and 600 A.D. The base is 402 m^2 (132 sq ft) and it is 70 m (231 ft) high. Although it is not as tall as the Pyramid of Cheops,

its volume of 3,770,000 m^3 or 5,000,000 cu yd is approximately 1.5 times greater (Fig. 5). At the time of the Spanish Conquest, there was a small temple on the flat top. It was replaced by a Roman Catholic Church which is still in use.

The pyramid is constructed of light-colored tuff boulders about 0.6 m (2 ft) diam in a matrix of dark volcanic ash and soil. Exploratory tunnels into the heart of the pyramid have found five (or possibly seven) smaller concentric pyramids with plastered faces. A painting of a giant grasshopper on one face is still grotesquely colorful.

Deep in the jungles of northern Guatemala, along the humid Gulf Coast of southern Mexico and in the tangled underbrush of the Yucatan Peninsula are the most magnificant structures of pre-Columbian North America, i.e., the Mayan temple pyramids (14,20). Commencing about 500 B.C. and ending between 1200 A.D. and 1400 A.D., complex religious centers resembling cities were constructed in the tropical lowlands. A wide variety of massive structures remain, many still choked by the jungle and awaiting archeologic study. Enough have been examined to demonstrate the evolution of advanced construction technology over a wide area (Fig. 6). Although each has its imposing structures, Tikal,

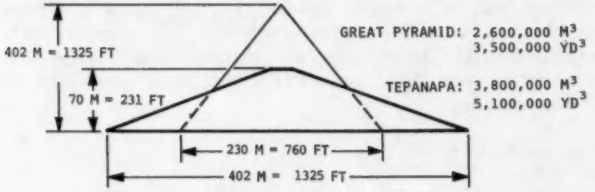

FIG. 5.—Comparison of Pyramid of Tepanapa, Cholula, Mexico with Pyramid of Cheops, Egypt

Guatemala represents one of the earliest and longest lived of these areas (1,2,20).

Temple I, Fig. 7 was completed about 700 A.D. near the climax of Tikal's 1000 yr history. It is 40 m^2 (130 sq ft) at the base, with the overall slope of its nine terraces 65°. It has a narrow truncated top, 30 m (100 ft) above the Plaza. On top is a small temple with a soaring crest or comb rising another 14 m (45 ft). Although other temple pyramids at Tikal are higher, and many in Yucatan, such as at Uxmal and Chichen Itza, are broader, Temple I remains an impressive example of the best Mayan construction. A stair leads up to the temple, so steep that one climbs it today with the aid of a chain. The pyramid surface is of well-fitted soft limestone blocks laid in courses.

Surface repair of the Tikal pyramids reveals that they were built of boulder-sized soft limestone rubble in a matrix of limestone chips and cemented with lime mortar. Tunnels into the pyramids reveal smaller, older pyramids within (1,2). Large carvings on the older pyramid surfaces, hidden by the larger, later enveloping construction, can be seen in exploration adits, excavated by archaeologists (Fig. 8).

The quarries from which the soft limestone blocks were cut and the rubble obtained are still in use, furnishing fresh blocks for restoration of the structures

(Fig. 9). Deep, narrow slots were first cut, using tools of chert or flint. The rock was then broken apart by prying or wedging in the slots.

Adobe

Adobe is a universal construction material used throughout the Americas as well as in the Old World. Technically it is unburned soil (clay) brick, but the term has been applied to other forms of dried soil construction.

Sun-dried brick is a form of artificial stone used in arid regions where local rock is difficult to shape or is absent. Based on data from sites in the western United States, a wide variety of soil materials have been used, the major

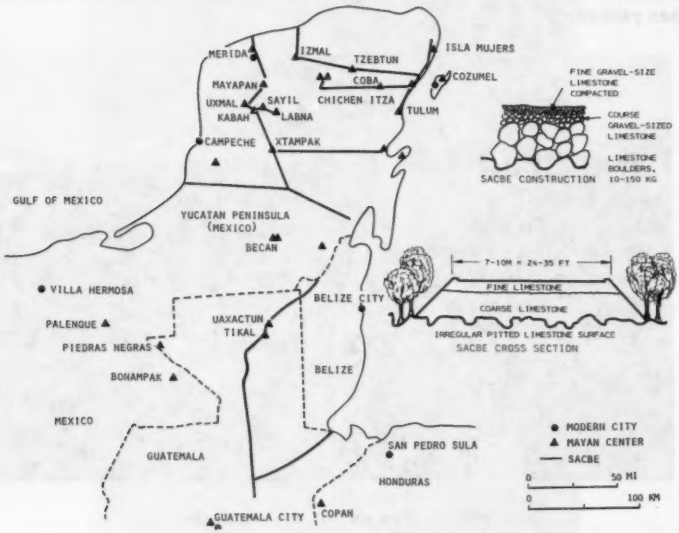

FIG. 6.—Mayan Centers and Roads

requirements are sufficient cohesion to provide strength when dry and enough inert filler such as sand, fine gravel, and even straw, grass, or twigs to minimize shrinkage. Based on unpublished tests by the writer, unconfined compressive strengths range from 100 kN/m^2–nearly 700 kN/m^2 (15 lb/sq in.–nearly 1000 lb/sq in.). The tensile strength is typically 1/6 the unconfined compressive strength. Adobe resembles weak, plain concrete in its strength and ability to absorb repeated strain and tension. It resists static loads in walls up to 15 m (50 ft) high but crumbles under the dynamic loads of earthquakes.

Adobe balls and cones were used as masonry units in coastal Peru as early as 1000 B.C. Rectangular adobe blocks appeared shortly afterwards sometimes interlayered with stones. The largest adobe brick structure in the Americas was the pyramid of Pachamac, mentioned previously (11).

The Pueblo Indians of the United States southwest used both adobe and stone for construction depending on material availability. The Casa Grande of Arizona was built between 1350 A.D. and 1400 A.D. as a part of a village compound of the Hohokam, whose descendents may be the Pima Indians (9,25). Lenticular pancakes, typically 0.35 m^3 (1.3 cu ft) diam of firm silty clay were laid in very irregular noncontinuous courses and level tiers, 1.2 m (4 ft) wide and 0.5 m–0.75 m (1.5 ft–2.5 ft) high. Each tier was shaped to make flat vertical surfaces and then allowed to dry before adding the next, producing cold joints in which hand prints are still visible. Although all the soils in the walls were obtained from the site, there are significant variations between tiers, reflecting the different calcium carbonate percentages in the soil horizons excavated. The insides of the walls (and possibly the outside) were plastered with adobe and then painted.

FIG. 7.—Temple I, Tikal, Guatemala

Archeologists (25) have estimated that the 41,000 cu ft of walls required about 50,000 man-hours of labor, based on the excavation, mixing, and placing of each soil pancake. A village of 20 families could have built it in a year or two after allowing for their farming and hunting. Similar adobe construction has been found in other southwestern United States pueblos.

Masonry Walls

The temple platforms and pyramids are massive, requiring much labor, but limited ingenuity. Walled structures, which also evolved from simple heaps of stones, required advanced technology to provide stability against overturning by wind, earthquakes, and security against enemy attack.

The first walls in the Americas were of cobbles, stone slabs, or adobe with clay binder for mortar, about 2 m high. They appeared along the coast in Peru

about 2500 B.C. Similar cobble and mud walls were built along the sandstone cliffs of the southwestern United States to enhance the shelter provided by the sandstone overhangs.

Wall construction evolved rapidly in the southwestern United States, using flat sandstone flags about 30 cm^2 (1 sq ft) by 3 cm–5 cm thick, laid in courses, with the stones in successive courses overlapping to form a bond. The earliest construction used rough flags selected for uniform size. In later construction,

FIG. 8.—Stone Face 2.5 m (8 ft) High Revealed in Exploratory Tunnel into Pyramid at Tikal, Guatemala

the broad surfaces and one edge of the stone were chipped to provide a rectangular outer face of uniform thickness. A good example is Pueblo Bonito, Chaco Canyon, N.M., built about 1000 A.D. The higher walls consisted of outer casings of bonded and faced flat stones with cores of rough flat stones crudely interlayered (bonded) with the facing. An understanding of the greater stress at the base of the wall is reflected in the greater width at the base, 1 m (3.3 ft) tapering to 0.3 m (1 ft) at a height of about 8 m (25 ft). The masonry was laid with

stone chips and clay mortar to level the rough split stone surfaces. Lateral stability was provided by cross walls; the rooms were typically 2 m–4 m wide and long.

Coursed masonry walls were used more sparingly in Meso-American construction. Some of the temple complex of Teotihuacan, Mexico, included coursed masonry of tuff blocks, 25 cm × 50 cm, on the outer face. There are a few Mayan (700 A.D.–1200 A.D.) walls of soft limestone, generally laid without mortar. The blocks were of varying sizes, from 20 cm to about 50 cm high, but uniform in each course. The typical length to width ratio of the blocks ranged from 1.1–1.4.

Masonry walls were constructed extensively in the Peru-Bolivia highlands. Most of the earlier walls, 200 B.C.–600 A.D. were laid with more or less rectangular

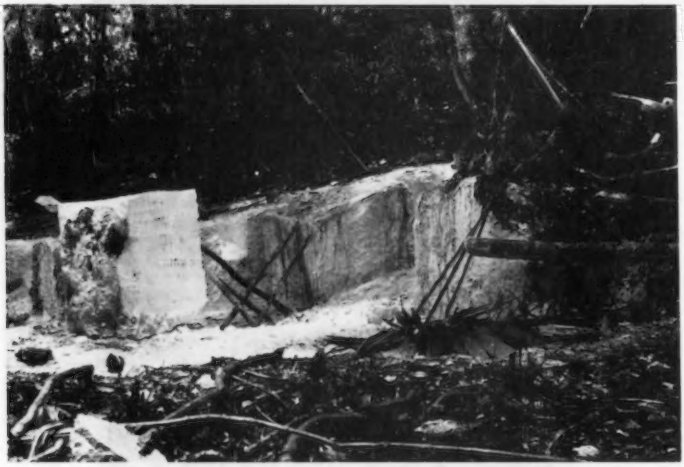

FIG. 9.—Ancient Quarry in Soft Limestone, Tikal, Guatemala Furnishing New Blocks for Restoration Work

blocks of unequal height, as in Fig. 10. This required notching of the corners to fit successively higher courses together. The fitting was very precise and most of the walls were laid without mortar. At Tihuanaco, Boliva, some of the stones were held together by I-shaped copper cramps, forced into dumbbell shaped notches cut between adjoining stones. The use of the wall was reflected in the quality of construction in the later Inca masonry, 1200 A.D.–1500 A.D. Terrace walls in rural areas were built of roughly trimmed rectangular blocks of varying sizes, laid in courses that were not necessarily level nor of equal height. Military structures such as the Fort of Sacsahuaman near Cuzco (Fig. 10) were made of huge, more or less rectangular blocks, laid in irregular courses, with blocks of unequal size notched to fit together. The fitting of these limestone blocks was very precise, with either very thin clay mortar or no mortar at

all. The surface texture of the stones suggests that they were shaped by pounding with small hard stones, followed by surface grinding with stones and sand. According to Inca tradition, recounted by de LaVega (10), the blocks were dragged from the nearby quarry by hundreds of men utilizing twisted vine ropes and either wood skids or rollers. Earth ramps were constructed to place the upper blocks. The construction of Sacsahuaman, completed about 1480 A.D., required 50 yr utilizing tax labor, about 120 days/yr/person, and a legendary labor force of more than 20,000. One large block, the "Weary Stone," was never trimmed or lifted in place. According to Inca legend (10), it was so weary after being dragged to the fort site that it wept blood from two holes in one corner. More likely it was the laborers who wept—3,000 were killed when it fell from a slope during hauling.

FIG. 10.—Inca Wall of Notched Rectangular Blocks: Fortress of Sacsahuaman, Cusco, Peru

Because of the irregular coursed, notched corners, and close fitting, the walls have demonstrated unusual resistance to earthquakes compared with the uniform coursed, mortared walls built in the same areas by the Spanish conquerors. Some historians have speculated that the notched form represents a conscious effort for greater stability. However, if this were true, it would be used on the most important structures, i.e., religious and governmental buildings. However, uniform, continuous, coursed (unnotched) masonry was reserved for the most sacred buildings in Cuzco, such as the Convent of the Virgins of the Sun and the Temple of the Sun. The writer believes that the notched masonry reflects a compromise between the ordered appearance of uniform coursed masonry and the labor required to produce uniformity from rock that did not split readily.

Mortar.—Mortar is employed to bed and cement the masonry units of walls and to plaster over a rough wall to provide a smooth surface, often for decorating. A low to moderate plasticity clay was the most widely used material throughout the Americas. It is durable if protected from wetting.

When the masonry units were so irregular that thick mortar was required, shrinkage became a problem. Pebbles and stone chips were forced in the mortar joint to steady the stones, reduce the mortar volume, and minimize shrinkage. This practice was widespread in the United States southwest and in Meso-America.

In the United States southwest, caliche, a calcaerous silt or clay, is abundant near the ground surface and has been employed for mortar probably because of availability. It has the property of hardening somewhat, in alternating damp-and-dry conditions, and becoming slightly water resistant.

FIG. 11.—Composite Masonry Wall with Rubble Core, Uxmal, Yucatan, Mexico

The Mayans discovered that burned limestone would reharden slowly into soft rock upon wetting and subsequent exposure to air. Lime was produced by burning limestone fragments on firewood racks (20). The mortar was a mixture of lime, limestone dust, soil (if abundant), and probably volcanic ash. Although the Egyptians and Persians used gypsum mortar, lime mortar apparently did not appear in the Old World until a few hundred years B.C. The Mayans used it possibly as early as 500 B.C. for masonry construction as well as plaster.

Composite Construction.—The Mayans made extensive use of massive composite wall construction. The interior of the wall was coarse, rubble masonry, cemented with clay or lime mortar and chips of stone into a homogeneous mass. A veneer of stone masonry, precisely fitted and coursed, covered the surface, providing the illusion of a masonry block wall (Fig. 11). The practice can be seen in early structures at Tikal, about 200 B.C. and some of the latest

at Chichen Itza and Uxmal, 1200 A.D. to 1400 A.D.

Wattle and Daub.—Wattle and daub is a form of reinforced adobe or a wood-soil-plaster composite. The reinforcement is a grid of wood poles 5 cm–10 cm (2 in.–4 in.) diam spaced 1 m–2 m (3 ft–7 ft) apart. Between them is an open matting or wattle made of parallel (but sometimes loosely woven) reeds or thin poles 1 cm–2 cm or (3/8 in.–3/4 in.) diam, 1 diam or 2 diam apart. Low plasticity clay mortar is applied to both sides to form a wall 8 cm–15 cm or (3 in.–6 in.) thick. Such a contemporary house in Yucatan is seen in Fig. 12. The deteriorating clay daub exposes the underlying wattle. The age of this form can be judged from its representations, in a Mayan carving on a structure named the "Nunnery" (although its use is not known) of Uxmal. Similar houses can be seen today throughout the Mayan areas, in other parts

FIG. 12.—Wattle and Daub House, near Chichen Itza, Yucatan

of Meso-America (and in Kenya and adjacent areas of East Africa).

Retaining Walls.—Retaining walls served two purposes in the pre-Columbian Americas: (1) Agricultural terraces; and (2) support of steep slopes. The civilizations of the Andes Highlands of Bolivia and Peru built extensive terrace walls to make level land on steep slopes and to conserve runoff. Most were of untrimmed, small boulders laid in crude courses (Fig. 13).

Walls to support steep slopes were a part of the structures of Monte Alban in Mexico and Mayan Copan in Honduras. They appear to be incidental to the structures to which they are attached and not built specifically for retaining.

Pueblo Bonito, Chaco Canyon, N.M., is built at the toe of a sandstone cliff. Soft shaley layers near the base of the cliff were weathering and eroding, allowing the massive sandstone above to tilt outward from a vertical joint crack (Fig. 14). The pueblo builders constructed a wall at the toe of the cliff to retain

the weathering rock and to prevent further deterioration, probably about 1000 A.D. For more than 800 yr it functioned. In 1941 the cliff collapsed demolishing the wall and a portion of the pueblo.

Foundations

Foundations in the Americas were usually simple. Although the bottom of a high masonry wall was sometimes wider than the top, there was no enlarging of the base in contact with the ground to make a footing. At the sites of the larger Mayan and Mexican structures, rock was usually shallow; therefore, foundation bearing was no problem. The same is probably true of the western South American structures; however, foundations are not mentioned in archeo-

FIG. 13.—Inca Agricultural Terrace, Abandoned 400 yr Ago but Still Intact, Machu Pichu, Peru

logical reports. Some of the precisely fitted Inca masonry walls rest on crudely laid rubble below the ancient ground level. This suggests that a trench was dug, filled with stones, and the wall placed on top. The trench width and depth, however, are not significantly greater than the wall thickness.

Wood columns in most North American construction were placed in holes about 1 m deep, and backfilled with soil to provide lateral support during construction and (probably without intent) some vertical support for the eventual load. Stone columns of the Mayans and Mixtecs usually sat on the stone platform of the temple complex; separate foundations were not required.

The Pueblo Indians in the vicinity of Chaco Canyon, N.M. used prefabricated stone disks at the bases of the columns for the Great Kivas. Three or four, about 1 m diam and 4 cm thick, were stacked like pancakes under each column.

Wood piles served as both foundations and unsupported columns in areas of wet soil. The Spanish explorers found Indians in Lake Maricaibo on the north coast of South America living in pile-supported houses over the water. They named the area Venezuela: "Little Venice." There are similar pile supported houses in the area today; the only change is the substitution of wood-plank siding and corrugated iron roofs for the indigeneous pole and thatch.

Similar wood pile supports were used in the Valley of Mexico where the Aztecs built Tenochtitlan, the first Mexico City, in a marshy arm of Lake Texcoco (14). Excavations for modern construction have uncovered wood pile foundations for houses, and to retain soil fill for roadways. Although there are no records of how the piles were driven, the writer observed men driving wood piles in the loose sands at Acapulco, Mexico in 1940, Fig. 15. They raised a wood hammer about 25 cm (10 in.) diam and 60 cm (2 ft) long, by

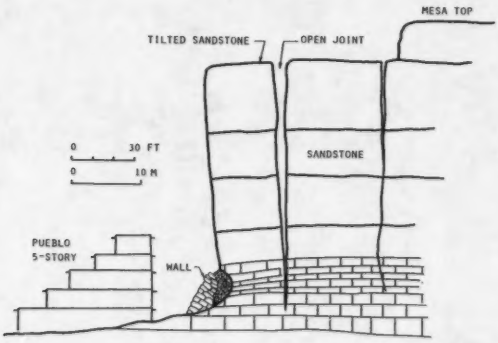

FIG. 14.—Retaining and Erosion Prevention Wall Pueblo Bonito, Chaco Canyon, New Mexico

handles, and dropped it about 60 cm on top of the 10 cm diam wood pole while standing on a wood platform fastened to previously driven piles.

Transportation Routes

Transport of people and commodities developed late in the pre-Columbian Americas. There is evidence of loosely organized trade in the finding of native copper in mounds in Georgia, which probably came from the only known source in Michigan, far away.

Similar trade in mica and flint between different areas of the eastern United States is inferred from grave artifacts. The trade routes, which were also used by the early European explorers, were water courses and loose networks of foot paths, 0.6 m wide, which probably evolved from hunting trails. There was little need for more. The only beasts of burden were men, women, and occasionally dogs. The largest boats were only canoes or rafts. In the Andes of South America, the llama, a mini-camel, still carries loads of about 50 kg (100 lb) but has never pulled a load. Coastal ocean commerce developed late,

primarily in the Yucatan area and to a small extent along the North Pacific Coast of the United States and Canada.

Surprisingly, systems of wider "highways" are found in many areas. Because these routes focus on major settlements and religious centers, archeologists speculate that they were required for processions or perhaps for armies moving in compact units.

The best known are the Inca roads in Peru and Ecuador (22,23). One 5,400 km or 3,200 miles long followed the high valleys in the Andes, from the administrative capital at Cuzco, Peru northward into Ecuador and southward into Chile. A second road followed the coast linking the irrigated valley civilizations across the sandy deserts. They were connected by east-west roads. In the plains they were merely trampled paths, marked by rows of stones 3

FIG. 15.—Pile Driving by Hand, Acapulco, Mexico, 1949

m–6 m apart, and swept clean of sand regularly. The roads were essentially straight, up and down the mountainsides, and across streams 5 m–7 m (16 ft–23 ft) wide. In the mountains they included causeways across low wet areas, retaining walls, paving, stone stairways up steep slopes (Fig. 16) and parallel marker stones. Suspension bridges spanned narrow canyons and tunnels pierced steep obstructions. At intervals of 7.5 km (4.5 miles) there were distance markers. Relay stations were built 2.5 km (1.5 miles) apart for messengers who ran the interval, passed messages and perishable food to the next runner, and then rested. At larger intervals, about a one day walk or 20 km–30 km (12 miles–18 miles), there were rest stations for official travelers and supply warehouses for small military parties. Possibly the litter parties that carried the nobility and their military escorts determined the road width. There were no vehicles and only occasional llama pack trains. Parts of the Inca road system are still

in use, while others lie in disuse because of the steepness of the pathways or because they are lost under the desert sands.

The Mayans likewise had an extensive road system called "Sacboebs" connecting many of their cities and religious centers (Fig. 6). Many can be traced today as lines of different growth in the jungles of Guatemala and the scrubby forests of Yucatan. The ground surface in much of the Mayan area is extremely rough, deeply pitted from the solution of the soft limestone, making cross country travel difficult. Causeways 8 m–10 m (25 ft–33 ft) wide were constructed with level surfaces and in straight lines.

The causeways were built of small limestone boulders, topped with limestone chips and limestone sand to form a smooth surface, anticipating the ideas of McAdam, the Scottish engineer, centuries later and an ocean apart. A stone

FIG. 16.—Inca Road near Machu Pichu, Peru

cylinder, 4 m long and 0.65 m (13 ft × 2 ft) diam weighing 5 ton, found adjacent to a road suggested a roller to Mexican geotechnical engineers (18). They found that 15 men could easily push it across freshly placed stones and compact the surface. (Some archeologists are skeptical of this explanation of the stone's use.) Most of the causeways have become overgrown with vegetation after centuries of disuse. A few sections have been restored by the Mexican Highway engineers; it is likely that many others remain to be discovered.

Archeologists of the United States National Park Service, studying air photographs of Chaco Canyon, N.M., for prehistoric irrigation channels, were surprised by faint linear features radiating from some of the ancient pueblos (5). The lines go straight across topographic features but are best defined on the uplands and mesas (Fig. 17). They were located on the ground and found to be cleared pathways 6 m–9 m (22 ft–30 ft) wide. Across bed rock, they were defined

by lines of cobble stones, and in some cases by leveling of high points in the rock. Some terminated in staircases down the cliffs. Across sandy ground the pathway was a shallow excavation. Despite seven centuries of neglect, these pathways or "roads" are still evident (Fig. 18). Their use is not known; archeologists speculate that they were paths from the cultivated fields and springs to the pueblos.

Although much of the transport of people and commodities into the Aztec Capital of Tenochtitlan was by canoe, there were major causeways across the

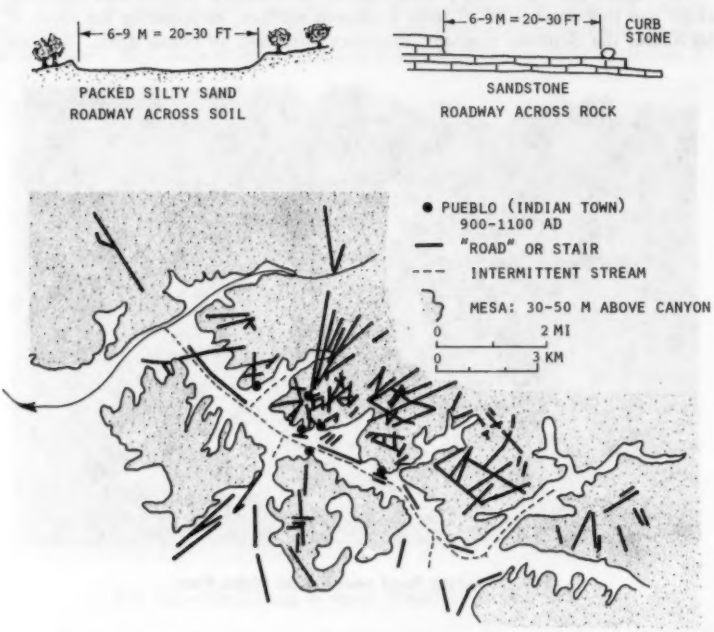

FIG. 17.—Road or Pathway System, Chaco Canyon, New Mexico (5)

marshes connecting it with the mainland (Fig. 19). Closely spaced pole piles formed parallel retaining walls (Fig. 20). Possibly reeds or canes were interwoven with the piles to produce a tighter wall with fewer piles. Earth fill from the adjacent marsh was placed between the pile walls forming an earth causeway with a canal for canoes on each side. There were occasional openings in the causeways to allow water circulation and passageway for boats. According to the Spanish conquerors, these were bridged with timbers which could be removed for military defense (4). Cortes, his soldiers, and Indian allies were nearly trapped by the Aztecs who opened the bridges during his first sortie into the city.

Water and Soil Management

Water and soil for agriculture are twin essentials to community living. In many regions of the Americas, highly seasonal rainfall was unfavorable to continuous settlement and agriculture. In coastal Peru, where the sea was a source of food, lack of any rain made life nearly impossible. In mountainous areas, steep slopes eroded and slumped when the permanent vegetation was destroyed by farming. Despite shortcomings of climate, some of the most advanced civilizations in the Americas developed in such areas. Water and soil management were the keys to their success.

Terracing, in steep terrain, with the aid of low rubble walls, retained both soil and runoff. There are remains of such rudimentary terraces in the south-

FIG. 18.—Chaco Canyon Road or Path across Sandstone Mesa

western United States, some possibly 2000 years old. In the Tehuacan Valley, southeast of Mexico City, terraces have been found in cultures dating from 900 B.C.

In South America, terracing in the Andean highlands and in coastal settlements probably began about 500 B.C. (11,23). Because of the continuity of community life in the Andean highlands, the terrace systems were improved and enlarged until the end of the Inca empire in the sixteenth century. There are many that remain in use today. Many others are in good physical condition despite four centuries of neglect, such as at Machu Pichu (Fig. 13). Others have crumbled; their remains are a testimony to better water and soil management than is practiced today in the same region. The terraces in some areas are as high as 2 m or 6 ft constructed on slopes typically 20°–30° or 2.7(H)–1(V)–1.7(H)–1(V) but occasionally steeper than 1–1 (Fig. 13). The rubble walls at Machu Pichu were

backfilled with soil, plus a filtered underdrain of sand over gravel to prevent soil saturation (and also to prevent hydrostatic pressure from overturning the wall) (15). Unfortunately, the technical knowledge and the political system that made it possible to build and maintain these terraces were destroyed by the European conquerors.

Water Diversion Canals.—Diversion of water from streams and springs to farm lands, and to terraces by canals or ditches, represents a logical step beyond terracing. Unlined ditches have been found in the southwest United States built by the Hohokum nearly 2,000 years ago (9). The builders diverted streams

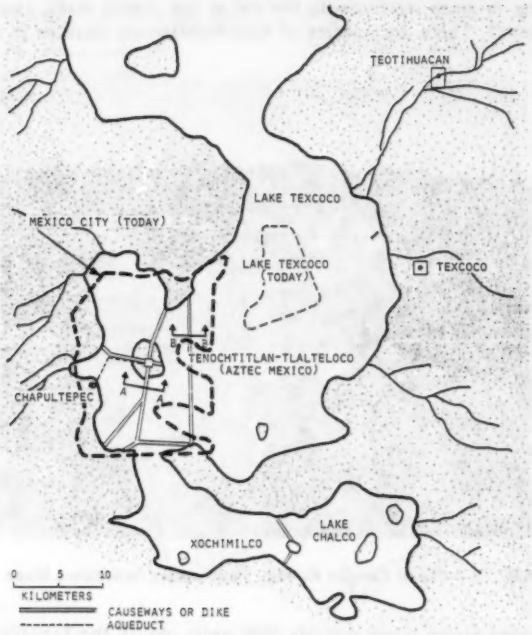

FIG. 19.—Causeways and Dike, Aztec Tenochtitlan (Mexico City), Mexico

using temporary dams of woven fiber matting supported by short poles driven into the stream bed. In Chaco Canyon, N.M., there are stone rubble structures built in dry gullies to divert thunderstorm runoff into cultivated fields (24).

In Coastal Peru, where there is no rainfall, agriculture 2,500 years ago depended on diverting water from the rivers which flowed from the mountains into the flat terraces alongside the arid flood plain. In the Andean highlands with seasonal rainfall, multiple use was made of the occasional dry weather springs. The water was collected in masonry channels, diverted first to fountains, and baths, and then into trenches leading to terraced fields (Fig. 21).

The Hierve el Agua Spring, about 20 km east of Milta in Mexico's Oaxaca Valley, is a combination terrace and canal system (Fig. 22) (7). Warm water, rich in magnesium and calcium bicarbonates, flows from several small springs on a steep hillside. The carbon dioxide is released in the air, precipitating the minerals as travertine, a soft limestone. Ordinarily, alkaline waters cannot be used for irrigation because the minerals inhibit plant growth. At this site the builders constructed an elaborate system of minicanals using the precipitating travertine (Fig. 23). The lengthy network prolonged the air exposure, enhanced precipitation, and reduced the mineral content. When the travertine built up, the soft deposits were recut forming new channels on top of the old. Today, more than 2,000 years after the system was begun, the minicanals are perched on travertine ridges 1/2 m–1 m high and 1/4 m–1/2 m wide. These ridges also help form terraces on the steep hillside (Fig. 24). At intervals along the terrace-canals there are pot-like enlargements. The archeologists believe that the water was handdipped from these to water the plants on the terraces (7). Other small canals with small cisterns for dipping water are found throughout ancient Mexico; some were derived from springs or small streams but a few utilized shallow well water.

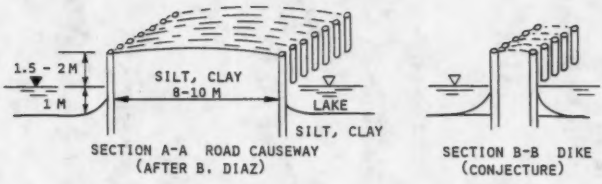

FIG. 20.—Cross Section of Road Causeways and Dikes of Tenochtitlan (4)

Water Storage.—In the Southeastern Gulf Coast of Mexico, the lowlands of Belize and Guatemala and the Yucatan Peninsula, there is little stream flow despite abundant rainfall. The runoff disappears into cavities in the soft, porous limestone. The occasional large open sinkholes, or cenotes, were the only natural source of water. These became the focal points for many Mayan Temple cities. The large cenote of Chichen-Itza, Yucatan was a sacred well. When the ground-water level dropped during dry weather, jewelry and sometimes humans were sacrificed into it to bring the water back.

At other Mayan Temple cities artifical reservoirs were constructed in the limestone to store surface runoff. Some were probably old solution pits in the rock, others were carved in the soft limestone. The pores of the rock were sealed with lime-limestone dust mortar and occasionally clay. Some at Uxmal and Sayil were covered to vinimize evaporation and included paved rainfall catchments (Fig. 25). At Tikal, there were a number of open reservoirs with areas of 1,000 m^2–10,000 m^2 and 2 m–5 m deep.

The "Mummy Lake" in Mesa Verde, Fig. 26(*a*) and 26(*b*), is a combination masonry and earth-storage reservoir in a runoff-collecting system on the sandstone mesa top. Storm water was diverted into it by blocking the collector ditch, which also fed water to small agricultural terraces (19).

Drain Systems.—Surface water drainage systems were incorporated in many of the temple city complexes of Meso-America and in the Andean Highlands where locally intense rainfall could accumulate on impervious masonry surfaces.

At Copan, Honduras, and Monte Alban, Oaxaca, Mexico, there are extensive stone-slab culvert systems, draining to nearby gullies and streams (13). Grooved stone bars were used as runoff channels at Copan. Similar grooved stone water conduits can be seen on the Andean highlands. It is possible that matching bars were joined to form closed water pipes.

There is some speculation that the stone drains of Monte Alban were also used for drainage of human waste. If so, they probably accummulated decomposing solids during periods of low rainfall because there are no springs on the mountain top and rainfall is highly seasonal.

FIG. 21.—Spring, Baths, and Water Diversion System at Tambumachy, Cuzco, Peru

At Dainzu, Southeast of Oaxaca, Mexico, there are extensive conduit systems of grooved stones and stone slab culverts. There are also burned clay pipes about 10 cm OD (Fig. 27). They brought spring water into the temple complex from a hill above.

A ribald sense of humor can be seen in roof drains for a temple in "Old Chichen," a part of Chichen Itza. The roof downspouts are in the form of a penis; when it rains, they discharge in a realistic manner.

Valley of Mexico.—The valley of Mexico (Fig. 19) was once occupied by a shallow lake between the surrounding volcanos. The early inhabitants excavated canals in the marshy lake margins and piled the excavated peaty, silty clays between to form low rectangular artifical island called *chinimpas* (14). Several crops per year were possible in the warm sunshine with the organic soils and their adjacent source of water. Human wastes were collected from nearby

settlements to enhance the natural fertility. The present "Floating Gardens of Xochimilco" (the remnant of an ancient south arm of the lake) still produce flowers and vegetables, although they are now mostly a tourist attraction.

The Aztec capital of Tenochtitlan (now Mexico City) in the western marshes of Lake Texcoco was an adaptation of the chinimpas (plus some older islands) to urban development. The island city was connected to the mainland by causeways (Figs. 19 and 20). Lake Texcoco was becoming saline because it had no outlet. The causeway isolated the western part of the lake, with its large fresh water inflow from springs and streams compared with its surface area from which water evaporated. By limiting the area of the cross-canal links to the more saline larger eastern area of the lake, the Aztecs were able to maintain freshwater around the city.

FIG. 22.—Hierva el Agua Canal and Terrace System Near Oaxaca, Mexico

Windstorms generated sufficient waves and water pileup on the main lake that the causeways were overtopped and parts of the Aztec City flooded on a few occasions. Shortly before Cortez's conquest, the Aztecs constructed an outer dike for the sole purpose of protecting the city and causeways from flood damage and salt-water contamination. Today, modern Mexico covers much of the old causeway and water control system, and Lake Texcoco has shrunk to a shallow salt pond.

Significance of Pre-Columbian Construction

The pre-Columbian civil works, with their unusual variety and size, are a tribute to those ancient engineers who conceived their designs and supervised their construction. The civilizations are dormant and the names of those

responsible for these achievements are lost. However, when these works are evaluated by modern standards, many are examples of what is good in engineering.

The first test of the value of engineering is its contribution to society's primary physical needs, i.e., shelter, water, food, communication, and defense. Enough examples of engineering works that meet each need remain unswallowed by jungle or unmelted by weather to demonstrate that they rival comparable structures of Europe and the Middle East of 2,500 yr–1,000 yr ago. As will be considered later, the works of the Americas exhibit neither the evolutionary growth of technology from one location to another nor the development with passing time that can be seen in the Old World (although this conclusion may be partially blamed on less archeologic study).

Structures that expose man's religious and spiritual feelings also fulfill a fundamental need. In size and grandeur the temples and pyramids of the Americans compare with those of the Egyptians, Babylonians, and Assyrians. In construction, they are more advanced, with their composite masonry core and fitted mosaic casings.

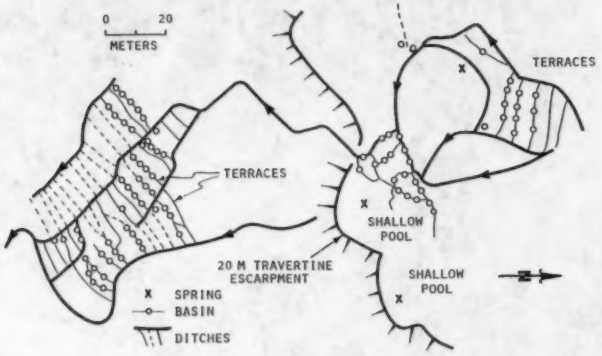

FIG. 23.—Plan of Hierva el Agua Canal and Terrace System (7)

A third test of technology is the adaptation to available materials. In this the pre-Columbian Americans excelled. Because long, heavy timber was scarce in the Andean highlands, the Valley of Mexico, Yucatan, and the arid southwestern United States, local stones and soil were exploited. As today, the soil was dirt cheap—a versatile, strong, durable material if handled correctly, a pile of mud if not. Even a child knows this instinctively and empirically; some modern engineers have forgotten it.

Soil was made into walls, and was used for the mortar for walls of stone, and the plaster that smoothed the surfaces. Reinforced with sticks and reeds, it became floors, roofs, and the walls of huts in areas where soil was too scarce for adobe block construction, or where moisture softened the blocks.

The geotechnical engineer can find a deeper meaning in this use of simple earthy materials. Many religions teach that man becomes a part of the earth when he dies, therefore, he must be made of earth. The ceremonial underground

pit or kiva of the Southwest Indian, is thought to represent the womb of the earth from which man springs. The civilized child sometimes finds comfort in a close space among rocks, a shallow pit in the ground, or a dark corner of a room. The earth, or rock mound that supports a temple, reflects man's (and all life's) dependence on the earth. The pit grave and the burial mound signify his return on death.

Thus, the geotechnical engineer can feel that he is working with something more fundamental than a mere construction material—he builds with life itself!

FIG. 24.—Detail of Raised Minicanal Constructed of Travertine

Unfortunately to some modern engineers, soil has a dirty connotation. However, to the Geotechnical Specialist, soil is a primary material for construction and dirt is something swept off the floor, or which he washes from his child's face.

The final test of technology is its ingenuity in transmitting an idea into a reality. The civilization of the Western world was born in Asia and Africa and matured in Europe and the post-Columbian Americas. The initial development

of technology was slow, with similar ideas emerging in widely spaced localities. Writing fostered the long distance communication of ideas and transmission of knowledge from one generation to the next. After the development of writing, technology developed at a rapidly increasing rate through the synergism of independent (nuclear) technologies.

Development in the Americas was different. Man appeared only recently, compared to Africa and Asia, as recently as 12,000 years (or perhaps as long as 50,000 years ago). The settlements were dispersed and their life was dependent on hunting and food gathering. Primitive technologies arose spontaneously in widely separate areas, about 3,000 years ago, much later than in the Old World. However, they evolved at least as rapidly as those in the Old World during comparable time spans.

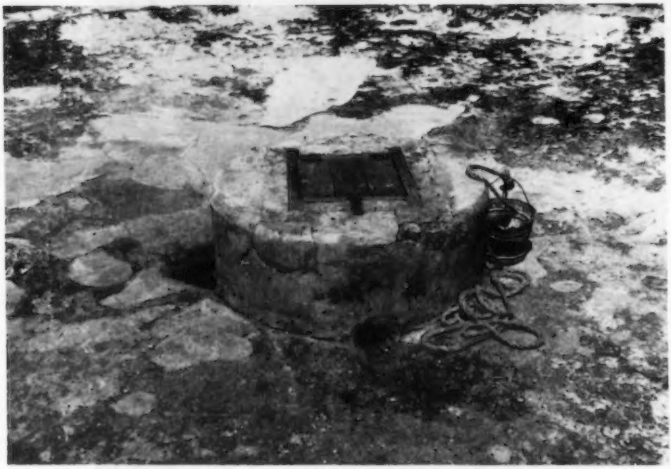

FIG. 25.—Paved Rainfall Catchment 10 m diam above Cistern, Sayil, Yucatan, Mexico

There were also other major differences in the development in the Americas. The lack of a logic system and mathematical computation inhibited an orderly understanding of the mechanics of technology. The lack of written language inhibited the synergism between geographically isolated areas as well as the transmission of technology to succeeding generations.

With these differences between the Old and New Worlds, many historians have speculated on the origin of the technologies that produced the ingenious works that are being uncovered.

Old World Contacts.—There were legends of both the Incas in Peru and the Aztecs in Mexico that describe bearded, light-skinned gods landing from large ships. However, the stories were embellished with such fanciful details that they could be entirely imaginary. There are a few scattered finds of pre-Columbian European artifacts. Recent small-craft crossings of the Atlantic

demonstrate that skilled seamen, such as the Phoenicians, could have crossed to the Americas, probably because of bad navigation. The chances of a safe return were small, which would explain no records of such voyages. There are fragmentary stories of Norse expeditions to "Vineland" but conflicting evidence of its location. Certainly there are no records of major expeditions that might have brought Old World skills to the Americas.

The evidence of comparative technology is also weak. There are some similarities, e.g., weaving, burned clay pottery, adobe, and pyramids. However, a detailed comparison shows that the similarities are superficial. The American stone pyramids are far steeper than those of the Old World. Most were built box-in-box and of rubble with only a veneer of faced stone. Their primary use was in religious ceremonies; burial was secondary.

Some of the most important Old World advances are absent such as the wheel and metallurgy (except for Western South America, remote from Atlantic

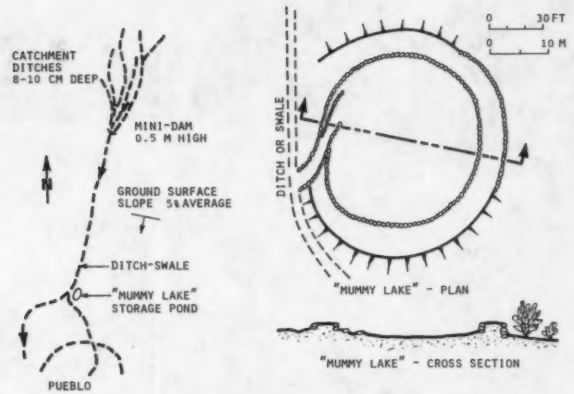

FIG. 26(*a*).—Plan and Cross Section, Mummy Lake Reservoir, Mesa Verde, Southwest Colorado (19)

crossings). Most important, there was neither a system of logic nor written communication. By way of contrast, there are some New World ideas that may have predated those in the Old, e.g., lime mortar and composite masonry using a rubble core with only a thin facing of finished stone work.

The absence of Old World diseases, such as smallpox, in the Americas before Columbus is also evidence of little or no communication. Large segments of the indigenous people were wiped out by Old World infections after contact with the early explorers.

The available evidence suggests that although contact was possible, there was no significant transfer of technology from the Old World to the New.

Creatures from Space.—The idea of extraterrestrial communication is intriguing, but entirely lacking in evidence. *The Chariots of the Gods* strains at comparing the weird stylized costumes of the Mayan gods with the modern space suit

and suggesting that the Nazca lines were landing fields for space craft. We can understand the ancient Hebrews explaining still older megalith construction (lavstones) by stating, "There were giants in the earth in those days." There is little excuse for such a viewpoint today (21).

The extraterrestial hypothesis as voiced by Von Daniken is developed by a logic of elimination: (1) the huge structures built today are the product of modern technology; (2) the ancient people possessed no such technology; (3) they did build some extraordinary structures; and (4) because they had no modern technology, they must have received supernatural help.

This conclusion is based on the unstated assumption that the ancients could not have contrived an innovative, admittedly primitive technology to produce their structures. It is a form of intellectual snobbery that cannot admit the

FIG. 26(*b*).—Mummy Lake Dike, Mesa Verde, Southwest Colorado

potential for achievement without the tools and gadgets which we now possess.

Indigenous Ingenuity.—The alternative to the hypotheses of Old World influence and extraterrestial intervention for the New World construction achievements is indigenous ingenuity. The word "engineer" is derived from ingenious, the capacity to contrive something new. It is related to genie, the mythical being with magic powers to create. Confronted with a problem, the engineer (the ingenious one) contrives a plan to transform the available materials into a solution. The plan becomes a reality through the organization of labor.

The available evidence supports this hypothesis. Each of the widely separated pre-Columbian civilizations exhibited a logical technical evolution within its geographic nucleus. The problems were common among the different civilizations. However, each evolution was somewhat different, reflecting different materials and different ideas, e.g., the Maya built their temple bases of limestone rubble

bonded with lime mortar and cased with cut stone; the Mexicans at Cholula used volcanic stones in a soil-volcanic ash matrix; and the peoples of the Andean highlands fitted large stones together.

Although there were rapid technological developments between 2,500 and 500 years ago, many were forgotten before the Old World conquest. Moreover, the technology of one nuclear civilization did not appear to influence that of its near neighbors. Each invented its own, more or less independently. When a society deteriorated, its technology was largely forgotten. The lack of an effective means of recording and transmitting ideas was a major deficiency of the pre-Columbian Americas. In my opinion, this loss confirms the indigenous nature of their origin.

For Today.—A study of the past is of greatest value in its message to the

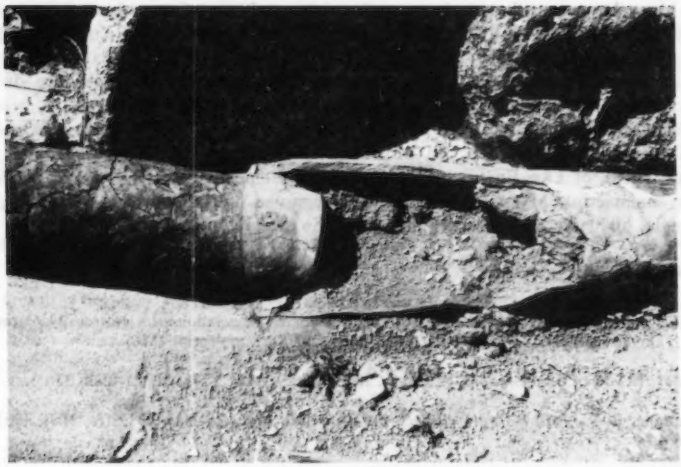

FIG. 27.—Drain Pipe, 10 cm OD, Dainzu, Oaxaca, Mexico

present and future. To the geotechnical engineer, our pre-Columbian heritage can reinforce our dedication to the earth. The Western Indians revered it as their mother or grandmother, the Judeo-Christian tradition maintains that we were created from it, our childish instinct is to play in it, and as engineers, we build with it. Thus, our work with the earth as a raw material and a foundation for our creations is more fundamental than child's play or an intellectual exercise for the laboratory.

The arrested development of pre-Columbian technology is a warning that communication and interchange of ideas is vital to development. Concepts that remain within a nuclear society eventually die with it. We continue to waste effort in "reinventing the wheel."

Finally, these achievements remind us that the most important factor in achievement is man's innate ingenuity—the essence of engineering. Modern

technology has enabled us to build bigger, faster, and even better. However, the complexity and beauty of our scientific tools causes some of us to fall in love with them instead of their use. The past remains us that man has produced magnificently with little except his ingenuity and labor.

The ancient Hebrews were closer to the truth than they realized when they conclude, "There were Giants on the Earth in Those Days." There were giants of ingenuity, fulfilling their potential.

Karl Terzaghi was such a giant. He generated new ideas 50 years ago that have transformed engineering. We can express this ingenuity if we aren't seduced by our own tools. We too can be giants, and society will be the better.

Acknowledgments

Many have contributed observations, data, and ideas from which this paper has been compiled. Particularly, R. E. Gray, F. ASCE, G.A.I., A. Rico Rodriguez, Departmento Geotechnica, S.O.P. Mexico, T. Lyons, Chaco Research Center, New Mexico, and R. G. Vivian, Arizona State Museum made obscure data available and provided personal insights. Warren Bennet conducted a brief demonstration on desert varnish on the Mojave Desert, Calif. Teresa Groves, Librarian, Marlene Barnes, and Chris Shattuck, secretaries and Robert Alexander, Draftsman, of Law Engineering provided the technical assistance for preparing the manuscript. My wife, Frances, accompanied and encouraged me through jungle, highland, and desert in pursuit of the elusive ancients.

Appendix I.—Bibliography

deLanda, D., *Yucatan before and after the Conquest,* Translation with Notes, W. Gates, ed., Dover Publications, Inc., New York, N.Y., 1978, (Manuscript 1566).

Innes, H., *The Conquistadors,* Alfred A. Knopf, Inc., New York, N.Y., 1969, 336 p.

Lanning, E. P., *Peru before the Incas,* Prentice-Hall, Inc., Englewood Cliffs, N.J., 1967, 216 p.

Spiden, H. J., *A Study of Mayan Art,* Dover Publications, New York, N.Y., 1975, 285 p. (originally *Memoirs,* Vol. 6, Peabody Museum of American Archeology and Ethnology, Harvard University, Cambridge, Mass., 1913).

Appendix II.—References

1. Adams, et al., *Tikal Reports 5–10,* University Museum, University of Pennsylvania, Philadelphia, Pa., 1961.
2. Coe, W. R., *Tikal: A Handbook of the Ancient Mayan Ruins,* University Museum, University of Pennsylvania, Philadelphia, Pa., 1967, p. 124.
3. Von Daniken, E., *Chariots of the Gods,* Putnam's G. P. and Sons, New York, N.Y., 1969.
4. Diaz, B., *Conquest of New Spain,* Translated from Spanish by J. M. Cohen, 1963, Penguin Books, Harmondsworth, Middlesex, England, 1963, (Manuscript 1576).
5. Ebert, J. I., and Hitchcock, R. K., "Chaco Canyon's Mysterious Highways," *Horizon,* Autumn, 1975, p. 49.
6. Erasmus, C. J., "Monument Buildings, Some Field Experiments," *Southwestern Journal of Anthropology,* Vol. 21, No. 4, 1965, pp. 277–299.
7. Flannery, K. V., and Kirkby, A. T., "The Use of Land and Water Resources in

the Past and Present Valley of Oaxaca, Mexico," *Memoirs of the Museum of Anthropology*, Vol. 1, No. 5, University of Michigan, Ann Arbor, Mich., 1973.
8. Genesis 6:4.
9. Haury, E. W., "The Hohokum," *National Geographic*, May, 1967, pp. 670–696.
10. de LaVega, G., *The Incas, Royal Commentaries*, Translated by Jolas, Discus-Avon-Prion Press, New York, N.Y., 1961, (Manuscript 1610–1616).
11. Mason, J. A., *The Ancient Civilizations of Peru*, Penguin Books, Baltimore, Md., 1961.
12. McIntyre, L., "Mystery of the Ancient Nazca Lines," *National Geographic*, May, 1975, pp. 716–728.
13. Paddock, J. ed., *Ancient Oaxaca*, Stanford University Press, Stanford, Calif., 1966, p. 36.
14. Peterson, F. A., *Ancient Mexico*, Putnam's G. P. and Sons, New York, N.Y.
15. Polo, N., *Macu Picu*, Editorial de Cultura Andina, Cuzco, pp. 279–298.
16. Reed, N. A., Benett, J. W., and Porter, J. W., "Solid Core Drilling of Monks Mound: Technique and Findings," *American Antiquity*, Vol. 33, Apr., 1968, pp. 137–148.
17. Reiche, M., *Mystery on the Desert*, Nazca, Peru.
18. Rico, R. A., and Castillo, H. Del, *La Ingenieria de Suelos en las Vias Terrestres*, Vol. 1, Editorial Limuasa, S. A. Mexico, 1974, p. 134.
19. Roh, A. H., "Prehistoric Soil and Water Conservation on Chapin Mesa, Southwestern Colorado," *American Antiquity* Vol. 28, No. 4, Apr., 1963, pp. 441–455.
20. Stierlin, H., *Mayan Architecture*, Office Du Livre, Fribourg, Switzerland, 1964.
21. Thiering, B., and Castle, E., et al., *Some Trust in Chariots*, Popular Library, New York, N.Y., 1972.
22. Von Hagen, V. W., *Highway of the Sun*, Revised Edition, Plata Publishing Co., Ltd., Chur, Switzerland, 1975.
23. Von Hagen, V. W., *Realm of the Incas*, 2nd ed., Mentor Books, New York, N.Y., 1961.
24. Vivian, R. G., "Prehistoric Water Conservation in Chaco Canyon," *Final Report, National Science Foundation Grant GS 3100*, Arizona State Museum, Tucson, Ariz., 1972.
25. Wilcox, T. R., and Schenk, L. O., *The Architecture of Casa Grande and its Interpretation*, Archeological Series 115, Arizona State Museum, Tucson, Ariz., 1977.

JOURNAL OF THE GEOTECHNICAL ENGINEERING DIVISION

EFFECT OF WETTING AND DRYING ON SHEAR STRENGTH

By Mehter Mohamed Allam[1] and Asuri Sridharan[2]

INTRODUCTION

The earth cover in tropical and semitropical regions undergoes large fluctuations in its water content as the seasons change. Literature suggest that such changes both lead to degradation of the parent rock to form soil, and result in the aggregation of soil particles and in interparticle bonding which can impart an intrinsic effective stress to the natural soil. The study reported herein was conceived to examine to what extent the shear strength properties of a disturbed natural soil are affected when it is subjected to repeated wetting and drying.

LITERATURE REVIEW

The soils in large parts of the earth's land surface are partially saturated to considerable depths and are known as desiccated soils. These soils are subjected to repeated wetting and drying as a result of climatic changes. In arid areas with deep water tables, soil humidities are controlled by atmospheric humidities to depths of 20 ft (6 m) or more (17). Changes in color and arid soluble constituents and the gain and loss of other constituents can occur as a result of climatic changes (14). The action of water on the soil consists of solution, hydrolysis, and decomposition of the soil compounds (6,8). It has been reported (1) that alternate wetting and drying, resulting in the buildup and breakdown of soil granules, is partly responsible for a continuous increase in the percentage of water stable aggregates. The extent to which discrete or elementary, nonaggregated soil particles are grouped to form larger, more or less stable aggregates is a function of several factors such as the grain size distribution, amount of

[1]Asst. Prof., Dept. of Civ. Engrg., Islamiah Inst. of Tech., Bangalore, India.
[2]Assoc. Prof., Dept. of Civ. Engrg., Indian Inst. of Science, Bangalore 560012, India.

Note.—Discussion open until September 1, 1981. To extend the closing date one month, a written request must be filed with the Manager of Technical and Professional Publications, ASCE. Manuscript was submitted for review for possible publication on January 10, 1980. This paper is part of the Journal of the Geotechnical Engineering Division, Proceedings of the American Society of Civil Engineers, ©ASCE, Vol. 107, No. GT4, April, 1981. ISSN 0093-6405/81/0004-0421/$01.00.

clay, type of clay minerals present, nature of the saturating cation populations, and presence and solubility of excess entities as well as organic decomposition and organic cementing agents (3,9,26).

Several ways, including wetting and drying, have also been reported (13) by which individual soil particles can become more or less permanently linked together and in effect grow into large particles. Chemical attack by suitable reagents on the majority of soil components is capable of producing covalently bonded, macrolatticed compounds possessing considerable potential strength, and under suitable conditions this can be achieved by alternate wetting and drying cycles (10). Repeated wetting and drying of some soils can result in increased strength due to aluminum oxide bonds being generated in the initial states, and also due to the recrystallization of ferric oxide in the later stages (8). In certain cemented clays, Al, Fe, Mg, and Ca compounds act as cementing agents and influence their compressibility (11,15). Removal of these bonds by chemical treatment results in loss of the apparent preconsolidation pressure.

TABLE 1.—Chemical Composition of Natural Soil (Red Earth)

Chemical determination (1)	Amount present, as a percentage (2)
Silica (SiO_2)	60.18
Alumina (Al_2O_3)	19.59
Ferric Oxide (Fe_2O_3)	7.96
Titanium Oxide (Fe_2O_3)	0.65
Potassium Oxide (K_2O)	1.02
Sodium Oxide (Na_2O)	0.86
Magnesium Oxide (MgO)	0.58
Calcium Oxide (CaO)	0.56
Loss on ignition	8.36
Manganese Oxide (MnO)	0.09

It has been also reported that the effect of desiccation is similar to that of heavy overconsolidation (5).

From the available literature it can be concluded that repeated wetting and drying of a soil can generate bonding between particles which can influence its shear strength properties. This may be a source of the bonding present in desiccated soils (2,23). This paper investigates the effect of repeated wetting and drying on the shear strength behavior of a natural soil.

Experimental Work

For this study a disturbed sample of desiccated soil was taken from the yard of the Soil Mechanics Laboratory, Indian Institute of Science, Bangalore, India. This soil is locally described as Red Earth and its chemical composition is presented in Table 1. It can be classified as a nonlateritic soil on the basis of the criteria given by Martin and Doyne (4,6), as its silica to alumina ratio = 3.0. Its grain size distribution is shown in Fig. 1, and it is composed of about 70% sand, 25% silt, and 5% clay. Kaolinite is the dominant clay mineral

present, and the x-ray diffraction pattern for this soil is presented in Fig. 2. Its index properties are: liquid limit = 32.1%; plastic limit = 18.7%; shrinkage limit = 17.5%; and $G = 2.6$.

The oven dried (110° C) soil was sieved through BS Sieve No. 7 and statically compacted into cylindrical triaxial test specimens of 1-1/2 in. (38 mm) diam and 3 in. (76 mm) height in an apparatus (16) having a water content of 16% and a dry density of 1.79 g/cm^3. The water content of the specimens when fully saturated is 17.5% and is equal to the shrinkage limit of the soil. This dry density was selected so that drying would result in negligible shrinkage, if any, taking place.

The specimens thus prepared were allowed to first dry in air under controlled conditions, till there was no change in weight, before being dried in an oven for 24 h at a temperature of 110° C. At the end of this drying process, which constituted the first drying cycle, the specimens were cooled in air and arranged in trays lined with blotting paper and completely covered with fine sand which was then saturated with distilled water. The specimens, thus subjected to their

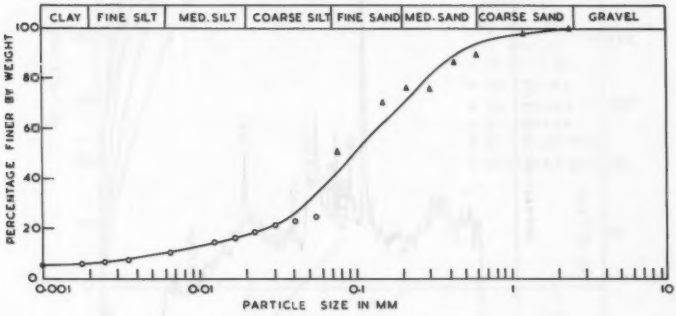

FIG. 1.—Grain Size Distribution of Red Earth

first rewetting cycle, absorbed moisture from the saturated sand surrounding them with little erosion taking place. After rewetting had taken place for 3 days, the specimens in the trays were placed in an oven and dried for 3 days at a temperature of 110° C. After cooling, rewetting was repeated in the manner previously described. Successive wetting and drying cycles were performed until some specimens had undergone as many as 59 rewetting cycles but had suffered negligible erosion and cracking.

Specimens were selected at random from the trays at the end of their 1st, 25th, 40th, 50th, and 60th drying cycle and were subjected to isotropically consolidated undrained shear tests in the conventional triaxial shear apparatus after being saturated. The saturation of the specimens was done in the triaxial apparatus itself in the following manner and constituted the 1st, 25th, 40th, 50th, and 60th rewetting cycle. The dry specimens were set up in the triaxial apparatus under an initial all-round pressure of 5 psi (34.5 kPa) and were allowed to imbibe deaired water from the top and bottom drainage lines for 24 h. Next, distilled deaired water was circulated upwards through the specimens for a

period of 48 h via the bottom drainage line at a pressure of 4 psi (27.6 kPa) to flush out trapped air in the specimens. Measurement of water content at the end of the shear tests indicated that this procedure resulted in a degree of saturation as high as 99.5% in the specimens. The specimens were then consolidated isotropically to the desired pressures and sheared with an axial strain rate of 0.08% per min, which was found adequate for the equalization of pore pressures mobilized during shearing.

Some specimens were treated with 250 ml of 0.2*N* EDTA (disodium salt of ethylene-diamine tetra acetic acid) solution after having undergone 50 and 60 rewetting cycles. The EDTA is a chemical that would remove carbonates,

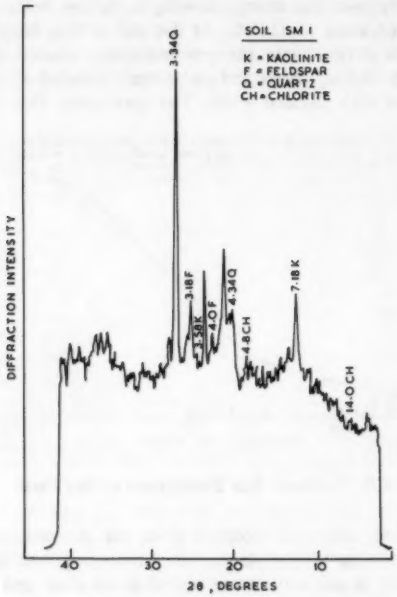

FIG. 2.—X-ray Diffraction Pattern for Red Earth

gypsum, and iron compounds, that is, it would remove materials that could act as particle cementing agents (11). The EDTA was circulated upwards through the specimens at a pressure of 4 psi (27.6 kPa). The spent solution, collected from the top drainage exit, was chemically analyzed. The specimens were next flushed with distilled deaired water prior to consolidation to the required pressures, and were sheared in the undrained condition.

For comparison purposes, some field saturated undisturbed triaxial test specimens of the same soil were extracted and subjected to isotropically consolidated undrained shear tests in the laboratory. Remolded specimens were also prepared from the same soil, taking care to attain the water content and

void ratio present in the saturated undisturbed specimens, and were subjected to identical tests.

Theoretical Considerations

In this study it has been assumed that no significant volume changes occur in the soil specimens due to cyclic wetting and drying. For this reason the

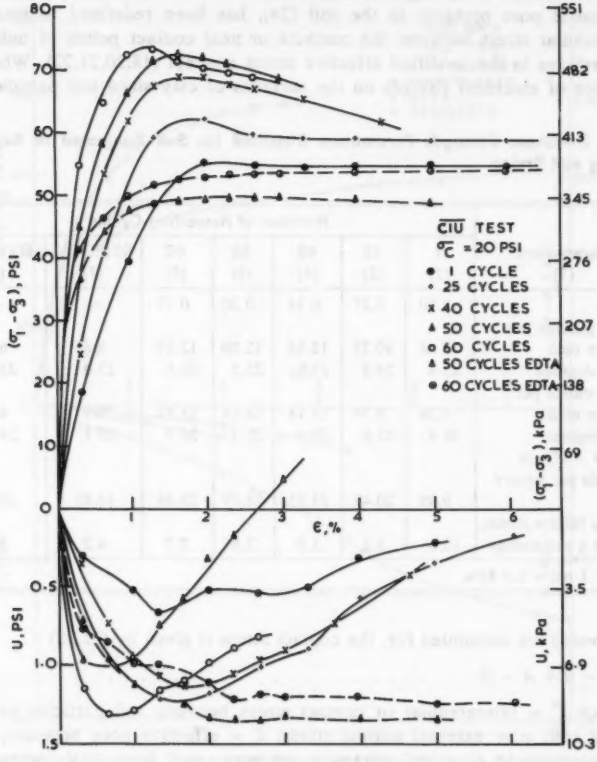

FIG. 3.—Typical Deviator Stress-Axial Strain and Pore Pressure Curves for Wetting and Drying Specimens

specimens were remolded at water contents near the shrinkage limit. Further, as was confirmed by inspection at the end of the wetting and drying cycles, cracking and erosion due to the drying and wetting process would be minimal. It has been assumed that whatever minute volume changes were likely to occur took place at the end of the first drying cycle, and at this stage all the specimens would possess no desiccation bonds. With successive wetting and drying cycles,

the specimens are expected to develop desiccation bonds in increasing numbers and gain the properties of undisturbed desiccated soils, and thus tend to be analogous to them in behavior. As the specimens are tested only in the saturated state, the influence of suction stresses is considered to be eliminated and any cohesion intercept obtained is attributable only to the intrinsic effective stress present. This intrinsic effective stress is anticipated to be imparted by the desiccation bonds generated.

The effective stress, originally defined as the excess of the total stress over the neutral pore pressure in the soil (24), has been redefined to mean the intergranular stress between the contacts or near contact points of individual soil particles in the modified effective stress concept (18,20,21,22). When the presence of electrical charges on the surfaces of clay sized soil particles and

TABLE 2.—Shear Strength Parameters Obtained for Soil Subjected to Repeated Wetting and Drying

Parameters (1)	Number of Rewetting Cycles						
	1 (2)	25 (3)	40 (4)	50 (5)	60 (6)	50(EDTA) (7)	60(EDTA) (8)
B	0.30	0.27	0.24	0.20	0.17	—	—
C_{cu}, in pounds per square inch	7.08	10.73	12.54	12.80	12.87	6.85	6.84
ϕ_{cu}, in degrees	25.4	24.3	23.6	25.5	26.6	23.4	23.2
C', in pounds per square inch	5.24	9.79	11.14	13.49	13.95	4.9	4.98
ϕ', in degrees	28.9	25.6	25.6	25.1	26.1	25.1	24.8
$\sigma'' = (A - R)$, in pounds per square inch	9.49	20.43	23.25	28.79	28.48	10.46	10.78
Average failure strain, ϵ_f, as a percentage	10.5	8.2	5.9	2.8	2.7	4.2	5.0

Note: 1 psi = 6.9 kPa.

other bonds are accounted for, the contact stress is given by (21,22)

$$\bar{C} = \sigma - \bar{u} + A - R \quad \ldots \ldots \ldots

easily evaluated independently. It is this intrinsic effective stress that is expected to be affected by subjecting the soil to repeated wetting and drying.

Test Results

Stress-Strain Response.—Some typical deviator stress-axial strain and pore water pressure-axial strain curves obtained from $\overline{CIU}$ shear tests on specimens

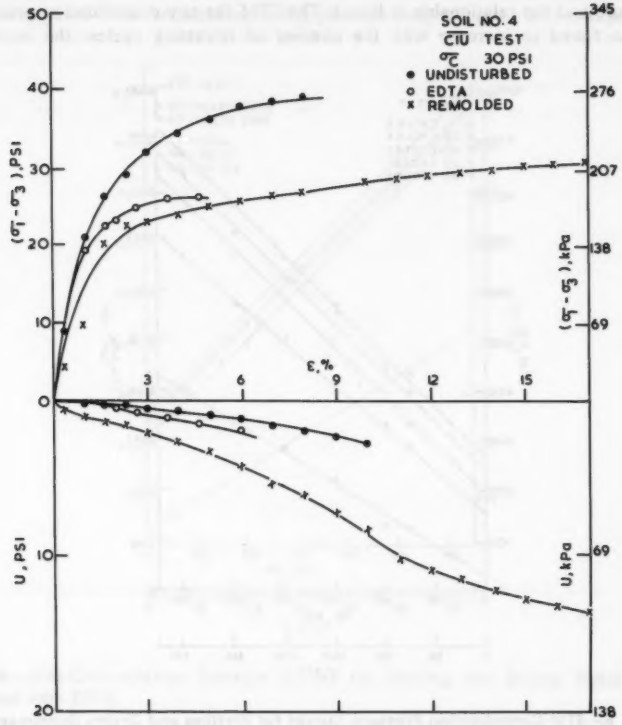

FIG. 4.—Typical Deviator Stress-Axial Strain and Pore Pressure Curves for the Soil in its Undisturbed and Remolded Conditions

which had undergone 1, 25, 40, 50, and 60 cycles of rewetting are shown in Fig. 3. It is seen that the shear strength [defined as $(\sigma_1 - \sigma_3)_{max}$] progressively increases, the axial strain at failure decreases (Table 2), and the soil fabric rigidity increases as the cyclic wetting and drying process repeats. The deviator stress-strain curves show pronounced peaks indicating that failure tends towards the brittle type. Fig. 4 presents some typical deviator stress-axial strain curves obtained from $\overline{CIU}$ shear tests on saturated undisturbed and remolded specimens

of the same soil. Striking resemblance with the specimens subjected to cyclic wetting and drying is observed if the first rewetting cycle is considered analogous to the remolded condition.

It was found that these deviator stress-strain curves could be transformed into rectangular hyperbolas (12,19), and the values for the initial tangent modulus (ITM) obtained from these transformed curves have been plotted against consolidation pressure (σ_c) for different numbers of rewetting cycles undergone prior to shearing (Figs. 5 and 6). The ITM is found to increase with consolidation pressure and the relationship is linear. The ITM for any consolidation pressure is also found to increase with the number of rewetting cycles: the increase

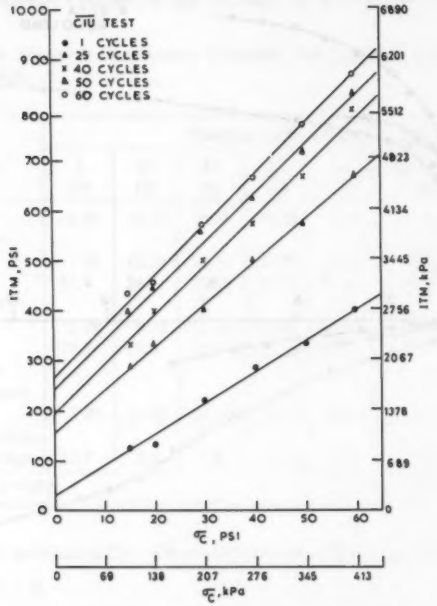

FIG. 5.—ITM-Consolidation Pressure Curves for Wetting and Drying Specimens

is as much as 9 times over the value for the first rewetting cycle when the soil has undergone 60 cycles of rewetting. A similar observation can be made when the undisturbed and remolded conditions are compared (Fig. 7). Fig. 8 presents the variation of the ITM ratio (defined as the ratio of ITM for any rewetting cycle to that for the first rewetting cycle) with consolidation pressure for specimens sheared after undergoing 25, 40, 50, and 60 rewetting cycles. The ITM ratio is found to decrease nonlinearly with increase in consolidation pressure for any rewetting cycle. This decrease is dependent on the slopes of the ITM-σ_c curves for any rewetting cycle and the first rewetting cycle,

and on the value of ITM at $\sigma_c = 0$. Fig. 8 also presents the variation of ITM ratio for undisturbed and remolded soils. The behaviors are similar. Fig. 3 also presents the stress-strain response of specimens treated with EDTA prior to shearing after having undergone 50 and 60 cycles of rewetting. A decrease in shear strength, an increase in axial strain at failure (Table 2), and a decrease in soil fabric rigidity as compared with the corresponding untreated specimens' behavior is noticed. Fig. 6 shows the ITM-σ_c curves obtained for EDTA treated specimens. The decrease in the ITM on treatment with EDTA is seen to be small compared with the increase taking place on subjecting the soil to repeated

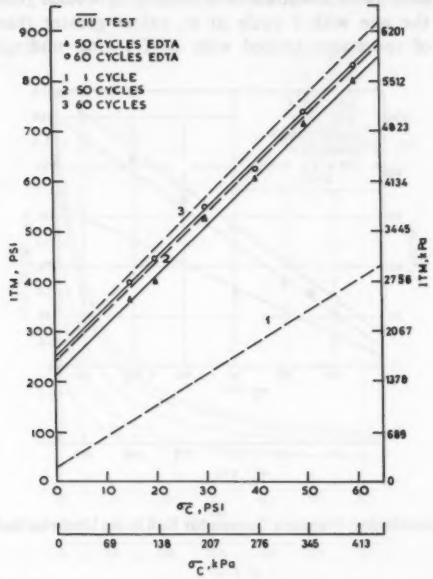

FIG. 6.—ITM-Consolidation Pressure Curves for Wetting and Drying Specimens Treated with EDTA

wetting and drying. A similar observation is made in the case of undisturbed soil (Fig. 7).

From the foregoing it can be concluded that the increase of ITM with the number of rewetting cycles is due more to changes in soil fabric resulting from wetting and drying than to the generation of bonds in the specimens.

Pore Pressure Parameters.—Table 2 presents the average values of B measured for specimens subjected to 1, 25, 40, 50, and 60 rewetting cycles. The low B value of 0.3 for the first rewetting cycle can be possibly attributed to the fact that specimen preparation was by compaction. Further, it is seen that the average B value decreases as the number of rewetting cycles increases. The

B value of a saturated soil is dependent on the soil skeleton's compressibility, which is itself dependent on the shearing resistance at particle contacts, and hence on the intrinsic effective stress present. The decrease in B value with increase in the number of rewetting cycles is a clear indication that repeated wetting and drying increases the intrinsic effective stress present. This is further corroborated by the data for the undisturbed desiccated soil (Table 3), which show a smaller B value as compared with the remolded soil in which desiccation bonds have been destroyed by remolding.

From the A_f-σ_c curves presented in Fig. 9 it is seen that although there is no definite trend in A_f values as the number of rewetting cycles increases, samples which have been rewetted to a number of cycles resulted in smaller A_f values than the one with 1 cycle at σ_c values greater than about 20 psi. The A_f values of specimens treated with EDTA after undergoing 50 and 60

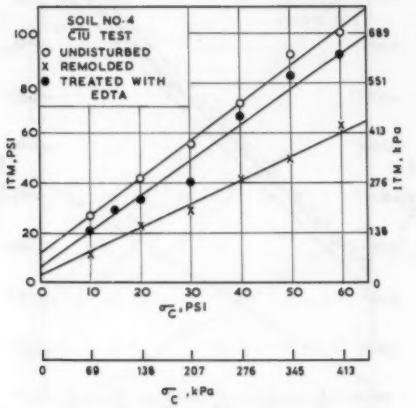

FIG. 7.—ITM-Consolidation Pressure Curves for Soil in its Undisturbed and Remolded Conditions

cycles of rewetting are more than the corresponding ones without treatment. Fig. 10 presents the A_f-σ_c curves obtained for the undisturbed and remolded soil, and also after treating it with EDTA. While EDTA removes the bonds generated by wetting and drying and thus reduces the intrinsic effective stress present, it does not alter the soil fabric. It has already been seen earlier that fabric also contributes to the ITM of the soil. The reduced intrinsic effective stress results in reduced shearing resistance at particle contacts. Therefore larger amounts of the applied deviator stress (but smaller compared to those of the first rewetting cycle specimens) are supported by the pore water pressures mobilized during shearing, and hence A_f values greater than those for the untreated 50 and 60 rewetting cycle specimens are obtained. The data for the undisturbed and remolded soil further corroborate this conclusion.

Shear Strength.—Fig. 11 presents the shear strength-σ_c curves for specimens subjected to different numbers of rewetting cycles. The shear strength-σ_c

relationship is linear in the range of σ_c used, and it is seen that the shear strength increases with the number of rewetting cycles. The increase in shear strength with the number of rewetting cycles clearly shows that the latter contributes additional intrinsic effective stress to the soil by generating some bonds. Fig. 12 presents the corresponding data for the undisturbed and remolded soil. The effect of treating undisturbed soil with EDTA is also shown. The reduction in shear strength on remolding may be attributed to the disruption of desiccation bonds in the soil. Fig. 11 also shows the shear strength obtained on treating 50 and 60 rewetting cycle specimens with EDTA. The reduction in shear strength which occurs on treatment with EDTA indicates that the bonds induced by wetting and drying are chemical in nature and therefore similar

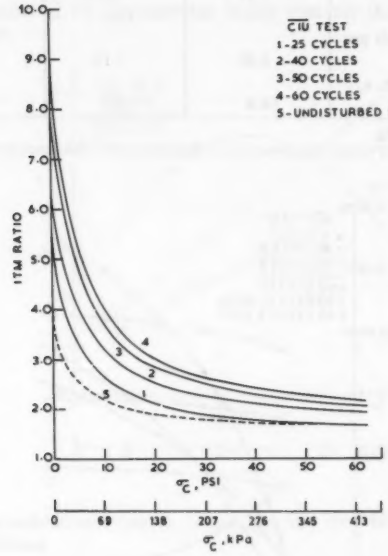

FIG. 8.—ITM Ratio-Consolidation Pressure Relationships for Wetting and Drying Specimens and for Undisturbed Soil

to the desiccation bonds present in desiccated soils. Since treating the 50 and 60 rewetting cycle specimens with 250 ml of 0.2N EDTA solution removed as much as 1 mg to 41 mg of Fe, 10 mg to 45 mg of Ca, 37 mg to 80 mg of Al, and 45 mg to 91 mg of Mg—similar quantities were detected from the chemical analysis of the spent EDTA solution collected from undisturbed soil—it can be concluded that cementing agents of Ca, Fe, Mg, and Al are produced by repeated wetting and drying, and that these bonds are responsible for the additional intrinsic effective stress occurring in the specimens.

It is seen from Fig. 11 that the shear strength of the treated specimens is less than that of the specimens subjected to only one rewetting cycle. Undisturbed

TABLE 3.—Shear Strength Parameters for Undisturbed and Remolded Red Earth

Parameters (1)	Undisturbed condition (2)	Remolded condition (3)	Treated with EDTA (4)
B	0.6	0.9	—
C_{cu}, in pounds per square inch	4.76	2.08	0.78
ϕ_{cu}, in degrees	19.3	16.7	16.7
C', in pounds per square inch	3.31	0.57	0.0
ϕ', in degrees	25.1	27.5	24.5
$\sigma''(A - R)$, in pounds per square inch	6.00	1.10	0
Average failure strain, ϵ_f, as a percentage	14.6	16.3	14.0

Note: 1 psi = 6.9 kPa.

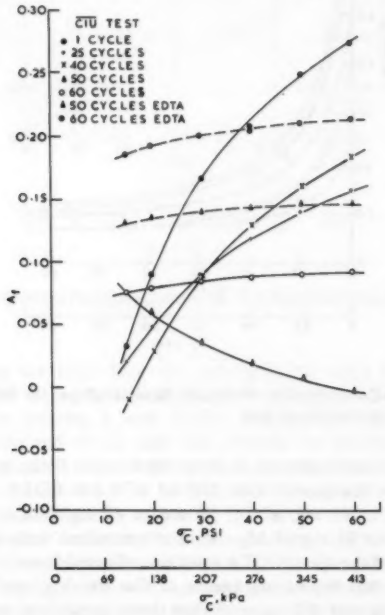

FIG. 9.—A_f-Consolidation Pressure Curves for Wetting and Drying Specimens

soil has a similar response when treated with EDTA (Fig. 12). This suggests that the wetting and drying process produces microcracks in the specimens, and suggests the presence of weaker planes in the undisturbed soils.

Fig. 13 presents the sensitivity ratio (defined as the ratio of shear strength for any rewetting cycle to that for the first rewetting cycle) versus consolidation pressure curves for specimens sheared after undergoing 25, 40, 50, and 60 rewetting cycles. It is seen that the sensitivity ratio increases with the number of rewetting cycles, since the shear strength itself increases. Also, the sensitivity ratio for any number of rewetting cycles decreases nonlinearly with increase in σ_c. This is because the ratio depends on the slopes of the shear strength-σ_c relationships and on the values for shear strength at $\sigma_c = 0$. Fig. 13 also presents the sensitivity ratio (ratio of shear strength undisturbed to remolded) for the undisturbed soil. Its maximum value (2.15) is somewhat larger than for the 60 rewetting cycle specimens (1.64).

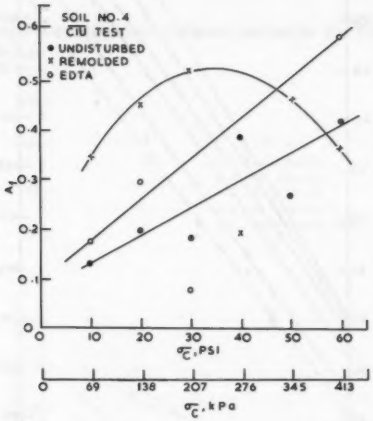

FIG. 10.—A_f-Consolidation Pressure Curves for the Soil in its Undisturbed and Remolded Conditions

The sensitivity ratio (Fig. 13) and the ITM ratio (Fig. 8) exhibit similar trends for changes in σ_c. Also, if the first rewetting cycle specimens are considered analogous to the remolded specimens, it is seen that the decrease in sensitivity ratio is of a smaller order than the decrease in the ITM ratio with increase in σ_c.

Shear Strength Parameters.—Table 2 presents the shear strength parameters in terms of total and effective stresses obtained from $\overline{\text{CIU}}$ shear tests on specimens subjected to different numbers of rewetting cycles. It is seen that the specimens which have undergone only one rewetting cycle possess significant cohesion intercepts in terms of both total and effective stresses. This can be attributed to the stress history effects involved in the preparation of the specimens by static compaction, and also to the shrinkage stresses occurring in the first drying cycle.

It is seen that the cohesion intercept increases in terms of both total and effective stresses as the number of rewetting cycles increases, showing an increase in the intrinsic effective stress present in the specimens. This further confirms that repeated wetting and drying induces bonds in the specimens. The angle of shearing resistance displays a slight decrease, and this can possibly be attributed to microcracks occurring in the specimens due to repeated wetting and drying taking place (2). Table 3 presents the shear strength data for the undisturbed

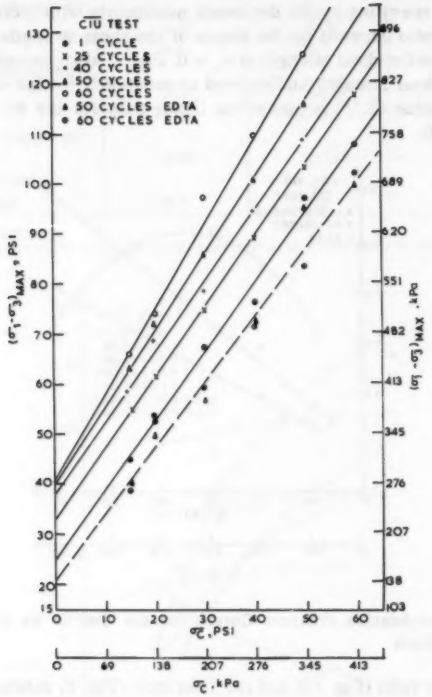

FIG. 11.—Shear Strength-Consolidation Pressure Curves for Wetting and Drying Specimens

and remolded soil. A decrease in the value of the total stress parameters and in the effective cohesion is seen to occur on remolding.

The 50 and 60 rewetting cycle specimens with were treated with EDTA prior to shearing yield cohesion intercepts (in terms of both total and effective stresses) which are less than those for specimens subjected to one rewetting cycle only, while their angles of shearing resistance correspond more closely to those for the 50 and 60 rewetting cycle untreated specimens. A similar effect is seen to occur when the undisturbed soil was treated with EDTA (Table 3). This

is because the treatment with EDTA is very effective in removing the bonds generated by wetting and drying, while microcracks and other defects remain

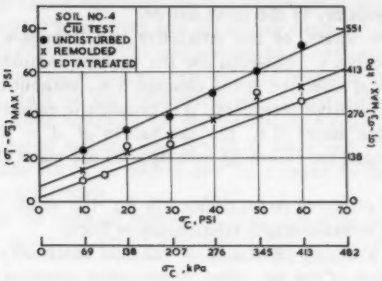

FIG. 12.—Shear Strength-Consolidation Pressure Curves for the Soil in its Undisturbed and Remolded Conditions

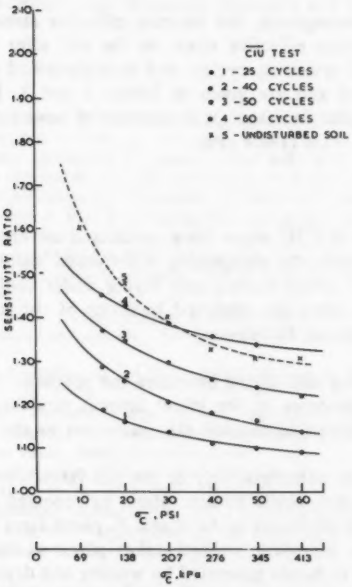

FIG. 13.—Sensitivity Ratio-Consolidation Pressure Curves for Wetting and Drying Specimens and for Undisturbed Soil

unaltered. Since varying amounts of Fe, Mg, Ca and Al ions were removed by EDTA, it is concluded that repeated wetting and drying induces some chemical

bonds in the soil. Since the strength and deformation behavior of the desiccated undisturbed soil and that of the specimens subjected to repeated wetting and drying show good resemblance, it can be concluded that the bonds present in both cases are possibly of the same nature.

Intrinsic Effective Stress, or Net Attractive and Repulsive Pressures.—From the cohesion intercepts C' obtained for the various samples (Tables 2 and 3) with the conventional effective stress concept (i.e., without taking into account the attractive and repulsive pressures), it is possible to estimate the contribution of intrinsic effective stress (i.e., the net values of $A - R$) to the effective stress (Eq. 1) provided the following assumptions are made (22):

1. The modified effective stress defined in Eq. 1 is valid.
2. The effective stress-strength relationship is linear.
3. The angle of shearing resistance ϕ' remains essentially the same with or without consideration of the net values of attractive pressures.
4. All shearing resistance in the soil is of a frictional nature. In other words, if the true effective stress is known, then the cohesion intercept should become zero.

In view of these assumptions, the intrinsic effective stress $\sigma'' = C'/\tan \phi'$. The values of intrinsic effective stress in the soil after it has undergone a specified number of rewetting cycles, and in undisturbed and remolded soils, have been computed and are given in Tables 2 and 3. It can be seen that the net $(A - R)$ value increases with number of rewetting cycles and could reach as high as 28.79 psi (198.4 kPa).

Conclusions

From the results of $\overline{\text{CIU}}$ shear tests conducted on specimens prepared in the laboratory by statically compacting a disturbed natural soil (Red Earth) and subjecting it to cyclic wetting and drying under controlled conditions in the laboratory, and from the observed behavior of the undisturbed soil, the following conclusions can be drawn:

1. Repeated wetting and drying increases the stiffness of the soil fabric, as is seen from the increases in the initial tangent modulus ITM (as much as 9 times). The brittleness of the soil also increases as the wetting and drying repeats.
2. Decreases in the compressibility of the soil fabric occur due to increases in the intrinsic effective stress brought about by repeated wetting and drying. This is shown by the decreases in the B and A_f parameters.
3. An increase in the shear strength takes place as the intrinsic effective stress increases due to bonds generated by wetting and drying.
4. The cohesion intercept is found to increase as the wetting and drying process repeats, further confirming that the process generates bonds and hence intrinsic effective stress in the soil.
5. The maximum value of the ITM ratio (9.0) exceeds that for the sensitivity ratio (2.15). A similar trend (3.8 and 1.64) is observed when these ratios are compared for the soil in its undisturbed and remolded states.

6. Results for EDTA treated specimens show the increase in ITM ratio due to wetting and drying to be due more to changes in soil fabric than to generation of bonds.

7. Treatment with EDTA decreases the shear strength significantly, indicating that the bonds generated by wetting and drying are chemical in nature.

8. Considering the first rewetting cycle specimens as analogous to the remolded state, and specimens subjected to a larger number of rewetting cycles as analogous to the undisturbed state of the desiccated soil, remarkable similarity in the strength and deformation behavior for the undisturbed state and when the soil is subjected to repeated wetting and drying is observed. This suggests that the desiccation bonds found in nature can be created in the laboratory also by repeated wetting and drying.

9. The increase in the intrinsic stress (net attractive pressure) due to repeated wetting and drying has been quantitatively calculated with reasonable assumptions.

Acknowledgments

The writers acknowledge the cooperation and financial assistance extended by the Council for Scientific and Industrial Research and the Indian Institute of Science, India.

Appendix.—References

1. Alderfer, R. B., "Seasonal Variability in the Aggregation of Hagerstown Silt Loam," *Soil Science*, Vol. 62, No. 2, 1946, pp. 151–168.
2. Allam, M. M., "Shear Strength and Volume Change Behaviour of Desiccated Soils," thesis presented to the Indian Institute of Science, at Bangalore, India, in 1977, in fulfillment of the requirements for the degree of Doctor of Philosophy.
3. Arca, M. N., and Weed, S. B., "Soil Aggregation and Porosity in Relation to Contents of Free Iron Oxide and Clay," *Soil Science*, Vol. 101, No. 3, 1966, pp. 164–170.
4. Bawa, K. S., "Laterite Soils and Their Engineering Characteristics," *Journal of the Soil Mechanics and Foundations Division*, ASCE, Vol. 83, No. SM4, Proc. Paper 1428, November, 1957.
5. Blight, G. E., "Strength Characteristics of Desiccated Soils," *Journal of the Soil Mechanics and Foundations Division*, ASCE, Vol. 92, No. SM6, Proc. Paper 4966, Nov., 1966, pp. 18–37.
6. Drachev, S. M., "Solubility of the Solid Phase of Soil in Water," *Soil Science*, Vol. 35, No. 1, 1933, pp. 75–83.
7. Grant, K., "Laterites, Ferricretes, Bauxites and Silicretes," presented at the August 18–24, 1974, 2nd International Congress of the International Association of Engineering Geology, held at San Paulo, Brazil (Preprint IV-31).
8. Grant, K., "The Composition of Some Australian Laterites and Lateritic Gravels," presented at the August 18–24, 1974, 2nd International Congress of the International Association of Engineering Geology, held at São Paulo, Brazil (Preprint IV-32).
9. Gupta, K. G., and Sen, A., "Aggregation of the Soil due to Growth of Rhizobium sp. from some Common Cultivated Legumes," *Soil Science*, Vol. 94, No. 2, 1962, pp. 345–348.
10. Ingles, O. G., "Bonding Forces in Soils—Part I: Natural Soils—The Physical Factors Responsible for Cohesive Strength," *Proceedings*, Australian Road Research Board, Vol. 1, Part 2, 1962, pp. 999–1013.
11. Kenney, T. C., Moum, J., and Berre, T., "An Experimental Study of Bonds in a Natural Clay," *Proceedings*, 1st Geotechnical Conference of Oslo, Norway, 1967, pp. 65–69.
12. Kondner, R. L., "Hyperbolic Stress-Strain Response: Cohesive Soils," *Journal of*

the Soil Mechanics and Foundations Division, ASCE, Vol. 89, No. SM1, Proc. Paper 3429, February, 1963, pp. 115–144.
13. Lambe, T. W., "A Mechanistic Picture of Shear Strength in Clay," presented at the ASCE Research Conference on Shear Strength of Cohesive Soils, held at Boulder, Colorado, 1960.
14. Lipman, C. B., and Waynick, D. D., "A Detailed Study of Effects of Climate on Important Properties of Soils," *Soil Science,* Vol. 1, No. 1, 1916, pp. 5–48.
15. Loiselle, A., Massiera, M., and Usha, S. R., "A Study of the Cementation Bonds of the Sensitive Clays of the Outardes River Region," *Canadian Geotechnical Journal,* Vol. 8, No. 3, 1971, pp. 479–498.
16. Nagaraj, T. S., "Soil Structure and Strength Characteristics of Compacted Clays," *Geotechnique,* Vol. 14, No. 1, 1964, pp. 103–114.
17. Russam, K., "The Prediction of Subgrade Moisture Conditions for Design Purposes," *Proceedings of the 1st International Research and Engineering Conference on Expansive Clays,* College Station, Texas, 1965, pp. 233–236.
18. Sridharan, A., "Some Studies on the Strength of Partly Saturated Clays," thesis presented to Purdue University, at West Lafayette, Indiana, in 1968, in partial fulfillment of the requirements for the degree of Doctor of Philosophy.
19. Sridharan, A., and Narasimha Rao, S., "Hyperbolic Representation of Strength, Pore Pressures and Volume Changes with Axial Strain in Triaxial Tests," *Proceedings of the 1st Symposium on Strength and Deformation Behaviour of Soils,* Indian Geotechnical Society, 1972, pp. 33–42.
20. Sridharan, A., and Venkatappa Rao, G., "Physico-chemical Mechanisms Controlling the Strength, Consolidation and Swelling Behaviour of Clays," *Proceedings of the 1st Symposium on Strength and Deformation Behaviour of Soils,* Indian Geotechnical Society, 1972, pp. 11–16.
21. Sridharan, A., and Venkatappa Rao, G., "Mechanisms Controlling Volume Change of Saturated Clays and the Role of the Effective Stress Concept," *Geotechnique,* Vol. 23, No. 3, 1973, pp. 359–382.
22. Sridharan, A., and Venkatappa Rao, G., "Shear Strength Behaviour of Saturated Clays and the Role of Effective Stress Concept," *Geotechnique,* Vol. 29, No. 2, 1979, pp. 177–193.
23. Sridharan, A., and Allam, M. M., "Shear Strength Behaviour of Bangalore Soil," presented at the December, 1975, IGS Speciality Conference held during the 5th Asian Regional Conference on Soil Mechanics and Foundation Engineering, held at Bangalore, India.
24. Terzaghi, K., "Die Berechnung der Durchlassigkeitsziffer des Tones aus dem Verlauf der Hydrodynamischen Spannungserschienungen Sitz," *Akad. Wissen. Wien,* Vol. 132, 1923, pp. 105–124.
25. Watson, J. H., and Stojanovic, B. J., "Synthesis and Bonding of Soil Aggregates as Affected by Microflora and its Metabolic Products," *Soil Science,* Vol. 100, No. 1, 1965, pp. 57–62.

JOURNAL OF THE GEOTECHNICAL ENGINEERING DIVISION

MEASUREMENT OF POROSITY IN NATURAL SAND DEPOSITS

By S. A. Denekamp[1] and Y. Tsur-Lavie[2]

INTRODUCTION

Porosity and relative density of natural sand deposits depend both on textural properties (grain size, sorting, etc.) and on environmental conditions during sedimentation. The extent to which each of these factors affects porosity is of considerable interest in civil engineering, hydrology, and geology. Information on the subject is limited however, mainly because of technical difficulties in obtaining and handling undisturbed sand samples. Studies of porosity in natural sand deposits which were conducted in the past were generally based on samples obtained by driving a sampler into the unconsolidated sand, a procedure which always caused considerable disturbance of the sand. Accordingly, results lacked accuracy (3,4,9,11).

In the present study a technique was developed in which undisturbed samples are obtained by hardening the sand prior to sampling. Porosity is measured on small cubes cut from the sand samples. Some preliminary results obtained in dune sand are presented and serve to illustrate potential uses of the technique.

RETRIEVAL OF SAMPLES IN FIELD

Undisturbed samples were obtained by impregnating the sand deposit with a hardening material. Two types of organic hardeners were used: A solution containing 5% cellulose acetate in acetone and a polyester resin.

The method of impregnation is as follows: A thin-walled cylinder (a bottomless tin can) is pushed a few centimeters into the sand deposit, the hardening solution

[1]Sr. Lect., Faculty of Civ. Engrg., Technion, Haifa 32000, Israel.
[2]Sr. Lect., Faculty of Civ. Engrg., Technion, Haifa 32000, Israel.

Note.—Discussion open until September 1, 1981. To extend the closing date one month, a written request must be filed with the Manager of Technical and Professional Publications, ASCE. Manuscript was submitted for review for possible publication on June 24, 1980. This paper is part of the Journal of the Geotechnical Engineering Division, Proceedings of the American Society of Civil Engineers, ©ASCE, Vol. 107, No. GT4, April, 1981. ISSN 0093-6405/81/0004-0439/$01.00.

is then poured into the cylinder and allowed to filter slowly into the sand so that a "bulb" of impregnated sand is formed below the cylinder. After hardening, the bulb of impregnated sand is removed and transferred to the laboratory. The size and the shape of the hardened sample depends on the amount of

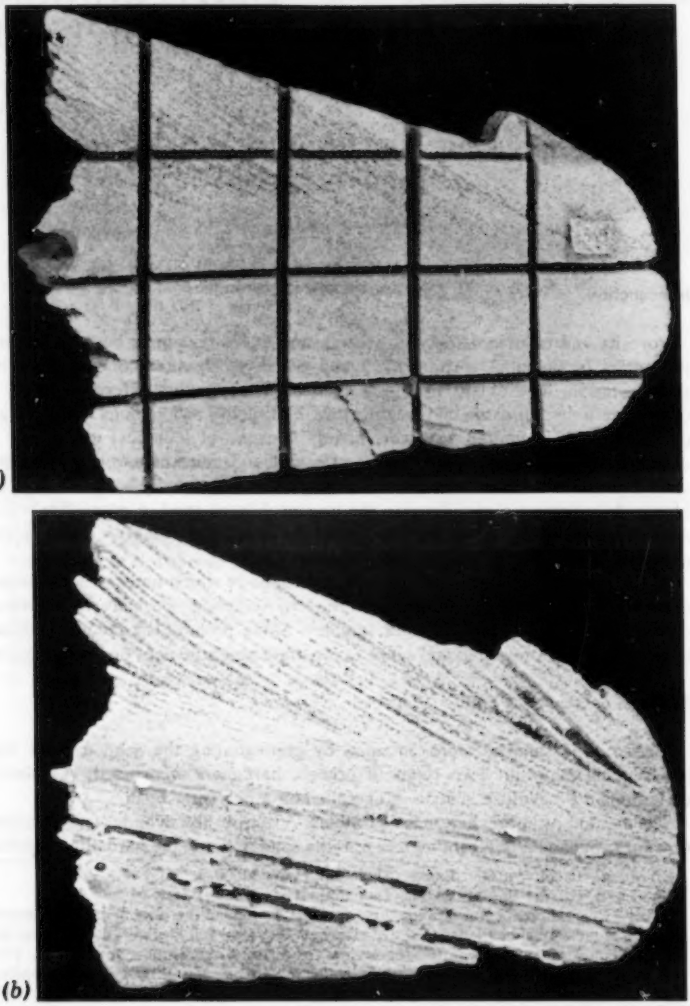

FIG. 1.—(*a*) Hardened Sand Sample Cut into Cubes; (*b*) Corresponding "Peel" Showing Internal Structure of Sand

impregnating liquid and the cylinder's diameter. In the present study cylinders 15 cm diam were used and about 600 cm^3 of liquid was used per sample. The samples obtained were about 20 cm wide and 15 cm deep.

Impregnating with cellulose acetate is relatively simple. Hardening occurs through evaporation of the acetone which proceeds so slowly that even fine-grained sand is completely impregnated before hardening sets in. Complete hardening requires about a week. The use of acetate for impregnation in the field is limited however, because of the long drying period required, and because it fails to harden when the sand is soaked or submerged. Good results with acetate are obtained in dry to medium wet dune sand but not, e.g., on tidal flats, where hardening must be fast and where the high water content prevents drying. For such conditions the quick hardening polyester resin must be used.

Measuring Porosity

Cubes measuring about 3 cm in each direction are easily cut from the hardened sample (Fig. 1). Porosity measurements are performed on each cube. The procedure consists of determination of the cube's volume by weighing in a liquid of known density, removal of the organic cementing material by heating, and volume measurement of the grains in a pycnometer.

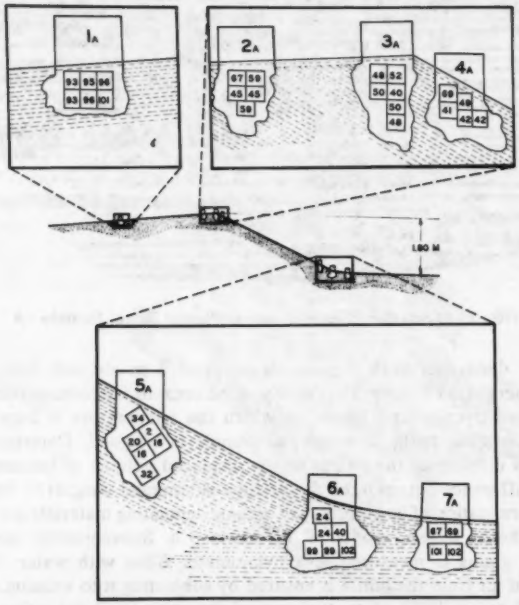

FIG. 2.—Location of Samples and Cubes: Relative Densities are Indicated, as a percentage

The technique used for measuring the volume of the cubes requires all pores to be completely sealed. The intergranular pores in the hardened samples obtained in the field, however, are only partly filled with hardening material, in particular where cellulose acetate is used. The acetate fills only a fraction of the pore volume and gives the samples a porous and spongy appearance. Complete sealing of the intergranular space is achieved by reimpregnating the cube samples with polyester resin. The cubes are submerged in resin and subjected to vacuum ensuring the complete filling of the pores. One difficulty encountered when reimpregnating sand cubes cemented with cellulose acetate is that they soften during the process and therefore may be disturbed. This is prevented by applying a thin protective coating of polyester which is allowed to soak into the cube's faces and harden before the main phase of impregnation under vacuum.

The volume of the cubes is determined as follows. The cubes are weighed with an analytical balance to which they are attached by means of a thin wire.

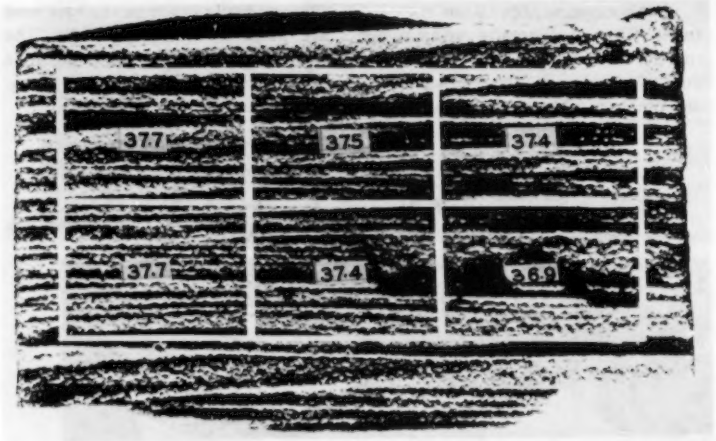

FIG. 3.—Accretion Deposits, upper Part of Dune, Sample 1A

Weighing is done first with the sample suspended in air and then with the sample submerged in benzene. The density of the benzene is accurately determined in a calibrated pycnometric bottle, in which the temperature is kept equal to that in the benzene bath, in which the sample is weighed. Determination of volume is by division of the weight of the displaced volume of benzene (which equals the difference between the dry and the submerged weight) by its density.

After determination of its volume, the organic cementing materials are removed from the cube by heating at 500° C for about 3 h. Subsequently, the volume of the sand grains is measured in a pycnometer filled with water. Complete evacuation of air from the bottle is ensured by subjecting it to vacuum. Porosity is calculated by on basis of the volume of the grains and the volume of the cube.

Loss of mineral matter due to heating should be accounted for while computing

porosity. For the determination of loss of mineral matter, sand samples were first heated to a (standard) temperature of 105° C and then to a temperature of 500° C. The loss of weight was 0.3%–0.35% for the tested beach and dune sands (which are mainly composed of quartz but contain up to 10% calcite). Thus the porosity determinations were modified by adding 0.3% to the measured volume of the sand grains.

The reliability of this procedure of porosity determination in the field was

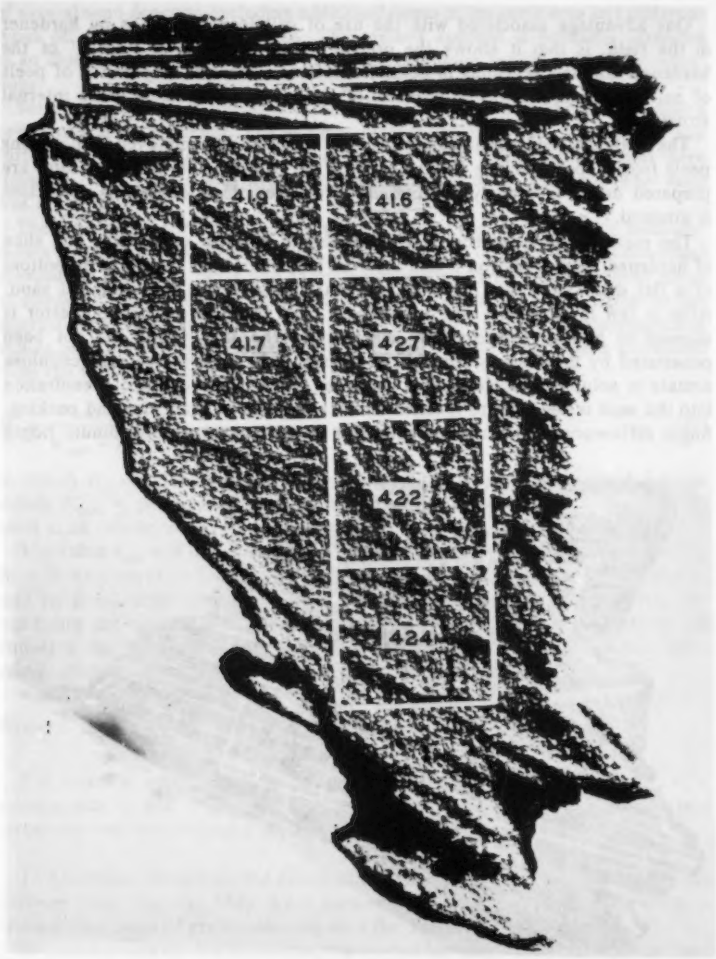

FIG. 4.—Slip Deposits, upper Part of Dune, Sample 3A

verified by applying the technique to sand of known porosity, obtained by compaction in a Proctor mold. The porosity measured in cubes cut from the hardened sand obtained from the mold was 37.3%–37.5%, after allowing for a loss of 0.3% of mineral matter. The porosity as determined in the Proctor mold was 37.5%.

Preparation of Peels

One advantage associated with the use of cellulose acetate as an hardener in the field, is that it allows the preparation of replica's or "peels" of the hardened samples, revealing in detail its internal structure. Preparation of peels of hardened sand allows the porosity of the sand to be related to its internal structure.

The method of peel preparation is basically similar to that employed for obtaining peels from deposits in the field (2). Since the peels of the hardened sand are prepared under laboratory conditions, a relatively high degree of perfection is attained.

The method employed for the preparation of peels is as follows. The slice of hardened sand is laid on a thin layer of polyester resin covering the bottom of a flat dish. The resin is allowed to soak upwards into the hardened sand. After a few minutes the slice is removed from the dish and the polyester is allowed to harden. Subsequently that part of the slice which has not been penetrated by the resin is removed by washing the slice in acetone (cellulose acetate is soluble in acetone, but polyester is not). The depth of penetration into the sand is sensitive to textural differences such as grain size and packing. Slight differences in texture are reflected by the appearance of minute ridges

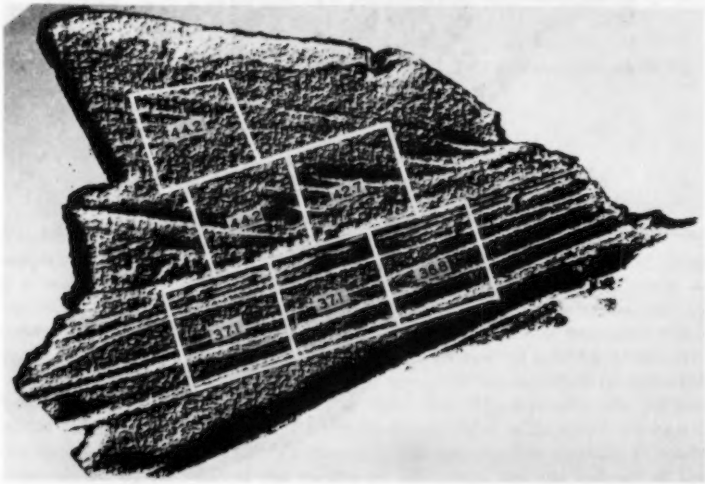

FIG. 5.—Slip Deposits, lower Part of Dune, Sample 6A

and grooves which parallel the sand layering. The internal structure of the sand is thus revealed.

Porosity Measurements in Dune

The study was performed on a small Barchan type dune in the near shore area along the Haifa Bay (Israel). It formed part of a more extensive investigation of natural sand deposits, including additional dunes in the same area and different types of sand deposits elsewhere. The present account is primarily intended as an illustration of the previously described technique and its potential applications.

Seven samples were obtained after being impregnated in the field, using a cellulose acetate hardener. The samples were taken from the dune's back, slip surface, and foot (Fig. 2). Textural properties of the sampled dune sand were found to vary only slightly, with a mean grain size of 0.18 mm. The sand was dry to damp.

The procedures for obtaining the sample, performance of porosity measurements on cubes cut from the samples, and preparation of peels were as described previously. Since the peels and the cubes were prepared from adjacent slices of hardened sand, the distribution of porosity values could be related to the internal structure of the sand. In addition to values of porosity, the corresponding values of relative density were also determined. These values were calculated from the following equation:

$$D_r = \frac{n_{max} - n}{n_{max} - n_{min}} \quad \ldots\ldots\ldots\ldots\ldots\ldots\ldots\ldots\ldots\ldots\ldots\ldots\ldots\ldots (1)$$

in which D_r = relative density; n = natural porosity as determined for the cubes; n_{min} = porosity of sand in its densest state; and n_{max} = porosity of sand in its loosest state.

The value n_{min} was obtained following ASTM D1557. The sand was compacted in a Proctor mold in five equal layers with 25 blows/layer. A 10-lb hammer and an 18-in. drop were used. The value n_{max} was obtained by pouring the sand into the mold and controlling the intensity of deposition by holding the funnel a few centimeters above the surface of the sand in the mold. As a result of these tests n_{min} was determined as 37% and n_{max} as 46.5%.

Results

The internal structure of the dune, as revealed by the peels (Figs. 3–5), corresponds to that of a typical Barchan dune (1). On basis of the internal structure, two types of sand deposits may be identified:

1. Accretion deposits show a pronounced layering which is horizontal or slightly inclined (see Fig. 3). They were formed through direct deposition from a wind-driven mass of grains saltating on a flat surface.
2. Slip deposits show a much less pronounced layering which is steeply inclined and formed by a process of rolling, sliding, and avalanching of sand grains on a steeply inclined slope (see Figs. 4 and 5).

Accretion deposits are found at the back of the dune and at the flat surface at the foot of the dune. Slip deposits are found at the inclined slip slope, at the leeward side of the dune. Fig. 4 showing sample 3A contains accretion deposits in its upper part and slip deposits in its lower part. The sample clearly reflects the process of dune movement showing traces of slip surfaces along which the progressive sand slides have taken place. Figure 5 showing sample 6A contains slip deposits in its upper part and accretion deposits in its lower part. It reflects the encroaching of the avalanching sand over an even surface at the foot of the dune.

Accretion deposits show low porosities (36.8%–37.7%) and high relative densities (93%–102%). These values may be attributed to the high energies involved in the saltation process in which individual grains hit the surface with considerable force. The process is analogous to the deposition of sand in the laboratory by dropping individual grains from some height. Porosities which are obtained in this way are known to approach those produced by laboratory compaction (7,8).

Slip deposits show high porosities (39.9%–46.3%) and low relative densities (2%–69%). These values are explained by the mechanism of deposition which involves avalanching of large masses of sand grains. There exists a similarity between this mode of deposition and that employed for the production of maximum porosity in a Proctor mold. The process limits the movement of individual grains which are therefore locked into an open packing. Significantly, the largest porosities were encountered in the lower part of the slip slope near the foot of the dune, where the process of deposition is purely by mass avalanching. Lower porosities are encountered higher up on the slip slope where the sand is formed partly by the accumulation of sand grains rolling and jumping over the crest of the dune and where it is less disturbed by sliding and avalanching.

Analysis

Karol (6) suggests a method of sampling unconsolidated sediments by means of grouting in boreholes. The writer claims that the relative density can be evaluated indirectly from the uniaxial compression strength of the hardened specimens, however no supporting data were provided.

A method for the measurement of porosity in sand which was impregnated by an hardening material has been described by Windisch and Soulie (12). The measurement is performed by microscopic inspection of thin sections prepared from the hardened sand. The thin sections are scanned systematically along transverses, using a point-counting technique. Porosity was determined statistically employing a procedure described by Kahn (5) for the determination of porosity in rocks.

In our own experience the following difficulties are associated with the previously described method:

1. The problem of obtaining a sufficiently sharp optical definition of the grain outlines in a standard thin section 0.03-mm thick (which is about 10% of a medium-sized sand grain).
2. The tendency of grains to dislodge during preparation of thin sections.
3. The necessity to scan a very large number of transverses in order to obtain a statistically reliable value for porosity.

The method used in the present study for the determination of porosity in hardened sand seems to be more accurate and reliable than the previously described method, and, in addition, it is technically easy to perform. One limitation inherent to the method is, however, that it can give accurate results only in sands with a low content of minerals which are affected by heating. In many sands this limitation does not apply.

The study of hardened sand is especially suited to the determination of small scale density variations in natural sand masses, a subject about which present knowledge is insufficient. One limitation in the application of the technique in the present study was that because lack of suitable hardening materials, samples could be obtained only from a small depth. This limitation may be overcome in the future by offering better control over viscosity and hardening time so that sand bodies may be impregnated and hardened at considerable depth, i.e., by means of boreholes. We believe that some of the commercially available organic hardeners used for grouting of boreholes could be successfully applied (10).

Appendix.—References

1. Bagnold, R. A., *The Physics of Blown Sand and Desert Dunes*, Methuen, London, England, 1954.
2. Bouma, A. H., *Methods for the Study of Sedimentary Structures*, John Wiley and Sons, Inc., New York, N.Y., 1969.
3. Brauckhoff, K., "Trockendichte und Verdichtung Natürlich Abgelagerter und Künstlich Aufgebrachter Strand und Dünensande," *Wasserwirtschaft-Wassertechnik*, Vol. 19, No. 6, 1969.
4. Füchtbaur, H., and Reineck, H., "Porosität und Verdichtung Mariner Sedimente," *Sedimentology*, Vol. 2, 1963, pp. 294–306.
5. Kahn, J. S., "The Analysis and Distribution of the Properties of Packing in Sand-Size Sediments," "The Distribution of the Packing Measurements and an Example of Packing Analysis," *Journal of Geology*, Vol. 64, 1956, pp. 578–606.
6. Karol, R. H., "Use of Chemical Grouts to Sample Sands, Sampling of Soil and Rock," ASTM STP 483, American Society for Testing and Material, 1971, pp. 51–59.
7. Kolbuszewski, J., "An Experimental Study of the Maximum and Minimum Porosities of Sands," *Proceedings of the Second International Conference on Soil Mechanics and Foundation Engineering*, Rotterdam, Netherlands, 1948, pp. 158–165.
8. Kolbuszewski, J., "Discussions," *Fourth International Conference on Soil Mechanics and Foundation Engineering*, London, Vol. III, 1957.
9. Krumbein, W. C., "The 'Sorting out' of Geological Variables Illustrated by Regression Analysis of Factors Controlling Beach Firmness," *Journal of Sedimentary Petrology*, Vol. 29, 1959, pp. 575–587.
10. Richardson, E. A., and Hamby, I. W., "A New Process for Consolidation of Silty Sands using the EROSAND (R) Resin Process," American Institute of Mining, Metallurgy and Petroleum Engineers, 1968, *Preprint SPE. 2189*.
11. Shockley, W. G., and Garber, P. K., "Correlation of some Physical properties of Sand," *Proceedings of the 3rd International Conference of Soil Mechanics and Foundation Engineering*, Vol. 1, 1953, pp. 203–206.
12. Windisch, S. J., and Soulie, M., "Technique for Study of Granular Materials," *Journal of the Soil Mechanics and Foundations Division*, ASCE, Vol. 96, No. SM4, Proc. Paper 7389, July, 1970, pp. 1113–1125.

JOURNAL OF THE GEOTECHNICAL ENGINEERING DIVISION

STOCHASTIC FEM IN SETTLEMENT PREDICTIONS

By Gregory B. Baecher[1] and Thomas S. Ingra[2]

INTRODUCTION

Foundation design requires predictions of total and differential settlement. However, as soil strata are spatially variable and exploration effort limited, these predictions cannot be made with certainty. In deterministic modeling, in which the subsurface is characterized as a uniform or trending continuum, the only procedure for dealing with these uncertainties is sensitivity analysis. This leads to an assessment of the effect of uncertainties on "average" settlement, but cannot be used to assess the effect of spatial variability on differential settlement. A soil model based on spatially variable soil properties would broaden the spectrum of predictions that might be made, but for deterministic analysis requires more site information than feasibly available. Therefore, a model is desired which more precisely encodes uncertainties about soil properties than either random lumped parameter models or sensitivity analyses do, yet which avoids the simplistic soil mechanics assumptions of current stochastic models. Given the accelerating use of numerical models and the cost experience curve for computation, an obvious approach is to broaden finite element methods (FEM) to incorporate stochastic variability in soil properties. This paper reports the results of two-dimensional second-moment settlement analyses using finite element methods, and compares these results with one-dimensional uncertainty analyses already in the literature.

PREVIOUS STUDIES OF SETTLEMENT UNCERTAINTY

Previous studies of probabilistic settlement appearing in the literature can be grouped in three categories: random lumped parameter models; stochastic one-dimensional models; and stochastic finite element models. Random lumped

[1]Assoc. Prof. of Civ. Engrg., Massachusetts Inst. of Tech., Cambridge, Mass. 02139.
[2]Geotechnical Engr., Ardaman and Assocs., Orlando, Fla. 32809.

Note.—Discussion open until September 1, 1981. To extend the closing date one month, a written request must be filed with the Manager of Technical and Professional Publications, ASCE. Manuscript was submitted for review for possible publication on January 29, 1979. This paper is part of the Journal of the Geotechnical Engineering Division, Proceedings of the American Society of Civil Engineers, ©ASCE, Vol. 107, No. GT4, April, 1981. ISSN 0093-6405/81/0004-0449/$01.00.

parameter models propagate parameter uncertainty through deterministic equations in which soil properties are assumed uniform but uncertain. Stochastic models are distinct from lumped parameter models in that they assume spatial variability in the soil profile. The one-dimensional models address variation along vertical lines in the subsurface. Finite element models address variation from one element to the next.

One of the earliest lumped parameter models is that of Wu and Kraft (15), which propagates uncertainty in standard penetration test data through a Terzaghi and Peck correlation for the load necessary to cause one inch of settlement. This is a full-distribution model, assuming the standard penetration test resistance and model uncertainty to be normally distributed. Ramos (10) extended this model to include uncertainty in loads, in a second-moment formulation.

Hilldale (7) developed a one-dimensional settlement model in which modulus is characterized as a second-order stationary stochastic process. Settlement is calculated by integrating one-dimensional deformations induced by a deterministic elastic stress field. Similar models were developed by Resendiz and Herrera (11) and Diaz and Vanmarcke (5). The former model assumes independence of soil properties in adjacent layers, and constant variance within layers. The latter assumes soil properties to be autocorrelated within layers. Both are second-moment analyses.

Stochastic finite element techniques for two- (or higher) dimensional settlements were suggested by Cornell (3) in a general discussion of the applicability of second-moment techniques to linear systems, and developed by Ditlevsen (6) for solution by matrix techniques. Application of stochastic finite element methods to rock and soil mechanics has been made by Su, et al. (12), Paraseau (9) and Cambou (2). Dendrou and Houstis (4) have used a similar model for fluid flow. Su, et al. and Paraseau use Monte Carlo simulations to generate element properties from specified distributions, repeating the calculations to form a sampling distribution. In both studies, element properties were assumed to be independent and identically distributed (iid). This yields low variance output with marked sensitivity to element size, through an "averaging" of random fluctuations over larger and larger "sample sizes," as element dimensions are reduced. Cambou applied second-moment approximations to linear solutions of the finite element method which include autocorrelation among properties. The procedure for selecting element properties, and whether the iid assumption was made, was not discussed.

Formulation of Random Settlement Models

Existing probabilistic settlement models, including stochastic finite element methods, are extensions of deterministic techniques in which input parameters are allowed to vary. Thus, these models suffer the same limitations as deterministic models and should be seen only as refinements of existing techniques. Most analyses, the present included, concentrate on parameter variability and ignore both estimation error and model uncertainty. However, in principle, both latter sources of uncertainty can be incorporated with existing techniques.

In the present work, soil variability is modeled as one realization of a second-order stationary random field. Clearly, soil properties are not random, however, they are spatially variable. Since observations can only be made at

a finite number of locations, some assumption must be made to infer properties at unobserved locations. Following standard practice in geological modeling, the assumption is made that the statistical properties of the soil are spatially constant (i.e., stationary), and that spatial variability is introduced by random fluctuations about the mean or mean trend. This is purely hypothetical. The uncertainty, actually due to ignorance, is divided into two artificial components, "random" fluctuation and estimation error, to facilitate analysis.

The random fluctuation component of uncertainty is characterized by a point variance ("amplitude") and autocorrelation function ("waviness"). Both of these result from the way the modeling of spatial variability is made, and change if the flexibility of the mean trend is changed (Fig. 1). By increasing the flexibility of the mean trend, both the point variance and autocorrelation distance (i.e., the distance at which the autocorrelation reduces to a value of e^{-1}) are decreased, because more of the spatial variation is being explained by the deterministic trend. On the other hand, more parameters must be estimated for the more flexible trends, and this introduces more estimation uncertainty. Since the total

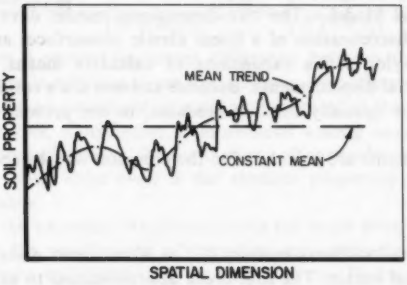

FIG. 1.—Stochastic Modeling of Soil Variability by Mean Trend Plus Random Fluctuation

uncertainty depends on both the random fluctuations and the estimation uncertainty, for practical purposes there may be an optimal level of flexibility in the mean trend for a fixed number of observations. The only way the total uncertainty can be reduced, however, is by increasing the number of observations (1).

One-Dimensional Models.—One-dimensional stochastic models of settlement integrate deformations along a vertical line due to an exogenously determined nonrandom stress field acting through a spatially variable modulus

$$\rho = \int_0^{z_0} \frac{\sigma_z}{M_z}\, dz \quad \ldots\ldots\ldots\

$$E[\rho] \cong \int_0^{z_0} \frac{\sigma_z}{E[M_z]}\, dz \quad \ldots\ldots\ldots\ldots\ldots\ldots\ldots\ldots\ldots\ldots\ldots\ldots\ldots\ldots (2)$$

and similarly $$V[\rho] \cong \int_0^{z_0}\int_0^{z_0} \frac{\sigma_{z_1}\sigma_{z_2} C[M_{z_1}, M_{z_2}]}{E^2[M_{z_1}]\, E^2[M_{z_2}]}\, dz_1\, dz_2 \quad \ldots\ldots\ldots\ldots\ldots (3)$$

in which $C[M_{z_1}, M_{z_2}]$ = the covariance of moduli at depths z_1 and z_2. The covariance of total settlement at any two points, a, b on the surface is

$$C[\rho_a, \rho_b] = \int_0^{z_0}\int_0^{z_0} \frac{\sigma_{z_a}\sigma_{z_b} C[M_{z_a}, M_{z_b}]}{E^2[M_{z_a}]\, E^2[M_{z_b}]}\, dz_a\, dz_b \quad \ldots\ldots\ldots\ldots\ldots\ldots (4)$$

in which $C[M_{z_a}, M_{z_b}]$ = the covariance of moduli along the two lines a and b. Typically, the profile is divided into layers and summations are used in place of integrations. If the point variance of modulus is large (i.e., coefficient of variation greater than about 0.2 or 0.3) a better approximation of $E[\rho]$ can be obtained by using the first three terms of the Taylor series expansion.

Two-Dimensional Model.—The two-dimensional model developed here uses a finite element discretization of a linear elastic subsurface, and uses the first two terms of Taylor series expansions to calculate means, variances, and covariances of nodal displacements. Because stresses are a result of the analyses and depend on the spatially random modulus, in the present model, stress is a random field.

Nodal displacements are calculated in the common way by solving the system of equations

$$[K]\{\rho\} = \{P\} \quad \ldots\ldots\ldots\ldots\ldots\ldots\ldots\ldots\ldots\ldots\ldots\ldots\ldots\ldots\ldots\ldots (5)$$

in which $[K]$ = the stiffness matrix; $\{\rho\}$ = a vector of nodal displacements; and $\{P\}$ = the load vector. The first-order approximation to expected displacements (i.e., first two terms in the Taylor series expansion) is

$$E[\{\rho\}] = E^{-1}[K]\{P\} \quad \ldots\ldots\ldots\ldots\ldots\ldots\ldots\ldots\ldots\ldots\ldots\ldots\ldots\ldots (6)$$

in which $E^{-1}[K]$ = the inverse of the matrix of expected stiffnesses.

First-order approximations for the variance and covariance require partial differentiation of the displacement vector with respect to element moduli. Differentiating Eq. 5 yields

$$[K]\frac{\partial\{\rho\}}{\partial\langle M\rangle_i} + \frac{\partial[K]}{\partial\langle M\rangle_i}\{\rho\} = \frac{\partial\{P\}}{\partial\langle M\rangle_i} \quad \ldots\ldots\ldots\ldots\ldots\ldots\ldots\ldots (7)$$

in which $\langle M\rangle_i$ = the average modulus within element i. Assuming the force vector $\{P\}$ to be independent of modulus gives:

$$[K]\frac{\partial\{\rho\}}{\partial\langle M\rangle_i} = -\frac{\partial[K]}{\partial\langle M\rangle_i}\{\rho\} \quad \ldots\ldots\ldots\ldots\ldots\ldots\ldots\ldots\ldots\ldots (8)$$

Rewriting and substituting $[K]^{-1}\{P\}$ for $\{\rho\}$ yields:

$$\frac{\partial\{\rho\}}{\partial\langle M\rangle_i} = -[K]^{-1}\frac{\partial[K]}{\partial\langle M\rangle_i}[K]^{-1}\{P\} \quad \ldots\ldots\ldots\ldots\ldots\ldots\ldots\ldots (9)$$

The solution of Eq. 9 results in a $n \times m$ matrix of differentials of the form:

$$\begin{bmatrix} \frac{\partial \rho_1}{\partial \langle M \rangle_1} & \frac{\partial \rho_1}{\partial \langle M \rangle_2} & \frac{\partial \rho_1}{\partial \langle M \rangle_3} & \cdots & \frac{\partial \rho_1}{\partial \langle M \rangle_m} \\ \frac{\partial \rho_2}{\partial \langle M \rangle_1} & \frac{\partial \rho_2}{\partial \langle M \rangle_2} & & & \frac{\partial \rho_2}{\partial \langle M \rangle_m} \\ \vdots & & & & \\ \frac{\partial \rho_n}{\partial \langle M \rangle_1} & \frac{\partial \rho_n}{\partial \langle M \rangle_2} & & & \frac{\partial \rho_n}{\partial \langle M \rangle_m} \end{bmatrix} \quad \ldots\ldots\ldots\ldots \quad (10)$$

in which n = the number of displacements; and m = the number of elements. With this matrix of differentials the $n \times n$ covariance matrix for total settlement is obtained from the first-order approximation

$$C[\rho_k, \rho_l] \simeq \sum_{i=1}^{m} \sum_{j=1}^{m} \left. \frac{\partial \rho_k}{\partial \langle M \rangle_i} \right|_{E[\langle M \rangle_i]} \left. \frac{\partial \rho_l}{\partial \langle M \rangle_j} \right|_{E[\langle M \rangle_j]} C[\langle M \rangle_i, \langle M \rangle_j] \quad \ldots\ldots \quad (11)$$

Eq. 11 indicates a second important difference between the one- and two-dimensional models, in addition to random stresses. Two-dimensional settlement uncertainties depend on uncertainties in the properties of all the elements through the $\partial \rho_k / \partial \langle M \rangle_i$ terms. Correlation is introduced among nodal displacements due to common dependence on the realizations of particular random variables. This correlation would exist even if the element properties themselves were mutually independent.

Calculation of the expected displacements is the same as in the deterministic case, as long as the coefficients of variation are relatively small (less than 0.2–0.3). For greater variability, the third term of the Taylor series expansion becomes non-negligible, which increases computational requirements (see, e.g., Ref. 6). Computation of variances and covariences is not as simple as the mean, and requires large matrix operations. However, treating Poisson's ratio as deterministic lessens the burden by reducing the terms of the global stiffness matrix to the form

$$k_{s,t} = \sum_{i=1}^{w} \langle M \rangle_i \alpha_i \beta_i \quad \ldots\ldots\ldots\ldots\ldots\ldots\ldots\ldots\ldots\ldots \quad (12)$$

$$\frac{\partial k_{s,t}}{\partial \langle M \rangle} = \sum_{i=1}^{w} \alpha_i \beta_i \quad \ldots\ldots\ldots\ldots\ldots\ldots\ldots\ldots\ldots\ldots \quad (13)$$

in which $k_{s,t}$ = a term in the global stiffness matrix $[K]$; w = the number of elements contributing to $k_{s,t}$; and α_i and β_i = coefficients depending on the element dimensions and Poisson's ratio. This approach is incorporated in the present model.

Assuming Poisson's ratio, ν, to be deterministic results in an underestimate of uncertainty. As shown by Cambou (2), however, uncertainty in vertical displacement is relatively insensitive to Poisson's ratio. Although this result is particular to Cambou's model, the relative insensitivity of settlement to

Poisson's ratio can also be derived by physical reasoning.

Differential settlement, defined as an absolute rather than relative magnitude

$$\Delta\rho = |\rho_i - \rho_j| \quad \ldots\ldots\ldots\

It is important to note that element variances and covariances differ from element to element, depending on their geometry and area. Previous studies which report strong sensitivity of solutions to element size have in some cases used constant statistical properties over differing element geometries and areas; this in itself could explain the sensitivity. With constant element variance, as the number of elements increases, the variance in nodal displacements approaches zero.

Computing element covariances for grids with many differing element shapes, sizes, and orientations is costly. Approximations, as used in the present study, are discussed in Appendix I.

Comparison of Settlement Predictions from One- and Two-Dimensional Models

The finite element grid used in the present study is coarse to reduce computational requirements (Fig. 2). Yet, the agreement between the finite element

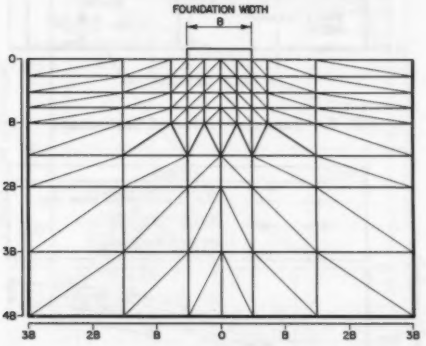

FIG. 2.—Finite Element Mesh for Two-Dimensional Model

model and exact elastic solutions is good (Fig. 3). By elastic solution, the stress on boundaries is less than 15% of the applied stress. The footing is assumed to be flexible, the base is a fixed boundary, and lateral boundaries provide horizontal restraint but allow vertical displacement. To facilitate comparison, the one-dimensional model used the same base geometry.

Two cases were considered: a homogeneous profile with spatially constant mean, point variance, and autocovariance function; and a nonhomogeneous profile with modulus increasing as the square root of depth, constant coefficient of variation and constant autocorrelation function (i.e., variance and covariance increase with depth). Two autocorrelation functions were used:

$$R(D) \propto \exp\left(\frac{-D}{R_0}\right) \quad \ldots\ldots\ldots\ldots\ldots\ldots\ldots\ldots\ldots\ldots\ldots\ldots \quad (20)$$

$$R(D) \propto \exp\left(\frac{-D}{R_0}\right)^2 \quad \ldots\ldots\ldots\

(COV) of modulus and the autocorrelation distance R_0. The following trends emerge:

1. For $R_0/B \to 0$, COV $[\rho] \to 0$, and for $R_0/B \to \infty$, COV $[\rho] \to$ COV $[M]$. These correspond to perfectly uncorrelated and perfectly correlated values of modulus, and agree with intuition.
2. For other values of R_0/B the one-dimensional model consistently yields larger total settlement uncertainty than the two-dimensional model.
3. COVs for different points on the footing differ by only about 10%.

Correlations among nodal displacements are shown in Fig. 5, and the implied differential settlement in Fig. 6. While the one-dimensional model yields consis-

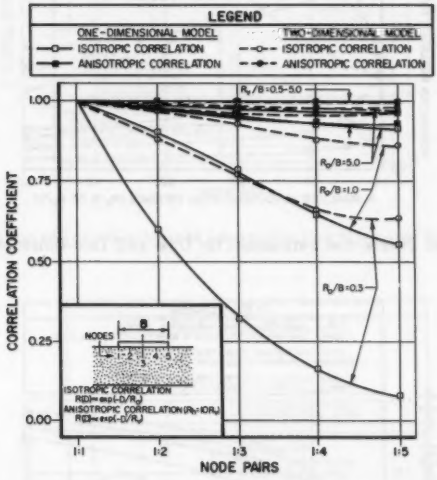

FIG. 5.—Correlation of Total Settlement Among Footing Nodes

tently higher predictions of differential settlement—because functional dependence on common subsurface elements is neglected—both models show the interesting result of a critical value of R_0/B which maximizes expected differential settlement. In retrospect, this is intuitive. The "worst" autocorrelation distance for differential settlement would seem to be in the range of $0.75B$–$1.0B$. Given typical autocorrelation distances in the range of 100 ft–200 ft (30 m–60 m), this would imply large differential settlements for mat widths of about the same dimension.

Introducing anisotropic correlation produces the results also shown in Figs. 4–6. Here the horizontal autocorrelation distance R_h was expanded to ten times the vertical, R_v. Numerically, this was accomplished by defining a new distance parameter D', obtained by shrinking the horizontal dimension ten times in calculating element properties. The apparent increase in variance of settlement

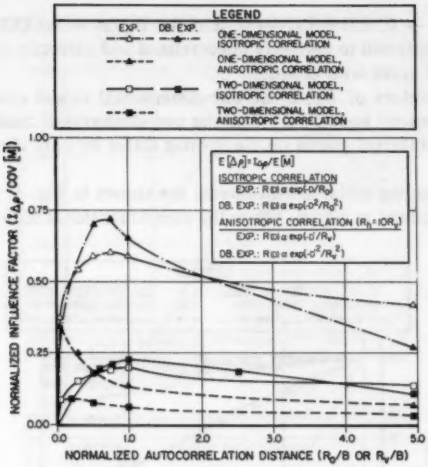

FIG. 6.—Implied Differential Settlement for One- and Two-Dimensional Models

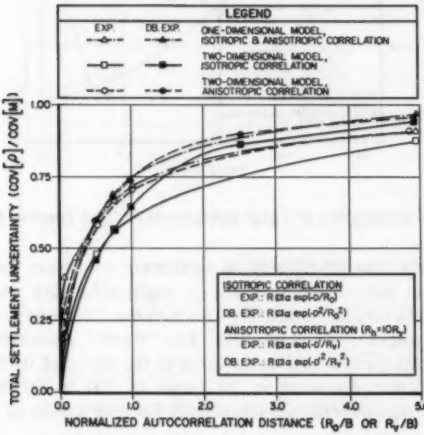

FIG. 7.—Total Settlement Uncertainty for One- and Two-Dimensional Models for Nonhomogeneous Profile

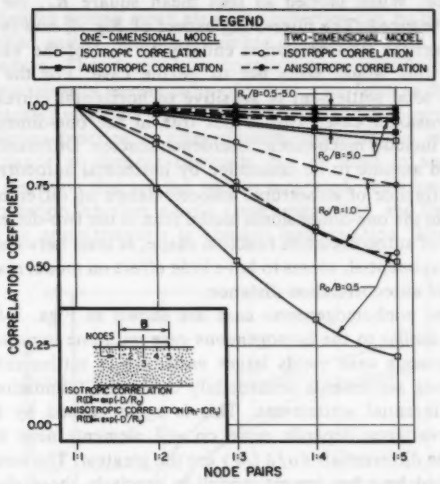

FIG. 8.—Correlation of Total Settlement Among Footing Nodes for Nonhomogeneous Profile

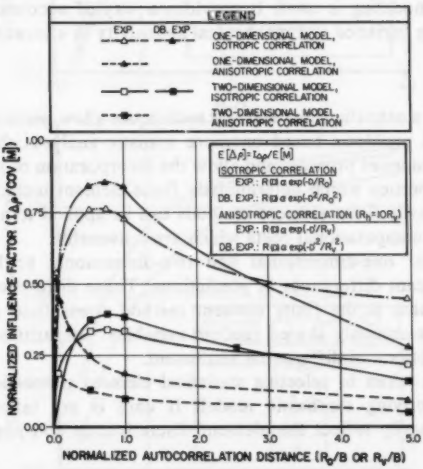

FIG. 9.—Implied Differential Settlement for One- and Two-Dimensional Models for Nonhomogeneous Profile

with the anisotropic model is more a matter of the data normalization than a real difference. When plotted as root mean square R_0, for example, the differences are reduced. The interesting aspect of Fig. 4, however, is that one would expect vertical autocorrelation entirely to control the variance of total settlement, and this would seem not to be the case. For the same vertical R_0, variance in total settlement is sensitive to horizontal correlation, at least in the two-dimensional case. This is not true in the one-dimensional model, which does not include mechanistic interdependencies. Differential settlement, which one would assume to be controlled by horizontal autocorrelation, seems to be so. The influence of anisotropic autocorrelation on differential settlement is more striking in the one-dimensional model than in the two-dimensional model.

The influence of autocorrelation function shape, at least between the exponential and double exponential, seems to have little effect on model results compared with the effect of autocorrelation distance.

Results for the nonhomogeneous case are shown in Figs. 7–9. Trends and conclusions are similar to the homogeneous case with one important exception. The nonhomogeneous case yields larger variances in settlement, and smaller correlations among settlements immediately under the foundation. This yields much larger differential settlements. This is again caused by the functional dependence. Covariance depends more on soil elements near the top of the stratum where the differentials $\partial \rho / \partial \langle M \rangle$ are the greatest. The nonhomogeneous case as formulated here has lowest moduli in precisely these elements, which even the correspondingly low-element variance does not entirely cancel. This is noteworthy, for it provides a vehicle for deciding the relative value of exploration data from different locations in minimizing errors of predictions, whether or not numerical modeling is used. It provides a way of accounting for both the spatially varying variance and mechanical sensitivity in allocating effort.

Conclusions

Second-order stochastic finite element techniques allow predictions to be made in random field problems based on more realistic analyses than current one-dimensional techniques provide, and allow the incorporation of spatial variability of material properties which deterministic finite-element techniques do not. In principle, stochastic finite element methods can be applied to a broad spectrum of problems, at computational costs which are reasonable.

Comparison of one-dimensional and two-dimensional settlement analyses indicates significant differences in predictions. These differences are primarily due to randomness in the finite element method stress field and mechanistic dependence on commonly shared random variables. Disparities are particularly distinct in predictions of differential settlement.

Care must be taken in selecting statistical element properties to accurately reflect the underlying stochastic model. If care is not taken, the resulting predictions primarily reflect the element discretization and not the underlying process.

Acknowledgment

This work was funded under PROJECT SEAGRANT, through the Massachusetts Institute of Technology Office of SEAGRANT Research.

APPENDIX I.—APPROXIMATIONS FOR ELEMENT COVARIANCES

While covariances among mean element properties can be calculated numerically as described earlier, the large number of element pairs (C_{72}^2) makes this a costly procedure. Therefore approximations were introduced. Eq. 19 is an averaging of covariances among pairs of points, one from each element. Thus, for widely separated elements (i.e., with respect to the autocorrelation distance) the autocorrelation function is approximately linear in the range of interest, and the covariance at element centroids can be used in an approximation. However, for elements that are not widely separated, the approximate linearity of the autocorrelation function is not a good assumption, and the use of centroid covariance in an approximation is brought into question. For closely spaced

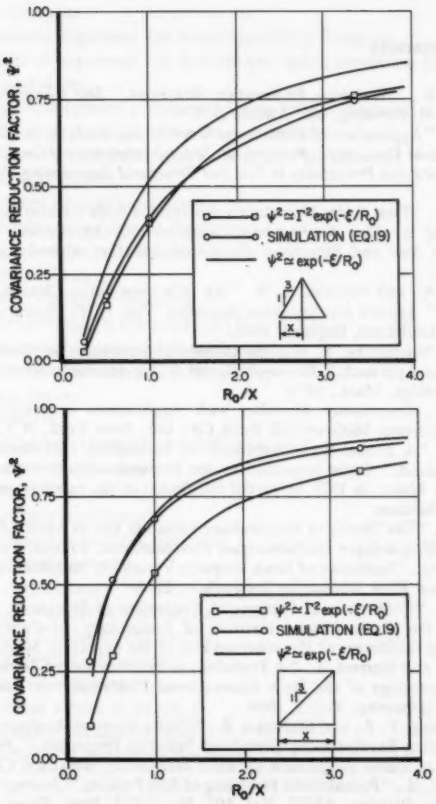

FIG. 10.—Approximations for Element Covariances

elements two approximations were considered, which seem to bound the range of element covariance as calculated from Eq. 19:

$$C[\langle M_i \rangle, \langle M_j \rangle] = \psi^2 V[M] \simeq V[M] R(\xi) \quad \ldots \ldots \ldots \ldots \ldots \ldots \quad (22)$$

$$C[\langle M_i \rangle, \langle M_j \rangle] = \psi^2 V[M] \simeq \Gamma^2 V[M] R(\xi) \quad \ldots \ldots \ldots \ldots \ldots \ldots \quad (23)$$

in which ξ = the vector separation distance between element centroids. The variance reduction factor Γ^2 is defined as $V[\langle M \rangle] / V[M]$, and ψ^2 is introduced as a covariance reduction factor. Results of these approximations are shown in Fig. 10 for two possible geometries. For geometric reasons Eq. 22 provides a better approximation than Eq. 23 when $R(\cdot)$ is approximately linear over the range of separation distances between pairs of points, one in each of the two elements. The reverse seems to be the case when $R(\cdot)$ is not approximately linear.

Appendix II.—References

1. Baecher, G. B., "Analyzing Exploration Strategies," *Site Characterization and Exploration*, C. H. Dowding, ed., ASCE, 1979.
2. Cambou, B., "Application of First Order Uncertainty Analysis in the Finite Elements Method in Linear Elasticity," *Proceedings Second International Conference on Application of Statistics and Probability in Soil and Structural Engineering*, Aachen, Germany, 1975.
3. Cornell, C. A., "First Order Uncertainty Analysis in Soils Deformation and Stability," *Proceedings of the First International Conference on Applications of Statistics and Probability in Soil and Structural Engineering*, Oxford University Press, London, England, 1971.
4. Dendrou, B. A., and Houstis, E. N., "An Inference-Finite Element Model for Field Applications," *Applied Mathematical Modeling*, Vol. 1, IPC Science and Technology Publications, Guildford, England, 1978.
5. Diaz, J., and Vanmarcke, E. H., "Settlement of Structures on Shallow Foundations: A Probabilistic Approach," *Research Report R74-9*, Massachusetts Institute of Technology, Cambridge, Mass., 1974.
6. Ditlevsen, O., *Uncertainty Modeling with Applications to Multidimensional Civil Engineering Systems*, McGraw-Hill Book Co., Inc., New York, N.Y., 1980.
7. Hilldale, C., "A Probabilistic Approach to Estimating Differential Settlement of Footings on Sand," thesis presented to the Massachusetts Institute of Technology, at Cambridge, Mass., in 1971, in partial fulfillment of the requirements for the degree of Master of Science.
8. Matheron, G., "The Theory of Regionalized Variables and its Application," *Les Cahiers du Centre de Morphologre Mathématigue*, Fountainbleau, France, Vol. 5, No. 5, 1971.
9. Paraseau, W. G., "Influence of Rock Property Variability on Mine Opening Stability," *Ninth Canadian Rock Mechanics Symposium*, 1973.
10. Ramos, J. A., "Predictions of Patterns of Settlement of Structures on Sand," thesis submitted to the Massachusetts Institute of Technology, at Cambridge, Mass., in 1976, in partial fulfillment of the requirements of the degree of Master of Science.
11. Resendiz, D., and Herrera, I., "A Probabilistic Formulation of Settlement Controlled Design," *Proceedings of the Sixth International Conference on Soil Mechanics and Foundation Engineering*, Vol. 3, 1969.
12. Su, Y. L., Wang, Y. J., and Stefanko, R., "Finite Element Analysis of Underground Stresses Utilizing Stochastically Simulated Material Properties," *Proceedings of the Eleventh United States Symposium on Rock Mechanics*, Berkeley, Calif., 1969.
13. Vanmarcke, E. H., "Probabilistic Modeling of Soil Profiles," *Journal of the Geotechnical Engineering Division*, ASCE, Vol. 102, No. GT11, Proc. Paper 13365, 1977, pp. 1247–1265.
14. Veneziano, D., and Antoniano, J., "Reliability Analysis of Slopes: Frequency Domain

Analysis," *Journal of the Geotechnical Engineering Division*, ASCE, Vol. 105, No. GT2, Proc. Paper 14378, 1979, pp. 165–182.
15. Wu, T. H., and Kraft, L. M., "The Probability of Foundation Safety," *Journal Soil Mechanics and Foundation Division*, ASCE, Vol. 93, No. SM5, Proc. Paper 5459, 1967, pp. 213–231.

Appendix III.—Notation

The following symbols are used in this paper:

A_i = area of element i;
a = element dimension;
B = boundation width;
b = element dimension;
$C[\cdot,\cdot]$ = covariance;
D = distance argument for autocorrelation function;
D' = distance argument for anisotropic autocorrelation function;
$E[\cdot]$ = expectation;
$\langle\cdot\rangle$ = expected (mean) parameter value within element;
I_ρ = influence coefficient for total settlement;
$I_{\Delta\rho}$ = influence coefficient for differential settlement;
$[K]$ = stiffness matrix;
$k_{s,t}$ = element of stiffness matrix;
M, M_z = modulus, modulus at depth z;
m_M = spatial mean of modulus;
P = vertical load;
$R(\cdot)$ = autocorrelation function;
R_0 = autocorrelation distance $[R(R_0) = 1/e]$;
R_h = horizontal autocorrelation distance;
R_v = vertical autocorrelation distance;
$\{P\}$ = load vector;
$V[\cdot]$ = variance;
w = number of elements contributing to $k_{s,t}$;
x = horizontal dimension;
z = vertical dimension;
α, β = arbitrary coefficient;
Γ^2 = variance reduction function;
ν = Poisson's ratio;
ξ = vector distance between element centroids;
ρ, ρ_i = total vertical settlement, at node i;
$\{\rho\}$ = nodal displacement vector;
$\Delta\rho$ = differential settlement;
$\Delta\rho_r$ = relative settlement;
σ_z = vertical stress at depth z;
σ^2 = variance parameter; and
Ψ^2 = covariance reduction function.

JOURNAL OF THE GEOTECHNICAL ENGINEERING DIVISION

IGNITION TEST FOR SOIL ORGANIC-CONTENT MEASUREMENT

By Abdul-Amir W. N. Al-Khafaji,[1] A. M. ASCE
and Orlando B. Andersland,[2] M. ASCE

INTRODUCTION

Soil organic matter includes plant and animal residues in various stages of decomposition together with soil microorganisms that are involved in these processes. Problems associated with decomposition in organic soils are often avoided by engineers because of uncertainties in organic-content measurement and lack of information on the effects of decomposition on soil engineering characteristics. In many cases decomposition rates are slow, so that the effects can be ignored. A decrease in strength or additional settlement during the service life of these materials may go unnoticed. In many cases the potential for problems is solved by organic-soil removal and replacement with mineral soils. A need exists for improved methods suitable for evaluation of the organic content, degree of decomposition, and prediction of future engineering properties.

Measurement of soil organic content requires that mineral solids be separated from organic solids. Destruction of the organic material by ignition is the method more commonly used by engineers. The high temperatures needed for the ignition test require that a correction be made for loss of surface hydration water from the mineral solids. Also, the ignition test provides only partial information on the degree of decomposition based on weight loss of organic solids. Both undecomposed organic matter and microorganisms formed during decomposition are destroyed by the high ignition temperatures. Information on the degree of decomposition and possible future decrease in the organic content would be useful on many engineering projects.

[1]Asst. Prof. of Civ. Engrg., Univ. of Detroit, Detroit, Mich. 48221.
[2]Prof. of Civ. Engrg., Michigan State Univ., East Lansing, Mich. 48824.

Note.—Discussion open until September 1, 1981. To extend the closing date one month, a written request must be filed with the Manager of Technical and Professional Publications, ASCE. Manuscript was submitted for review for possible publication on April 22, 1980. This paper is part of the Journal of the Geotechnical Engineering Division, Proceedings of the American Society of Civil Engineers, ©ASCE, Vol. 107, No. GT4, April, 1981. ISSN 0093-6405/81/0004-0465/$01.00.

Use of kaolinite with pulp fibers in preparation of model soils permitted precise control over the organic and mineral fractions, fiber type, and size. Nutrients added to the model soils, in proportions similar to those found in an average bacterial cell (13), and storage of anaerobic samples at a temperature close to 35° C helped accelerate decomposition in the laboratory. Measurement of organic content of decomposing soils by use of the ignition test is reviewed and a correction factor which appears suitable for use with natural organic soils is presented with an error analysis. A relationship between microorganism cell content, undecomposed organic matter, the mineral fraction, and the degree of decomposition has been developed. Several conclusions summarize the results on soil organic content measurement using the ignition test.

Experimental Work

The experimental work involved preparation of model organic soil samples, accelerated decomposition, and ignition tests. A brief description of the soil materials, sample preparation, decomposition photos, and ignition test are included.

Materials Studied.—The kaolinite included particles with 100% passing 40 μm, 93% passing 10 μm, and 42% passing 1 μm. The grain size distribution was relatively uniform. Consistency limits included a liquid limit of 47.8%, plastic limit of 27.5%, and plasticity index of 20.3%.

Pulp fibers included a range of sizes with a weighted average length of 1.6

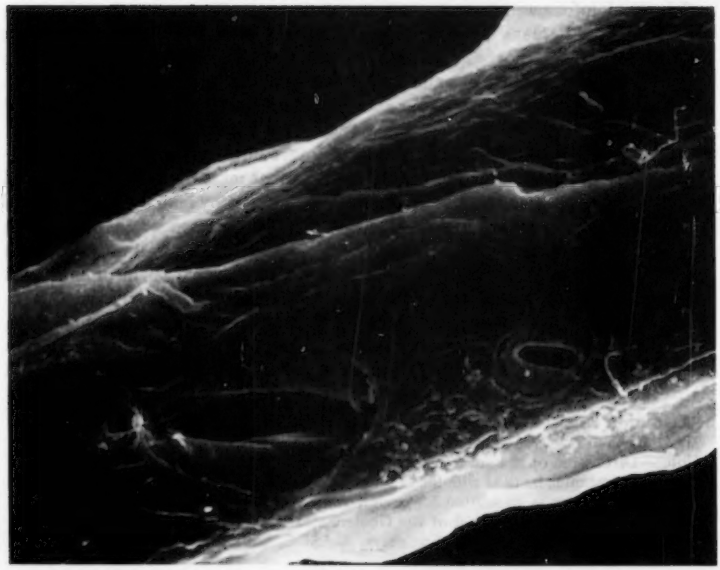

FIG. 1.—Surface Appearance of Pulp Fiber, 2000× Magnification (10)

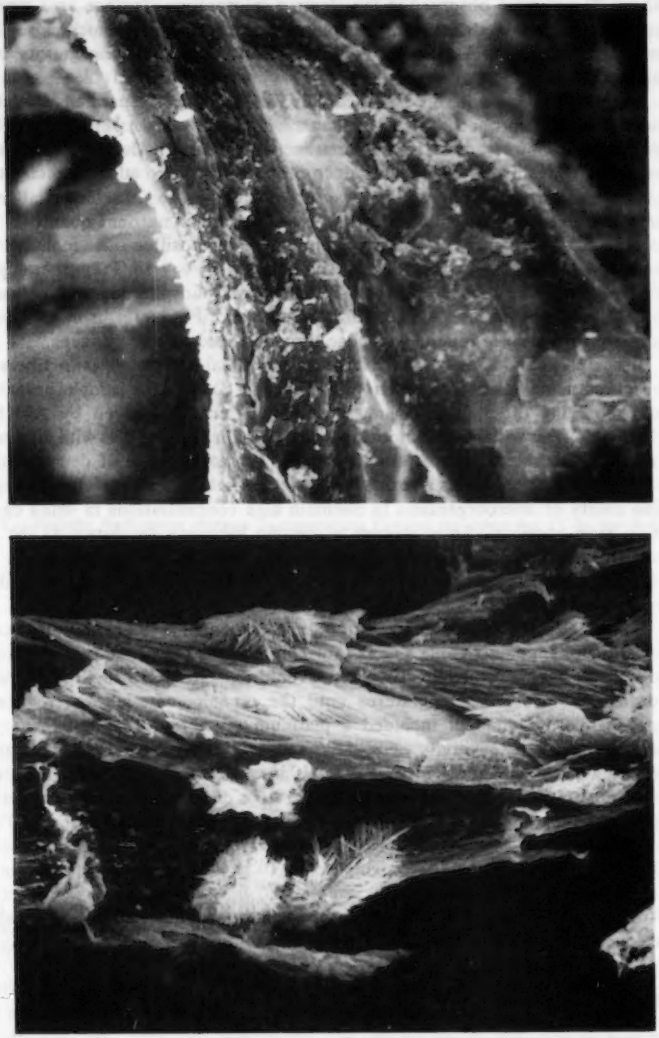

FIG. 2.—Partially Decomposed Pulp Fibers, 1000× Magnification (1): (*a*) Cracks at Fiber Surface Indicate Fiber Breakdown; (*b*) Advanced Stage of Decomposition Suggests Loss of Structural Integrity

mm, based on the test procedure given in Ref. 5, and typical diameters of about 20 μm were observed in the electron microscope. Surface area measurements, using the water vapor absorption method (7), gave values close to 133 m^2/g of dry fiber. A value of 1.54 was used for the specific gravity of the almost pure cellulose fibers.

Sample Preparation.—Freeze-dried pulp fiberboard was separated into a fluffy mass. Selected proportions of dry kaolinite and dry fiber were mixed. Next, distilled water was added in amounts needed to form a slurry. Nutrients and seed microorganisms, in predetermined proportions, were added directly to the clay-fiber slurry to help accelerate anaerobic decomposition of selected laboratory samples. Nitrogen served as the base by which other nutrient quantities were computed. Approximate ratios giving optimal decomposition rates included C/N = 30:1, P/N ≃ 1:5, and (Mg, Fe, K, Ca, and Na)/N ≃ 1:16. Pulp fiber supplied carbon, NH_4Cl supplied nitrogen, K_2HPO_4 for phosphorous and potassium, $MgSO_4$ for magnesium, $CaCl_2$ for calcium, and $FeCl_3$ for iron. About 1% (dry-weight basis) of municipal sludge provided seed microorganisms.

Decomposition Photos.—The extent of microbial attack on pulp fibers was observed using a scanning electron microscope. Details for sample preparation and mounting of samples on small aluminum stubs are given by Al-Khafaji (1). A pulp fiber with no decomposition, shown in Fig. 1, has holes with dimensions ranging from about 2 μm up to 15 μm. An advanced stage of decomposition, shown in Fig. 2, indicates a general breakdown of the fiber's structural integrity. The ability of microorganisms to maintain high concentrations in small cavities may have accelerated the process at certain locations as shown at the fiber surface in Fig. 2(*a*). Colonies of rod shaped bacteria are visible on the fiber surface in Fig. 2(*b*). These photographs help one visualize changes in the fibrous organic material due to decomposition.

Ignition Test.—Soil organic material is combustible whereas the mineral constituent is incombustible and ash forming. Separation of the two soil components was accomplished by firing an oven-dried (105° C) sample in a muffle furnace at specified temperatures until the organic material was reduced to an ash. Test equipment included a platinum crucible with lid, an analytical balance having a sensitivity of 0.1 mg, and an electric muffle furnace capable of maintaining selected temperatures within ±25° C. Weight-reduction curves for the materials, pulp fiber and kaolinite, were determined using temperatures ranging from 200° C to 900° C with oven-dried fiber sample sizes sufficient to yield minimum ash (or residue) weights of 10 mg–20 mg. For samples containing mineral fractions, oven-dry weights up to 10 g were used. After ignition and some cooling, the crucible with sample and lid was placed in a desiccator. When cooled to room temperature the weight was determined. The ash (or residue) fraction was determined from the equation

$$X_m = \frac{\text{weight of ash or residue}}{\text{oven dry sample weight}} \quad \ldots\ldots\ldots\ldots\ldots\ldots\ldots\ldots\ldots\ldots\ldots\ldots (1)$$

The organic fraction X_f, without corrections, was taken to be $(1 - X_m)$. A correction for loss of surface hydration water from the mineral fraction is developed in a later section. Organic fractions for the decomposing model soils were obtained in the same manner using small oven-dry samples.

Soil Organic Content

Soil organic material includes plant and animal residues in various stages of decomposition together with soil microorganisms that are involved in these processes. Background information, helpful in understanding soil organic-content measurement, is used in developing a correction factor for loss of surface hydration water from the clay minerals in multicomponent and natural soils. An error analysis helps evaluate the accuracy of soil organic-content measurements.

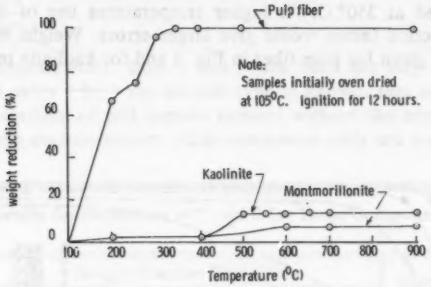

FIG. 3.—Weight Reduction Versus Temperature Curves (Ignition for 12 h) for Pulp Fiber, Kaolinite, and Montmorillonite (1)

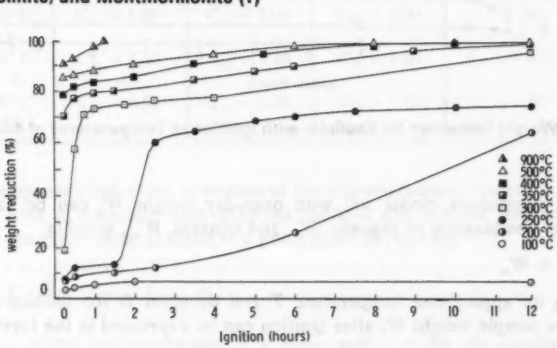

FIG. 4.—Weight Reduction for Pulp Fiber with Ignition at Temperatures of 100° C–900° C (1)

Background Information.—For engineering purposes the ignition test is the most common laboratory method used for measurement of soil organic content. The ignition test, described previously, can err by up to 15% due to loss of surface hydration water from the clay minerals (11). The American Society for Testing Materials (ASTM) standard method (Designation D 2974-71) of test for organic matter of peat materials involves the ignition test with no correction factor. Peat samples with small mineral fractions would lose little surface hydration

water. Skempton and Petley (14) indicate that mineral matter (oven dried at 105° C) loses about 3.8% by weight when ignited at 550° C. Arman (2) recommends use of oven-dried samples followed by combustion at 440° C with no correction factor. Franklin et al. (6) found that burning at 400° C–450° C until constant weight was attained gave reasonable organic contents.

To provide accurate information on change in organic content for the decomposing model organic soils, weight-reduction curves for the model soil components, pulp fiber and kaolinite, were determined as shown in Fig. 3. These curves show that at a temperature of 400° C maintained for 12 h there was a minimum loss of surface hydration water from the kaolinite. All the pulp fiber was ignited at 350° C. At higher temperatures use of the ignition test without a correction factor would give larger errors. Weight reduction versus time curves are given for pulp fiber in Fig. 4 and for kaolinite in Fig. 5.

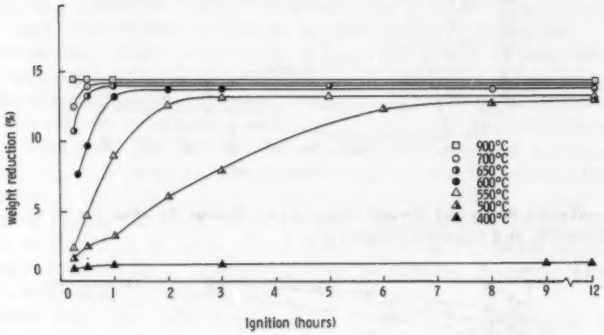

FIG. 5.—Weight Reduction for Kaolinite with Ignition at Temperatures of 400° C–900° C (1)

A two component model soil with oven-dry weight W_1 can be expressed as a linear combination of organic, W_f, and mineral, W_m, weights:

$$W_1 = W_f + W_m \quad \ldots \ldots \ldots

$$X_f = \frac{\frac{W_2}{W_1} - C_2(T,D)}{C_1(T,D) - C_2(T,D)} \quad \ldots\ldots\ldots\ldots\ldots\ldots\ldots\ldots\ldots\ldots\ldots\ldots (6)$$

and $X_m = 1 - X_f$ $\ldots\ldots\ldots\ldots\ldots\ldots\ldots\ldots\ldots\ldots\ldots\ldots\ldots\ldots\ldots\ldots\ldots\ldots (7)$

Selection of $T = 400°$ C and $D = 12$ h gives $C_1(T,D) = 0.00$ from Fig. 4 and $C_2(T,D) = 0.986$ from Fig. 5. Substitution into Eq. 6 and rearrangement of terms gives

$$X_f = 1 - 1.014\frac{W_2}{W_1} \quad \ldots\ldots\ldots\ldots\ldots\ldots\ldots\ldots\ldots\ldots\ldots\ldots\ldots\ldots\ldots\ldots\ldots\ldots (8)$$

for the model organic soils. Eqs. 6 and 7 are valid for any two-component soil. For special cases where the mineral type is known, this method provides a tool for measurement of soil organic content without the need for complete combustion of the organic matter. Multicomponent soils are considered in the next section.

TABLE 1.—Example Combinations of T and D for Three-Component Model Soil

Combination (1)	Weight Fraction Remaining			Sample weight for T and D (5)
	Pulp fiber (2)	Kaolinite (3)	Sand (4)	
$T_1 = 105°$ C $D_1 = 24$ h	$C_{11} = 1.00$	$C_{12} = 1.00$	$C_{13} = 1.00$	W_1
$T_2 = 500°$ C $D_2 = 1.5$ h	$C_{21} = 0.10$	$C_{22} = 0.95$	$C_{23} = 1.00$	W_2
$T_3 = 900°$ C $D_3 = 1.5$ h	$C_{31} = 0.00$	$C_{32} = 0.86$	$C_{33} = 1.00$	W_3

Multicomponent Soil.—An extension of the two-component system is possible for soils with n materials with different thermal and ignition characteristics. Consider the preceeding analysis in a generalized form, thus

$$W_j = \sum_{i=1}^{n} C_{ij}\bar{W}_i; \quad j = 1, 2, \ldots, n \quad \ldots\ldots\ldots\ldots\ldots\ldots\ldots\ldots\ldots\ldots\ldots\ldots (9)$$

in which i = the ith component of a given soil; j = the jth combination of temperature T and duration D; C_{ij} = the weight fraction remaining of the ith soil component; and W_j = the total weight of the soil sample at the jth combination of T and D. For a three component soil ($n = 3$), summing Eq. 9 over i gives

$$W_j = C_{1j}\bar{W}_1 + C_{2j}\bar{W}_2 + C_{3j}\bar{W}_3 \quad \ldots\ldots\ldots\ldots\ldots\ldots\ldots\ldots\ldots\ldots (10)$$

Consider a three-component model soil which contains pulp fiber, kaolinite, and sand. Select three combinations of T and D; $(T_1, D_1) = (105°$ C, 24 h); $(T_2, D_2) = (500°$ C, 1.5 h), and $(T_3, D_3) = (900°$ C, 1.5 h). Data from Figs. 4 and 5 provide the information in Table 1 for the matrix in Eq. 10. For this example it was assumed that sand loses no surface hydration water. Using

the inverted matrix the weight of pulp fiber $\bar{W}_1$, kaolinite $\bar{W}_2$, and sand $\bar{W}_3$ may be determined.

$$\bar{W}_1 = 1.448\ W_1 - 4.474\ W_2 + 3.026\ W_3;\quad \bar{W}_2 = -1.316\ W_1 + 13.158\ W_2 - 11.842\ W_3;\quad \bar{W}_3 = 0.864\ W_1 - 8.684\ W_2 + 8.816\ W_3 \quad \ldots\ldots\ldots\ldots \quad (11)$$

Note that only the oven-dry weight W_1 and the ignition weights W_2 and W_3 are needed to determine the weight fractions of pulp fiber $X_1 = \bar{W}_1 / W_1$, kaolinite $X_2 = \bar{W}_2 / W_1$, and sand $X_3 = \bar{W}_3 / W_1$.

Natural Organic Soils.—In the usual case mineral type(s) present in natural organic soils are unknown and the methods described previously will be of limited value. The immediate question concerned possible use of these methods for natural organic soils. Further development was encouraged by the following facts:

1. Dehydration weight losses for most minerals at temperatures around 400° C fall between that experienced by quartz and bentonite (dominant mineral compo-

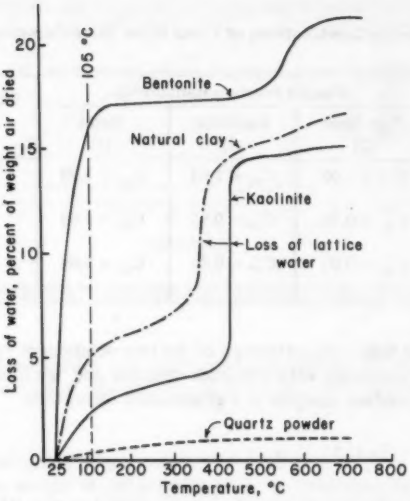

FIG. 6.—Dehydration Curves Showing Loss of Surface Hydration Water (9)

nent is montmorillonite) as shown in Fig. 6. These data give an upper bound for error due to mineral dehydration.

2. Composition of the soil organic matter is very complex and varies with age and origin, however, the main organic constituent is generally assumed to be similar to cellulose (6). With this assumption the spectrum of organic matter in soil becomes limited.

3. Since the mineral type is generally unknown, the temperature and duration of ignition must be selected so that a minimal loss of surface hydration water

occurs. Ball (3) indicated that critical dehydration for minerals occurs between 450° C and 600° C.

4. Complete combustion of pulp fiber occurs at 400° C as shown in Fig. 3. This fiber is similar in composition to many soil organic materials which are fully combustible at temperatures below 400° C (2,8).

Examination of Figs. 3 and 6 and recalling the four items previously listed, attention is directed to two facts. Regardless of the mineral type the weight loss due to mineral dehydration appears to be limited to about 2% at a temperature of 400° C provided that the soil samples were initially oven dried at 105° C. Skempton and Petley (14) observed that thermal dehydration curves for a number of common soil minerals (excluding montmorillonite) showed less than 3% weight loss due to dehydration at 400° C. Depending on sample size ignition at 400° C may be continued beyond 12 h until constant weight is attained.

It appears that soil organic content may be determined for most natural soils without regard for mineral content or origin. Consider Eq. 6 in the form

$$X_f = \frac{\frac{W_2}{W_1} - C_2(400^\circ\text{ C, }12\text{ h})}{C_1(400^\circ\text{ C, }12\text{ h}) - C_2(400^\circ\text{ C, }12\text{ h})} \quad \ldots\ldots\ldots\ldots\ldots\ldots \quad (12)$$

in which $C_1(400^\circ\text{ C, }12\text{ h}) = 0$ for the organic matter and $C_2(400^\circ\text{ C, }12\text{ h}) = 0.98$ for montmorillonite (Fig. 3). Substitution of these values into Eq. 12 gives the organic fraction X_f of a soil in terms of the initial oven dry weight W_1 and sample weight W_2 at 400° C after 12 h ignition, thus

$$X_f = 1 - 1.02\frac{W_2}{W_1} \quad \ldots\ldots\ldots\ldots\ldots\ldots\ldots\ldots\ldots\ldots\ldots\ldots \quad (13)$$

The mineral fraction is given by Eq. 7. The correction of 0.02 is smaller than the value 0.04 given by Skempton and Petley (14). Two possible reasons include their higher ignition temperature (550° C versus 400° C) and their assumption that the organic carbon = 0.58 × organic content. Broadbent (4) stated that the constant (0.58) is based on very old work and the value may range from 0.5–0.58. Greater accuracy would be attained if dehydration information on the mineral matter contained in a given natural organic soil were used in Eq. 12. A discussion on possible errors is given in the next section.

Error Analysis.—Advantages of the suggested procedure and correction factor become more apparent when errors associated with other ignition methods are evaluated. Three procedures considered include: (1) Samples air dried at 25° C before ignition at 900° C for 75 min; (2) samples oven dried at 105° C before ignition at 900° C for 75 min; and (3) samples oven dried at 105° C before ignition at 400° C for 12 h. Note that complete combustion of the organic matter occurs in all three procedures. The total weight loss fraction X_L experienced by the ignition soil samples can be written as

$$X_L = C_m X_m + X_f' \quad \ldots\ldots\ldots\ldots\ldots\ldots\ldots\ldots\ldots\ldots\ldots\ldots \quad (14)$$

in which C_m = the weight-loss fraction due to mineral dehydration; X_m = the mineral fraction; and X_f' = the true organic fraction. Note that C_m is dependent on temperature, duration of ignition, and mineral type. Recall that $(X_m + X_f')$

= 1, thus the true organic fraction $X_f' = (X_L - C_m)/(1 - C_m)$. Note that the experimental organic fraction X_f will always be greater than the true organic fraction X_f' since it includes loss of mineral surface hydration water. As a result the weight loss fraction due to ignition, X_L, with no corrections, is assumed to equal the organic fraction X_f.

Now determine the maximum possible difference (MPD) between the experimental and true organic fractions.

$$\text{MPD} = |X_f - X_f'| = \left| X_L - \frac{X_L - C_m}{1 - C_m} \right| \quad \ldots\ldots\ldots\ldots\ldots\ldots \quad (15a)$$

$$\text{or} \quad \text{MPD} = \left| C_m \frac{(1 - X_L)}{(1 - C_m)} \right| \quad \ldots\ldots\ldots\ldots\ldots\ldots\ldots\ldots \quad (15b)$$

Examination of Eq. 15 shows that the MPD is a linear function of the weight-loss fraction due to ignition. Note that the highest MPD that can be attained equals

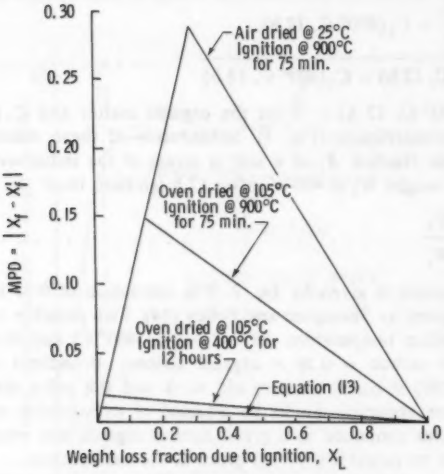

FIG. 7.—Maximum Possible Difference (MPD) Between Experimental and True Organic Fractions for Three Ignition Test Procedures (1)

C_m and this occurs only when $C_m = X_L$. This means that the maximum error in the ignition test will occur only when the weight-loss fraction equals that of the mineral fraction.

Consider first a soil sample that has been oven dried at 105° C followed by ignition at 900° C for 75 min. The maximum anticipated error in the organic fraction will be about 0.15 (Ref. 11). This represents the maximum possible weight loss due to surface hydration water for any mineral. If weight loss fractions are less than 0.15 ($X_L < 0.15$), this loss must be attributed to mineral dehydration and substitution of $C_m = X_L$ into Eq. 15 gives

$$\text{MPD} = \left| \frac{X_L(1 - X_L)}{(1 - X_L)} \right| = X_L \quad \text{for} \quad 0 \geq X_L \leq 0.15 \quad \ldots\ldots\ldots\ldots (16)$$

If the weight-loss fraction due to ignition, X_L, is greater than 0.15 it must be assumed that $C_m = 0.15$ and Eq. 15 becomes

$$\text{MPD} = \left| \frac{0.15(1 - X_L)}{(1 - 0.15)} \right| = |0.176(1 - X_L)| \quad \text{for} \quad 0.15 \leq X_L \leq 1.00 \qquad (17)$$

These relationships are shown in Fig. 7. Note that the MPD will be zero when $X_L = 1.00$. In this case the mineral fraction must be zero. A similar analysis was made for an air-dried sample and the new procedure as shown in Fig. 7. For the new procedure the 2% error is eliminated using the linear equation solution and the only error remaining is due to the presence of sand which experiences about 1% rather than 2% weight loss in surface hydration water. Thus the maximum error of ±1% may be expected for Eq. 13 using oven-dried samples (105° C) followed by ignition at 400° C for 12 h or until constant weight is attained.

Degree of Decomposition

Decomposition involves microbial activity with the formation of gases, water, new bacterial cells, and a decrease in the organic solids content. Completion of the process means that some organic material will remain, the non-degradable

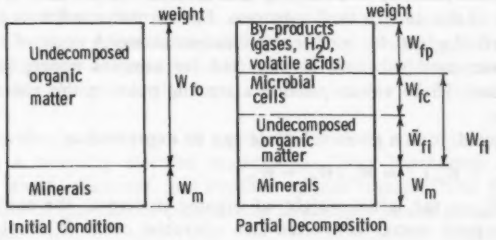

FIG. 8.—Schematic Diagram Showing Organic Soil Solids, before and after Partial Decomposition (1)

residue (humus). The ignition test for measurement of soil organic content does not distinguish between types of organic material, hence a correction factor is needed when computing the degree of decomposition based on the initial and final soil organic fractions.

Background Information.—Both aerobic- and anaerobic-decomposition processes result in substantial weight losses of organic matter. It is reasonable to take these weight losses as a quantitative measure of the degree of decomposition, X_{di}, thus

$$X_{di} = (W_{fo} - \bar{W}_{fi})(W_{fo})^{-1} \quad \ldots\ldots\ldots\ldots\ldots\ldots\ldots\ldots\ldots\ldots (18)$$

in which W_{fo} = the initial weight of organic matter in the soil and $\bar{W}_{fi}$ = the weight of undecomposed organic matter after partial decomposition as shown in Fig. 8. However simple Eq. 18 may appear, separation of the organic material from the inorganic fraction is very difficult. Define the initial organic fraction $X_{fo} = W_{fo}/(W_{fo} + W_m)$ and the organic fraction after partial decomposition $X_{fi} = \bar{W}_{fi}/(\bar{W}_{fi} + W_m)$ where symbols are as described in Fig. 8. Solve for W_{fo} and $\bar{W}_{fi}$, substitute into Eq. 18, and with rearrangement write

$$X_{di} = \left(1 - \frac{X_{fi}}{X_{fo}}\right) \frac{1}{(1 - X_{fi})} \quad \ldots\ldots\ldots\ldots\ldots\ldots\ldots\ldots \quad (19)$$

Determination of X_{fo} and X_{fi} using the ignition test permits computation of the degree of decomposition X_{di}.

Biomass Considerations.—Microorganisms in biological decomposition processes involve conversion of organic solids into stable humuslike products. The substrate (material on which the organisms live) is transformed into water, gases, volatile acids, and new microorganism cells (13). A schematic diagram showing the changes for a typical organic soil undergoing decomposition is shown in Fig. 8. The microorganisms are lumped with undecomposed organic matter in the usual ignition test for determination of organic content. Consequently, the degree of decomposition will always be greater than the value given by Eq. 19. The error would be corrected if the microorganism cell content were determined and subtracted from the current organic content.

Values for the biomass can be approximated using the Kjeldal method for organic nitrogen determination and McCarty's energetics model. McCarty (12) defined the cell yield, y, of a decomposed substrate as the ratio of the biomass to the mass of the decomposed substrate. For aerobic conditions the cell yield ranges from 0.15 g/g–0.4 g/g of decomposed substrate. A range of 0.05 g/g–0.20 g/g of decomposed substrate is predicted for samples undergoing anaerobic decomposition. These values provide a starting point in the absence of more precise data.

The cell yield, y, in a given substrate can be expressed as

$$y = W_{fc}(W_{fo} - \bar{W}_{fi})^{-1} = W_{fc}(W_{fc} + W_{fp})^{-1} \quad \ldots\ldots\ldots\ldots\ldots\ldots \quad (20)$$

in which W_{fo} = the initial weight of organic matter in the soil; W_{fc} = the weight of organic matter converted into microbial cells; $\bar{W}_{fi}$ = the weight of undecomposed organic matter; and W_{fp} = the weight of decomposition byproducts. The degree of decomposition defined by Eq. 18 can be rearranged to the form $(W_{fc} + W_{fp}) = X_{di} W_{fo}$. Substitution into Eq. 20 and rearrangement gives

$$X_{di} - yX_{di} = \frac{W_{fo} - W_{fi}}{W_{fo}} = \frac{1 - \dfrac{X_{fi}}{X_{fo}}}{1 - X_{fi}} \quad \ldots\ldots\ldots\ldots\ldots\ldots\ldots\ldots \quad (21)$$

Note that the right-hand side of Eq. 21 agrees with Eq. 19. Rearrangement of Eq. 21 gives the degree of decomposition

$$X_{di} = \frac{1}{(1 - y)} \left(\frac{1 - \dfrac{X_{fi}}{X_{fo}}}{1 - X_{fi}}\right) \quad \ldots\ldots\ldots\ldots\ldots\ldots\ldots\ldots \quad (22)$$

in which y = the cell yield; X_{fo} and X_{fi} = the initial and final organic fractions given by Eq. 13. The factor, $(1 - y)^{-1}$, is a biomass error term and it is dependent on environmental and microbial nutritional parameters related to the decomposition process. When estimating the degree of decomposition in an organic soil deposit one can use an approximate value for y, about 0.1 for the anaerobic case. The alternative solution would be to assume y equal to zero in Eq. 22. Values for X_{fo} and X_{fi} would be based on ignition test results.

Conclusions

Model organic soils prepared from kaolinite and pulp fibers have been studied relative to use of the ignition test for soil organic content measurement and evaluation of the degree of decomposition. These conclusions are intended to reflect the findings of this investigation and are limited to the soil materials used and to the test procedures employed.

1. Use of dehydration curves for kaolinite and pulp fiber made possible the elimination of major errors associated with the ignition test for soil organic-content determination. Linear equations and experimental coefficients permitted accurate organic-content measurements for various combinations of temperature and duration of ignition.
2. The degree of organic-solids decomposition, X_{di}, was defined in terms of the initial weight of organic matter, W_{fo}, and the weight or undecomposed organic matter after partial decomposition, $\bar{W}_{fi}$, in the form $X_{di} = (W_{fo} - \bar{W}_{fi})(W_{fo})^{-1}(1-y)^{-1}$. The cell yield, y, takes into account the fact that microorganisms formed during decomposition are also destroyed in the ignition test.
3. Ignition test data taken during different stages of decomposition may be used for computation of the degree of decomposition. This approach can be used to describe changes in the organic-solids content of field soil deposits with time.
4. Visual evidence of changes in a pulp fiber due to microbial activity were shown using a scanning electron microscope. Fiber breakdown included a reduction in length, diameter, and rougher surface features. The photographs illustrated some of the factors contributing to changes in soil properties during decomposition.

Acknowledgment

This study was supported by National Science Foundation Grant No. ENG75-13765 and by the Division of Engineering Research, Michigan State University. The kaolinite and pulp fiber were provided by the National Council of the Paper Industry For Air and Stream Improvement, Inc. Their support is gratefully acknowledged.

Appendix I.—References

1. Al-Khafaji, A. W. N., "Decomposition Effects on Engineering Properties of Fibrous Organic Soils," thesis presented to Michigan State University, at East Lansing, Mich., in 1979, in partial fulfillment of the requirements for the degree of Doctor of Philosophy.

2. Arman, A., "Engineering Classification of Organic Soils," *Highway Research Record, No. 310,* National Academy of Sciences—National Academy of Engineering, Washington, D.C., 1970, pp. 75–89.
3. Ball, D. F., "Loss on Ignition as an Estimate of Organic Carbon in Noncalcareous Soils," *Journal of Soil Science,* Vol. 15, No. 1, 1964, pp. 84–92.
4. Broadbent, F. E., "Organic Matter," *Methods of Soil Analysis, Part 2, Chemical and Microbiological Properties,* American Society of Agronomy, Inc., Madison, Misc., 1965, pp. 1397–1400.
5. "Fiber Length of Pulp by Classification, Suggested Method T233 su-64," Technical Association of the Pulp and Paper Industry, Atlanta, Ga., 1964.
6. Franklin, A. G., Orozco, L. F., and Semrau, R., "Compaction and Strength of Slightly Organic Soils," *Journal of the Soil Mechanics and Foundation Division,* ASCE, Vol. 99, No. SM7, Proc. Paper 9873, July, 1973, pp. 541–557.
7. "Instruction Manual of Perkin-Elmer Shell Model 212B Sorptometer," Instrument Division, Perkin-Elmer Corporation, Norwalk, Conn., 1961.
8. Keeling, P. S., "Some Experiments on the Low-Temperature Removal of Carbonaceous Material from Clays," *Clay Mineralogy, Bulletin No. 28,* Vol. 5, 1962.
9. Kelly, W. P., Jenny, H., and Brown, S. M., "Hydration of Minerals and Soil Colloids in Relation to Crystal Structures," *Soil Science,* Vol. 41, 1936, p. 259.
10. Khattak, A. S., "Mechanical Behavior of Fibrous Organic Soils," thesis presented to Michigan State University, at East Lansing, Mich., in 1978, in partial fulfillment of the requirements for the degree of Doctor of Philosophy.
11. MacFarlane, I. C., "Engineering Characteristics of Peat," *Muskeg Engineering Handbood,* Ivan C. MacFarlane, ed., University of Toronto Press, Toronto, Ontario, Canada, 1969.
12. McCarty, P. L., "Energetics and Bacterial Growth," *Fifth Rudolph Research Conference,* Rutgers, N.J., 1969.
13. McKinney, R. E., *Microbiology for Sanitary Engineers,* McGraw-Hill Book Company, Inc., New York, N.Y., 1962.
14. Skempton, A. W., and Petley, D. J., "Ignition Loss and Other Properties of Peats and Clays from Avonmouth, King's Lynn and Cranberry Moss," *Geotechnique,* Vol. 20, No. 4, 1970, pp. 343–356.
15. "Standard Methods of Test for Moisture, Ash, and Organic Matter of Peat Materials," *Designation: D2974-71,* American Society for Testing and Materials, 1972.

Appendix II.—Notation

The following symbols are used in this paper:

C = weight fraction remaining after ignition;
C_m = weight-loss fraction due to mineral dehydration;
D = duration of ignition;
MPD = maximum possible difference between experimental and true organic fractions;
T = temperature;
W = sample weight;
W_f = weight organic material;
W_{fc} = weight microbial cells;
W_{fi} = decomposed weight organic matter;
W_{fo} = initial weight organic matter;
W_{fp} = weight byproducts (gases, H_2O, volatile acids);
W_m = weight mineral material;
$\tilde{W}$ = weight of soil component;
$\tilde{W}_{fi}$ = weight undecomposed organic matter;
X = weight fraction;

X_{di} = degree of decomposition = $1/(1 - y)[1 - (X_{fi}/X_{fo})/(1 - X_{fi})]$;
X_f = organic fraction;
X'_f = true organic fraction;
X_{fi} = final organic fraction;
X_{fo} = initial organic fraction;
X_L = total weight-loss fraction;
X_m = mineral fraction; and
y = cell yield = $W_{fc}/(W_{fo} - \bar{W}_{fi}) = W_{fc}/(W_{fc} - W_{fp})$.

JOURNAL OF THE GEOTECHNICAL ENGINEERING DIVISION

CENTRIFUGE MODELING OF COAL WASTE EMBANKMENTS[a]

By Mosaid M. Al-Hussaini,[1] M. ASCE, Deborah J. Goodings,[2] Andrew N. Schofield,[3] M. ASCE, and Frank C. Townsend,[4] M. ASCE

INTRODUCTION

Current practice for the design and analysis of coal refuse embankments facilities as outlined by the Department of Interior (2) involves the use of various analytical solutions. Soil modeling utilizing centrifugal techniques to increase gravity forces offers an attractive method for verifying the available analysis procedures. In this context a series of model embankments with various geometries and materials properties were constructed of coal waste, accelerated using a 4-m radius centrifuge to 100–120 gravities, and subjected to various reservoir levels until failure occurred. Companion triaxial tests on specimens at similar model densities were performed to obtain shear strength and permeability parameters for comparing results of conventional seepage and stability analyses with those observed in the tested models.

CENTRIFUGE MODELING PRINCIPLES PERTINENT TO SEEPAGE AND STABILITY

The basic concept of centrifuge model testing is to create a scale model similar in material properties and boundary conditions to the prototype, and to subject the scale model to an acceleration such that the increase in self-weight stresses at any point matches those at corresponding points in the prototype.

[a]Presented at the October 22–26, 1979, ASCE Annual Convention and Exposition, held at Atlanta, Ga.

[1]Prof., Kuwait Univ.; formerly Research Civ. Engr., United States Army Engr. Waterways Experiment Station, Vicksburg, Miss.

[2]Engr., TAMS, New York, N.Y.

[3]Prof., Cambridge Univ., Cambridge, England.

[4]Prof., Univ. of Florida, Gainesville, Fla. 32611; formerly Research Civ. Engr., United States Army Engr. Waterways Experiment Station, Vicksburg, Miss.

Note.—Discussion open until September 1, 1981. To extend the closing date one month, a written request must be filed with the Manager of Technical and Professional Publications, ASCE. Manuscript was submitted for review for possible publication on October 22, 1979. This paper is part of the Journal of the Geotechnical Engineering Division, Proceedings of the American Society of Civil Engineers, ©ASCE, Vol. 107, No. GT4, April, 1981. ISSN 0093-6405/81/0004-0481/$01.00.

In the case of modeling embankment stability, the pertinent controlling factors are: (1) Height of embankment and strength of material; (2) seepage conditions; and (3) pore pressure dissipation. Assuming that steady-state seepage through an embankment can be represented by a flow net of N_f flow channels and N_d equipotential drops, then the rate of flow, q, at earth's gravity through a unit width of the embankment with permeability, k, is given by:

$$q = \frac{k \Delta h N_f}{N_d} \quad \ldots \ldots \ldots

of the model can be made through a thick transparent face of the strong box. Viewing was by either of two systems: (1) A closed-circuit television (CCTV) with the video camera located at the rotor and a 45-deg mirror mounted on the strong box (see Fig. 1); or (2) vertical flash photography synchronized as the model rotated past a stationary camera viewing through the centrifuge-pit

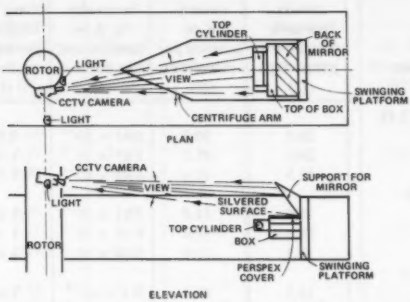

FIG. 1.—Schematic Diagram of Centrifuge Model and CCTV for Viewing

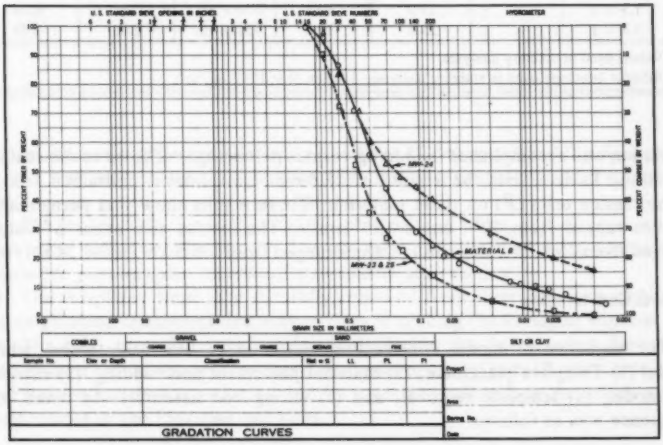

FIG. 2.—Grain-Size Distribution of Coal Waste Used in Centrifuge Models

safety cover. Additional details concerning the equipment have been presented in Refs. 3 and 7.

Materials.—Fig. 2 presents the grain-size distribution of the coal waste materials used in the models. These materials represent the minus 1.18-mm fraction of a coal waste embankment material sampled in the western United States. Material

TABLE 1.—Summary of Consolidated-Undrained Triaxial

Test identification (1)	At Shear Specimen Conditions		Permeability, k, in centimeters per second (4)	Maximum deviator stress, σ_d, in kilograms per square centimeter (5)	Induced pore pressure, $u - u_o$, in kilograms per square centimeter (6)
	Water content, w, as a percentage (2)	Dry density, d, in pounds per cubic foot (3)			
Material B; Gs = 2.43:					
B – 0.49 – 1	26.5	90.2	3.85×10^{-5}	0.92	0.20
B – 1.47 – 1	24.5	93.2	1.67×10^{-5}	1.23	1.06
B – 2.84 – 1	23.5	97.4	4.42×10^{-5}	1.67	2.36
MW 23; Gs = 2.50:					
–0.5 – 1	29.5	88.5	3.11×10^{-4}	1.05	0.23
1.5 – 1	25.6	91.4	3.26×10^{-4}	1.38	1.26
3.0 – 1	23.5	93.8	3.24×10^{-4}	2.05	2.39
MW 24; Gs = 2.43:					
0.5 – 1	18.5	99.1	2.8×10^{-8}	1.06	0.01
1.5 – 1	17.7	99.7	2.1×10^{-8}	1.60	1.06
3.0 – 1	16.3	101.4	1.01×10^{-8}	2.88	1.76
MW 25: Gs = 2.50:					
0.5 – 1	27.2	89.1	5.36×10^{-4}	1.34	0.14
1.5 – 1	25.9	89.8	3.72×10^{-4}	1.88	1.12
3.0 – 1	25.5	92.3	4.64×10^{-4}	2.06	2.29

[a] Values used in stability analyses.
[b] Bilinear envelope used in stability analyses; 1 lb/cu ft = 16.02 kg/m^3.

variation was accomplished by adding various percentages of fines to the scalped fraction. Table 1 lists the results of 35.6-mm consolidated undrained triaxial compression tests ($\bar{R}$) on these materials. These results show that permeability values ranged from 10^{-4} cm/s–10^{-8} cm/s. The results also show ϕ' values ranged from 26.9–34.7 deg and c' values ranged from 0.025 kN/m^2–0.24 kN/m^2.

Model Construction

The sequence of model construction consisted of five basic steps, which were: (1) Template placement; (2) material placement and rodding; (3) marking of model; (4) template removal; and (5) strong box assembly. In detail, the sequence was as follows:

1. Aluminum sheet templates outlining the slope, crest, and toe of the modeled embankment, and different sections such as the key and toe drain, were lightly oiled, and fitted and wedged in the strong box.
2. Subsequently, the sieved mine waste material and coarse drain material were placed behind the forming template. Since the material had been wet sieved and was stored under water, during placement it had a slushy consistency, and it was rodded not for density control, but rather to ensure that no voids remained behind the templates. After placement, the material was allowed to

Compression Tests on Coal Waste Model Material

AT MAXIMUM EFFECTIVE STRESS RATIO, σ_1/σ_3						
Effective minor stress, σ_3, in kilograms per square centimeter (7)	Principal effective stress ratio, σ_1/σ_3 (8)	Total Stress			Effective Stress[a]	
		Strain percent (9)	ϕ, in degrees (10)	C, in kilograms per square centimeter (11)	ϕ', in degrees (12)	C, in kilograms per square centimeter (13)
0.29	4.23	15.0				
0.41	4.01	15.0	8.1	0.33	34.7	0.025
0.58	3.92	13.78				
0.27	4.83	1.68				
0.24	6.71	6.76	9.5	0.36	30.5	0.23
0.61	4.37	10.24				
0.49	3.15	3.38				
0.44	4.59	10.18	15.1[b]	0.28[b]	26.9[b]	0.24[b]
1.24	3.32	13.60				
0.36	4.72	6.74	7.6	0.60	30	0.18
0.38	5.92	10.10				
0.71	3.88	10.19				

drain as the model and strong box were tilted to a 45-deg position. After drainage, the box and model were laid horizontally, the excess material was screeded away, and its moisture content was determined.

3. The model surface was then lightly spray painted white, and silvered nylon beads were placed on a 0.6 in. × 1.2 in. (15 mm × 30 mm) grid using a template to enhance photographic records of movements after testing.

4. The templates were then carefully removed from their positions and last minute patching operations undertaken prior to placing the Plexiglas window.

5. The final assembly step consisted of placing the lightly oiled Plexiglas window over the model, with its frame, and securing it by bolts. Sealing between the Plexiglas and box is accomplished by a sealant squirted on the edges prior to placement of the Plexiglas and bolts.

The test procedure then involved a delay in which balance calculations were completed, a counterweight was fitted at the other end of the balanced rotor arm, and the model package was secured to its swinging platform.

Test Results

The geometries of the models and corresponding prototype and post-test densities are listed in Table 2.

TABLE 2.—Geometries and Post-Test Densities of Coal Waste Centrifuge Models

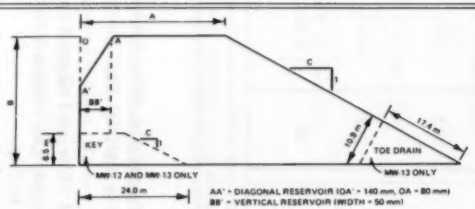

Test No. (1)	Geometry: Model A, in millimeter (2)	Model B, in millimeter (3)	Model C, in millimeter (4)	Reservoir Type (5)	Prototype[a] A, in meter (6)	Prototype[a] B, in meter (7)	Prototype[a] C, in meter (8)	Gravitational Acceleration g's (9)	Density, in pound per cubic foot[b] Wet (10)	Density, in pound per cubic foot[b] Dry (11)
MW-9	300	240	1.5	Vertical BB' = 50 mm	30.0	22.4	1.5	100	106.3	85.0
MW-10	295	260	1.5	Vertical BB' = 50 mm	35.4	28.7	1.5	120	88.4	78.2
MW-11	185	260	2	Diagonal	22.2	29.0	2	120	103.6	87.8
MW-12	185	260	2	Diagonal	22.2	29.0	2	120	104.3	88.4
MW-13	185	260	2	Diagonal	22.2	29.6	2	120	108.4	91.9
MW-23	315	195	2	Vertical BB' = 70 mm	31.5	18.6	2	100	95.8	85.5
MW-24	315	195	2	Vertical BB' = 70 mm	4.72	2.77	2	15	97.7	81.8
MW-25	315	195	2	Vertical BB' = 190 mm	31.5	18.6	2	100	106.6	87.4

[a] Prototype dimensions = model dimensions times the acceleration level.
[b] Densities used in stability analyses, 1 pound per cubic foot = 16.02 kilograms per cubic meter.

Model MW-9.—This model was slowly accelerated to 100 *g*, after which water was supplied to the reservoir from the feed pipe. A rapid rise in the piezometric levels at the base of the embankment was observed in the manometers, and the phreatic levels were also clearly observed to rise on the CCTV monitor. As the reservoir level surged upward, the phreatic level reached the position sketched in Fig. 3 and failure was observed to begin by seepage and erosion at the embankment toe. This initial erosion was followed by a succession of slip failures, which are indicated in Fig. 3. After these retrogressing failures, debris lay as a beach choking the exit and preventing further regression, but allowing seepage to flow. Additional water was then added to the reservoir which caused erosion of the slope and breaching of the model embankment.

In an analogous prototype experience, a coal waste embankment 73.6 ft (22.4 m) high would be constructed with a slope of 1 Vertical:1.5 Horizontal, with the reservoir filled with coarse rocks behind the embankment. A small stream would be directed into the reservoir and water begins to flow out from the embankment toe. Additional streamflow raising the reservoir level would then

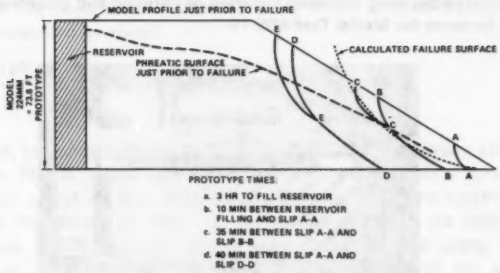
MODEL PROFILE JUST PRIOR TO FAILURE
RESERVOIR
PHREATIC SURFACE JUST PRIOR TO FAILURE
CALCULATED FAILURE SURFACE
MODEL 224MM = 73.5 FT PROTOTYPE
PROTOTYPE TIMES:
a. 3 HR TO FILL RESERVOIR
b. 10 MIN BETWEEN RESERVOIR FILLING AND SLIP A-A
c. 35 MIN BETWEEN SLIP A-A AND SLIP B-B
d. 40 MIN BETWEEN SLIP A-A AND SLIP D-D

FIG. 3.—Schematic Drawing Showing Location of Phreatic and Observed and Calculated Failure Surfaces for Model Test MW-9

cause erosion of the toe and slippages of the embankment face which lead to a stable beach with steady seepage underneath the embankment. A much larger streamflow would then be diverted into the reservoir, leading in rapid succession to a rise of the reservoir level, saturation of the coal waste embankment surface, water flow, erosion, and catastrophic breaching of the embankment. Using a scaling factor of N, the time from occurrence of the initial toe erosion until practically breaching the embankment would be 140 min.

Model MW-10.—This model was higher than Model MW-9 (as shown in Table 2) and was accelerated slowly to 120 *g*. At this stage the reservoir was filled in a more controlled fashion and attempts were made to determine seepage flow rates. The final increment of flow was perhaps applied too quickly and the phreatic line sketched in Fig. 4 probably does not reflect a steady-state condition. The full flow from the feed pipe was at a rate about 1/50 cu ft ($0.00056\ m^3$) in about 26 sec through the 6-in. (150-mm) wide model. This is equivalent to a seepage of about $2 \times 1/50 \times 120/26 = 0.185$ cu ft/sec/ft ($0.0172\ m^3/s$) of prototype embankment. The full flow from the feed pipe led to toe erosion and retrogressive slips sketched in Fig. 4. The location of the

two major slip surfaces BB and CC closely repeated the result of the test on model MW-9.

In terms of an analogous prototype experience, a coal waste embankment is built to a height of 94 ft (28.66 m). Flow of water from a reservoir through

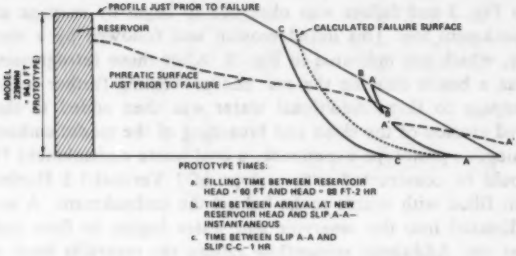
PROFILE JUST PRIOR TO FAILURE
RESERVOIR
CALCULATED FAILURE SURFACE
PHREATIC SURFACE JUST PRIOR TO FAILURE
MODEL 23INCHES = 94 FT (PROTOTYPE)
PROTOTYPE TIMES:
a. FILLING TIME BETWEEN RESERVOIR HEAD = 60 FT AND HEAD = 88 FT-2 HR
b. TIME BETWEEN ARRIVAL AT NEW RESERVOIR HEAD AND SLIP A-A—INSTANTANEOUS
c. TIME BETWEEN SLIP A-A AND SLIP C-C—1 HR

FIG. 4.—Schematic Drawing Showing Location of Phreatic and Observed and Calculated Failure Surfaces for Model Test MW-10

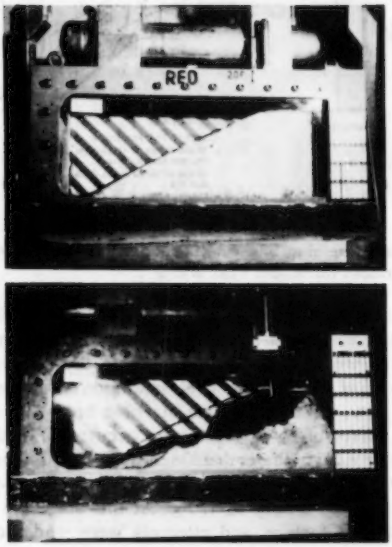

(a)

(b)

FIG. 5.—Model MW-11: (*a*) Prior to Centrifuge Test; (*b*) After Centrifuge Test

the embankment leads to erosion at the toe and retrogressive slips when the seepage flow is about 18.5 cu ft/sec (0.52 m^3/s) per 100 ft (30.5 m) of prototype embankment. The time between the initial observance of distress at the toe and major failure would be 1 h.

Model MW-11.—This model was constructed of material B (see Fig. 2) using a diagonal (sloping upstream face) reservoir filled with coarse waste material. The model was accelerated to 120 *g*, which corresponds to a notional prototype 95.3 ft (29.07 m) high. Fig. 5 shows the model before and after the test. The line of the original slope template is clearly visible in Fig. 5(*a*) and the dark mass of material at the back of the box can be seen to have settled by about 7% by the time full acceleration was reached. Supply of water to the reservoir was carefully controlled:

1. When the reservoir was at the equivalent of a 51-ft (15.56-m) head a flow rate to the model of 1/50 cu ft (0.00058 m^3) in 96 sec was measured. This rate corresponds to a flow through a notional prototype of about

$$2 \times \frac{1}{50} \times \frac{120}{96} = 0.05 \text{ cu ft/sec/ft } (0.00483 \text{ m}^3/\text{s/m}) \quad \ldots\ldots\ldots\ldots (2)$$

2. When the reservoir was at the equivalent of 74.8-ft (22.814-m) head the flow rate to the model was measured as 1/50 cu ft (0.00058 m^3) in 29 sec, which corresponded to about

$$2 \times \frac{1}{50} \times \frac{120}{29} = 0.17 \text{ cu ft/sec/ft } (0.016 \text{ m}^3/\text{s/m}) \quad \ldots\ldots\ldots\ldots (3)$$

At this stage, toe erosion began and led to a series of successive retrogressions, indicated in Fig. 6. After each slip, the accumulated debris formed a beach at a slope of about 10 deg, with steady seepage from the reservoir onto the beach. It is significant to note that the steel surface of the base of the box had not been roughened, and sliding may have occurred along this surface. The times of retrogression scaled by the factor $N = 120$ are also listed in Fig. 6. This factor $N = 120$ is based upon Malushitsky's (4) "modeling of models" and has not been confirmed. The rate of failure was accelerated by raising the reservoir to full height, after which the retrogression of erosion and slip eventually led to a catastropic breach of the reservoir wall and rapid erosion of a gully.

In analogous prototype experience, a coal waste embankment with slope of

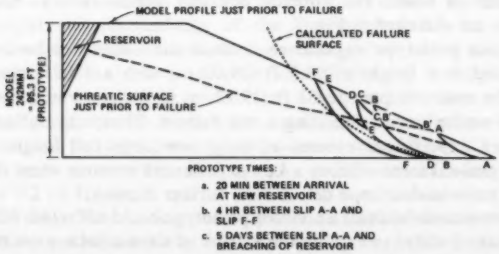
MODEL PROFILE JUST PRIOR TO FAILURE
RESERVOIR
CALCULATED FAILURE SURFACE
PHREATIC SURFACE JUST PRIOR TO FAILURE
MODEL 2.42MM = 95.3 FT (PROTOTYPE)
F E
D C
B
C B
B' A
F
F D B A
PROTOTYPE TIMES:
a. 20 MIN BETWEEN ARRIVAL AT NEW RESERVOIR
b. 4 HR BETWEEN SLIP A-A AND SLIP F-F
c. 5 DAYS BETWEEN SLIP A-A AND BREACHING OF RESERVOIR

FIG. 6.—Schematic Drawing Showing Location of Phreatic and Observed and Calculated Failure Surfaces for Model Test MW-11

1V:2H is built to a height of 95.3 ft (29.07 m). A steady supply of water from the reservoir through the base of the embankment leads to erosion at the toe when the reservoir is only three-fourths full. When the reservoir level is raised to full height, rapid retrogression leads to a breach of the reservoir wall. The time between initial observance of toe failure and catastrophic breaching of the embankment was 5 days.

Model MW-12.—This was a model of material B, with a diagonal (sloping upstream face) reservoir, and an inclusion of "key" material of coarse waste (2.36 mm–12.5 mm) at the center of the bank. Such a "key" feature had been included in the original waste embankment from which the model material had been obtained. The model was accelerated to 120 *g* in similarity with a notional prototype 95.3 ft (29.07 m) high. Reservoir filling proceeded slowly over a period equivalent to 2 days, by which stage the reservoir level was only at an equivalent prototype height of 63 ft (19.22 m) when toe failure began. The reservoir supply feed was interrupted to measure a flow of 1/50 cu ft (0.00058 m^3) in 72 sec, equivalent to

$$2 \times \frac{1}{50} \times \frac{120}{72} = 0.067 \text{ cu ft/sec/ft } (0.00644 \text{ m}^3/\text{s/m}) \quad \ldots\ldots\ldots\ldots (4)$$

of prototype. It is significant that failure was initiated at the toe when the

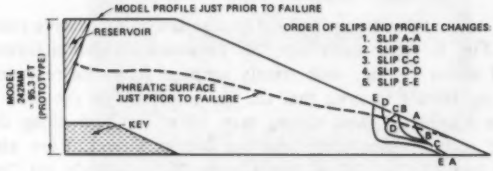

FIG. 7.—Schematic Drawing Showing Location of Phreatic Surface and Slips of Model Test, MW-12

reservoir level was only at two-thirds full height. Apparently the presence of the key material allowed seepage failure to be initiated and to progress under a lower reservoir head. The phreatic line just before failure, and the initial slip surfaces are sketched in Fig. 7.

In analogous prototype experience, a coal mine waste embankment would be constructed to a height of 95.3 ft (29.07 m) with a 1V:2H slope. A rapid raising of the reservoir pool to 63 ft (19.22 m) in 2 days would cause seepage through the embankment, initiating a toe failure. Thus, an embankment with a central key experiences erosion at only two-thirds full height; whereas a comparable embankment without a key experiences erosion when three-fourths full. Inability to remove slope debris halts further erosion.

Having thus established that a notional prototype could not retain full a reservoir of water, it was decided to explore the effects of a remedial toe drain to enhance embankment stability.

Model MW-13.—This model was constructed of material B (see Fig. 2) and had a toe drain constructed with about the same grain size as the "key" material.

However, this toe drain was to perform a more useful function; i.e., allow high seepage to pass safely without damage to the toe of the slope. The model was accelerated to 120 *g*. Water was subsequently supplied to the reservoir and the phreatic line rose higher than ever before; reaching an equivalent prototype height of 90.55 ft (27.62 m), at which it remained stable for the equivalent of 7 days without any distress at the toe of the bank. At this stage the seepage flow of 1/50 cu ft (0.00056 m^3) in 24 sec was equivalent to a prototype flow of

$$2 \times \frac{1}{50} \times \frac{120}{24} = 0.2 \text{ cu ft/sec/ft } (0.0193 \text{ m}^3/\text{s/m}) \quad \ldots\ldots\ldots\ldots\ldots (5)$$

This heavy seepage flow passed safely through the toe drain.

In an analogous prototype experience, a coal waste embankment containing an undrained "key" of coarse material, and downstream drainage control via a toe drain would be constructed on a 1V:2H slope to a height of 97.3 ft (29.68 m), at which condition it is stable. Subsequently, reservoir filling could be initiated and full reservoir capacity achieved. With this full reservoir head, the embankment could successfully allow the passage of seepage of 0.2 cu ft/sec/ft (0.0019 $m^3/s/m$) through the toe drain and remain stable.

Model MW-23.—Model MW-23 was constructed of material corresponding to gradation MW-23 in Fig. 2 and containing 8% fines. The model was accelerated to 100 *g*, and then the speed reduced to various levels, with different flow rates, to establish data to determine the permeability. At a throughflow rate of 1.21×10^{-3} cu ft/sec/ft or 112 $mm^3/s/mm$ of model width at 75 *g*, erosion occurred. Once initiated, the erosion was aggravated by the concentration of water drawn to that point; as the centrifuge speed was reduced from 100 *g* to 66 *g*, and the water supply ultimately increased to 3.54×10^{-3} cu ft/sec/ft (329 $mm^3/s/mm$) of model width, the erosion reached a clearly unacceptable level, forming a uniform blanket of debris across the model.

In analogous prototype terms, this model simulates several notional prototypes of different heights, permeabilities, and throughflows, but with constant strength parameters. A prototype embankment of height 60.7 ft (18.5 m), with permeability equal to 44 mm/s, impounding a reservoir 37.7 ft (11.5 m) deep, i.e., 62% of full capacity, and permitting a throughflow of 0.12 cu ft/sec/ft or 1.1×10^{-2} $m^3/s/m$ of embankment width is shown to be stable. By simultaneously changing height and permeability of the embankment for the same model throughflow, an embankment-dam passing a throughflow of 0.8×10^{-2} $m^3/s/m$ of embankment width from a reservoir 29.9 ft (9.1 m) in height or at 66% of full capacity is found to be unstable with respect to erosion. Once begun, the weakened point attracts more water, and the final eroded profile occurred when the notional prototype was an embankment-dam 39.4 ft (12 m) in height, with a prototype permeability of 9 mm/s, at full reservoir height passing a throughflow 0.2 cu ft/sec/ft or 2×10^{-2} $m^3/s/m$ of embankment width.

Model MW-24.—This model was prepared of material containing 34% fines (see Fig. 2) was accelerated to 9 *g* over 90 sec, and left at that speed for 13.5 min. It was further accelerated, and immediately upon achieving 15 *g*, it failed in a conventional rotational slip circle (Fig. 8), and the intact wedge of debris reclined at 16 deg to the horizontal.

In terms of analogous prototype experience, this model simulates a rate of construction failure. A prototype embankment with permeability equal to 3.8 mm/s is built to a height of 5.6 ft (1.7 m) over a 30-min period and then left to consolidate for 18 h. (Since embankment failure resulted from excessive rate of construction creating high pore pressures, the governing time factor comparing prototype with model is N^2 (3). Thus (13.5 min) $\times$ 9^2 $\div$ 60 = 18.2 h.) When, however, an attempt is made to increase the height of the embankment to 2.8 m, the slope immediately fails upon reaching that height.

Model MW-25.—This model of material containing 9% fines (see Fig. 2) was prepared identically to MW-23 but with a much wider vertical upstream face due to the decreasing supply of model soil. The model was accelerated to 100 *g* over 22 min, after which time various combinations of throughflows and centrifugal accelerations were tried to establish permeability. At 100 *g*, with a flow rate of 1.3×10^{-3} cu ft/sec/ft or 121 $mm^3/s/mm$ of embankment width, the slope was stable; for the same model flow rate, erosion began to occur when the speed of the centrifuge was reduced to 30 *g*. The erosion was permitted to continue at 30 *g* for 4 min.

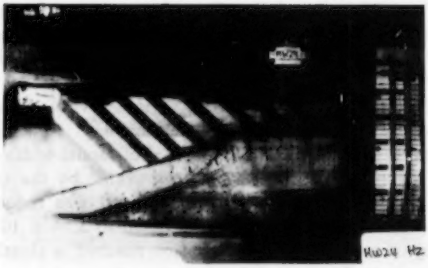

FIG. 8.—Model MW-24: Rotational Slip at 15 *g* Relative to State at 9 *g*

In analogous prototype experience, as in model MW-23, several different prototypes are simulated. An embankment of height 61.0 ft (18.6 m), impounding a reservoir 29.2 ft (8.9 m) high or 48% of capacity and passing flow of 0.13 cu ft/sec/ft or 1.2×10^{-2} $m^3/s/m$ of embankment width, was found to be stable. However, simultaneously decreasing the embankment height and permeability, so that the embankment was 18.4 ft (5.6 m) and reservoir depth was 15.4 ft (4.7 m) or at 84% capacity, and equivalent throughflow of 0.04 cu ft/sec/ft or 0.4×10^{-2} $m^3/s/m$ of embankment width caused erosion at the toe, constituting failure.

Seepage Analyses of Uniform Section

Six uniform prototype embankment sections were analyzed by conventional techniques to locate the phreatic surface and estimate isotropic permeability of the material. The phreatic surface location was calculated using Dupuit's parabolic assumption and Casagrande's location of the exit point (5). Isotropic permeabilities were estimated using Van Terson's (9) assumption for an embank-

ment resting on an impervious base; i.e.

$$q = ka \sin \alpha \tan \alpha \quad \ldots \ldots \ldots

surfaces, with the exceptions that the modeled surfaces are more linear than parabolic, their gradients are much steeper, and they intersect the downstream slope at lower elevations. However, in the case of the model embankments with diagonal reservoir faces, the lower vertical section simulates a vertical

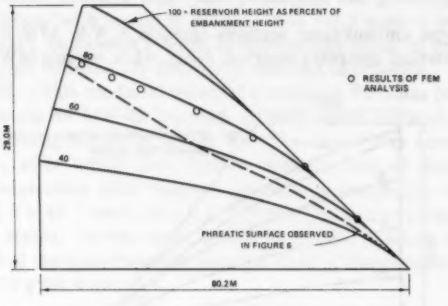

FIG. 11.—Comparison of Observed and Calculated Phreatic Surfaces for Centrifuge Model MW-11

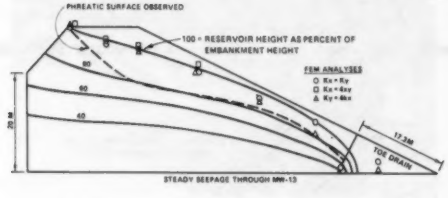

FIG. 12.—Comparison of Observed and Calculated Phreatic Surfaces for Centrifuge Model MW-13

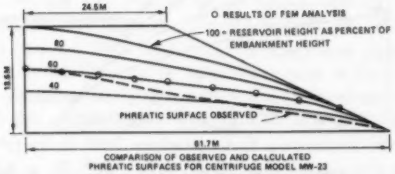

FIG. 13.—Comparison of Observed and Calculated Phreatic Surfaces for Centrifuge Model MW-23

cutoff, which is reflected as a free-fall tendency in the phreatic surface. For this reason, the observed centrifuge model phreatic surfaces deviate from the calculated values as shown in Fig. 11 for model MW-11 and later in Fig. 12 for model MW-13. In an attempt to understand the effect of the vertical cutoff on the phreatic surface of models with diagonal reservoirs, a two-dimensional

finite element method (FEM) seepage analyses (8) was performed. Model MW-11 with a diagonal reservoir was selected as representative, while MW-23 with a vertical reservoir was selected for comparison and control. The results of these FEM analyses are also presented in Figs. 11 and 13 and show that the FEM phreatic surface essentially duplicates Dupuit's (1) parabola for both reservoir conditions.

The coefficient of permeability per unit length, k, can be calculated using Eq. 1, the flow net and the measured quantity of seepage per unit length, q. For this case, the relationship

$$k = \frac{q}{h\,N}\left(\frac{N_d}{N_f}\right) \quad \ldots\ldots\ldots\

TABLE 3.—Estimates of Coefficient of Perme

Test number (1)	D_{10}, in millimeter (2)	$k \approx 100\ D_{10}^2$, in centimeters per second (3)	Flow rate, measured in model, q, in cubic centimeters per second per centimeter length (4)	Reservoir height, in meters (5)	Total height, as a percentage (6)
MW-10	0.0032	1.02×10^{-5}	1.464	22.7	79
MW-11	0.0032	1.02×10^{-5}	1.312	22.8	79
MW-12	0.0032	1.02×10^{-5}	0.528	19.2	66.2
MW-23	0.07	4.9×10^{-3}	1.06	11.5	62
MW-25	0.07	4.9×10^{-3}	1.21	8.9	48

[a] $k = q/(a \sin \alpha \tan \alpha)$.
[b] $k = q/h \cdot N \times 1/SF$.

to leakage occurring along the base or sides of the model, resulting in higher apparent permeabilities.

Stability Analyses with Seepage

It is important in centrifuge modeling not only to compare results with prototype events, but also with numerical forms of analysis. This section examines the factors of safety (FS) recommended for coal waste embankments (2), with those of the various models. In this fashion, the appropriateness of recommended procedures can be validated.

Stability analyses were performed utilizing the Corps of Engineers Modified Swedish Computer Program, as described in Ref. 6. Strength parameters utilized in these analyses were previously presented in Table 1. The stability analyses results are listed in the following:

Model	FS (modified Swedish)	Observed behavior
MW-9	0.79	Failed
MW-10	0.72	Failed
MW-11	0.70	Failed
MW-12	0.88	Failed
MW-13	1.26	Stable
MW-23	1.70	Stable
MW-25	1.70	Stable

These FS correctly, albeit conservative, predict phenomena observed in the centrifuge models. That is, models MW-9, MW-10, MW-11, and MW-12 were unstable and failed, while models MW-13, MW-23, and MW-25 were correctly predicted as stable. Failure of these latter models was by erosion, which is not considered by these analyses.

The conservative nature of the triaxial strength parameters and stability analyses is evident, and the recommended FS of 1.3–1.5 (2) is quite appropriate. A comparison between observed failure surfaces in the centrifuge models MW-9

ability, k, for Coal Waste Centrifuge Models

Distance from toe to seepage exit, a, in meters (7)	Gravitational acceleration, N (8)	Permeability k, in centimeters per second[a] (9)	Shape factor, N_f/N_d (10)	Permeability k, in centimeters per second[b] (11)
10.4	120	0.004	0.18	0.004
18.9	100	0.003	0.18	0.003
12.7	100	0.002	0.23	0.001
5.3	100	0.009	0.20	0.005
3.97	100	0.014	0.17	0.008

to MW-11 with the critical arcs estimated by the stability analyses are shown in Figs. 4–6. These critical arcs agree quite favorably with the failure surfaces observed in the models, which lends confidence to the FS derived by the analysis.

The effect of the toe drain (model MW-13) intercepting the phreatic surface and preventing seepage on the downstream slope obviously increased stability of the embankment. With the reservoir at maximum pool, the FS almost achieved recommended criteria.

Stability Analyses with No Seepage Forces (MW-24)

All of the previously examined centrifuge model tests were subjected to seepage except model MW-24, which failed prematurely while accelerating the model to prototype acceleration. This type of failure corresponds to a rate of construction failure that occurs when high pore pressures are created by the fill placement being too rapid. The prototype dimensions at failure are presented in Table 2, while Table 1 presents the parameters used in the stability analyses.

In analyzing stability for the end of construction case, the Corps of Engineers' practice is to rely on total strength parameters, as pore pressures are generally unknown for this case. However, as it is assumed that negative pore water pressures cannot be relied upon at low normal stresses, the lowest strength, effective or total, is used, resulting in a bilinear envelope. Despite this conservative approach, the results of the analyses provided a factor of safety value of 3.60, indicating stability; yet failure occurred.

Conclusions

Based upon the centrifuge models and materials tested, the following conclusions are appropriate:

1. Estimates of the phreatic surface based upon Dupuit's parabolic assumption and FEM seepage analysis agreed well with phreatic surfaces observed in models with vertical upstream slopes. However, in models with more realistic sloping upstream surfaces agreement was less favorable. Nevertheless, for both upstream

slope conditions, theoretical estimates of the phreatic surface were higher (and thus more conservative) than surfaces observed in the models. It is possible that steady-state seepage may not have been obtained for models.

2. Permeability estimates based upon seepage quantities measured through the models were of the order of 10^{-3} cm/s, while laboratory permeability values were of order of the 10^{-5} cm/s. This difference may be due to anisotropic permeabilities of the material or leakage along the sides of the models.

3. Stability analysis using the Corps of Engineers (modified Swedish) slope stability method agreed well, albeit conservatively, with observed model performance. Factors of safety ranged from 0.7 to 0.9 at the instant of failure for models with retrogressing slips. By comparison, factors of safety for stable embankments ranged from 1.3 to 1.7. Thus, from the standpoint of stability, the recommended minimum factor of safety of 1.3 is sufficient.

4. For embankments of cohesionless materials, permeability can govern the failure mode. In cases of low permeability, rate of construction may pose a problem, particularly when the initial water content is high, as in hydraulically placed fill. In case of intermediate permeability, pore pressures due to seepage can cause mass instability and retrogression. In cases of highly permeable material, or overtopping, erosion may pose a stability hazard.

5. Exiting of the phreatic surface on the downstream slope generally leads to erosion or mass instability. In this context, positive seepage control measures, e.g., a toe drain, are recommended.

Acknowledgments

The models described and resulting data presented herein were obtained from research conducted at Cambridge University, England, and the United States Army Engineer Waterways Experiment Station under sponsorship of the Spokane Mining Research Center, (SMRC), United States Bureau of Mines. Grateful appreciation is expressed to Bill Stewart of the SMRC who assisted in the testing program and was the technical monitor, and to R. G. James and C. H. Collison, of Cambridge, who assisted in the centrifuge model tests.

Appendix I.—References

1. Dupuit, J., "Etudes Theoriques et Partiques sur le Mouvement des Eaux dans le Canaux de Courerts et a Traves le Terrains Pereable," Paris, France.
2. *Engineering and Design Manual—Coal Refuse Disposal Facilities,* Department of the Interior, Mining Enforcement and Safety Administration, Washington, D.C.
3. Goodings, D. J., "Centrifugal Modeling of Slope Failures," thesis presented to the University Engineering Laboratories, University of Cambridge, at Cambridge, England, in 1979, in partial fulfillment of the requirements for the degree of Doctor of Philosophy.
4. Malushitsky, J. I., *The Centrifugal Model Testing of Waste-Heap Embankments,* Budivelnik Publishing House, Kiev, Russia, Draft Translation, 1977.
5. "Soil Mechanics Design, Seepage Control," *Engineering Manual 1110-2-1901,* Department of the Army, Office, Chief of Engineers, Washington, D.C., 1952.
6. "Stability of Earth and Rock-Fill Dams," *Engineering Manual 1110-2-1902,* Department of the Army, Office, Chief of Engineers, Washington, D.C., Apr., 1970.
7. Townsend, F. C., Goodings, D. J., Schofield, A. N., and Al-Hussaini, M. M., "Centrifuge Model Analysis of Coal Waste Embankment," *WES Technical Report G-79-18,* 1979.
8. Tracy, F. T., "A Plane and Axisymmetric Finite Element Program for Steady-State and Transient Seepage Proglems," *Miscellaneous Paper K-73-4,* United States Army

Engineer Waterways Experiment Station, CE, Vicksburg, Miss., 1973.
9. Van Terson, F. K., "Eenige Theoretisch Beschouivingen over Kivel," *De Ingenieur*, Berlin, West Germany, 1916–1917, p. 1940.

Appendix II.—Notation

The following symbols are used in this paper:

a = length of seepage surface along downstream slope;
c, c' = undrained, drained cohesive strength;
i = hydraulic gradient;
k = coefficient of permeability;
N = number of gravities acceleration or scale factor;
N_d = number of equipotential drop;
N_f = number of flow channels;
Q, q = flow rate;
α = slope angle;
γ = unit weight of water;
γ_s = unit weight of solids (soil);
σ_1, σ_3 = major, minor principal stress; and
σ_d = deviator stress.

JOURNAL OF THE GEOTECHNICAL ENGINEERING DIVISION

EARTHQUAKE-INDUCED LIQUEFACTION NEAR LAKE AMATITLAN, GUATEMALA

By H. Bolton Seed,[1] F. ASCE, Ignacio Arango,[2] Clarence K. Chan,[3] M. ASCE, Alberto Gomez-Masso,[4] and Rebecca Grant Ascoli[5]

INTRODUCTION

One of the effects of the February 4, 1976 Guatemala earthquake was the extensive liquefaction which occurred at the settlement of La Playa on the northeast shore of Lake Amatitlan. The settlement is located on a deltaic deposit near the mouth of a small river, Rio Villalobos, and consists mainly of a resort area with several newly constructed brick and cement-block houses surrounded by grass lawns and trees. An overall view of the area is shown in Fig. 1. The general area behind the shoreline is quite flat with the ground sloping gently up at about 2° away from the lake. The ground some distance from the beach is devoted to agriculture. The area of extensive liquefaction extended about 600 ft (180 m) behind the nearest shoreline and is marked by the shaded zone in Fig. 2. A second zone, where evidence of liquefaction was readily apparent but its effects were less severe, extended about 1,200 ft (360 m) behind the shoreline (see Fig. 2).

An excellent description of the geology of the delta and the nature of the damage has been presented by Hoose, et al. (2), and Krinitzsky and Bonis (4). As described by Hoose, et al., the Villalobos delta covers an area of about 16-1/2 km^2 of the northeastern portion of the Amatitlan basin, but only about 6% of the area was affected by liquefaction-induced ground failure during the

[1]Prof. of Civ. Engrg., Dept. of Civ. Engrg., Univ. of California, Berkeley, Calif. 94720.
[2]Sr. Project Engr., Woodward-Clyde Consultants, San Francisco, Calif.
[3]Research Engr. and Lect., Dept. of Civ. Engrg., Univ. of California, Berkeley, Calif. 94720.
[4]Sr. Staff Engr., Woodward-Clyde Consultants, San Francisco, Calif.
[5]Engr., INDE, Guatemala.

Note.—Discussion open until September 1, 1981. To extend the closing date one month, a written request must be filed with the Manager of Technical and Professional Publications, ASCE. Manuscript was submitted for review for possible publication on February 14, 1980. This paper is part of the Journal of the Geotechnical Engineering Division, Proceedings of the American Society of Civil Engineers, ©ASCE, Vol. 107, No. GT4, April, 1981. ISSN 0093-6405/81/0004-0501/$01.00.

FIG. 1.—Overall View of Liquefaction Zone at La Playa

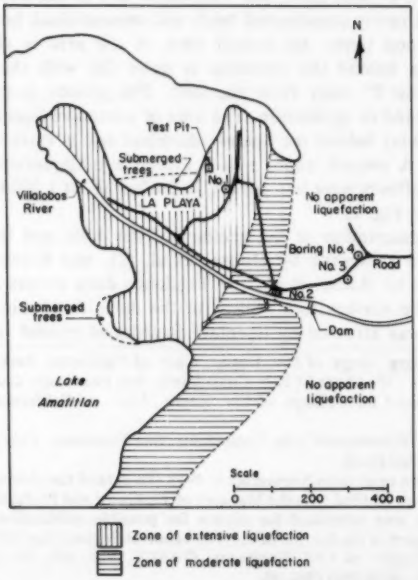

FIG. 2.—Boring and Test Pit Locations

1976 earthquake. The youngest, most active portions of the delta were those most severely affected. The river has changed its course at least three times in the past 80 yr, and the delta has had a rapid rate of deposition so that it now extends well out into Lake Amatitlan. The material deposited by the river is primarily pumice sand and gravel derived from extensive Quaternary deposits to the north of the lake. Detailed maps of the ground failures and evidence of liquefaction have been presented by Hoose, et al. (2), based on site inspection and aerial photographs. The zones shown in Fig. 2 are based largely on the work of these authors but were also confirmed by careful field inspections by three writers of the present paper.

Within the heavy damage zone (see Fig. 2) there was subsidence and flooding of beach areas, severe ground cracking with cracks ranging in size up to several

FIG. 3.—Ground Cracking in Zone of Extensive Liquefaction

meters (Fig. 3), severe damage to houses where they were located in areas of extensive ground cracking, as well as numerous sand boils. The ground cracking was generally more severe near the waterfront with crack widths decreasing progressively in size as the ground rose gradually in elevation towards the inland edge of the liquefaction area.

Of the 32 houses at La Playa, 29 were destroyed or damaged by differential lateral displacement, generally as a consequence of lateral spreading and subsidence. Fortunately, most of the houses at La Playa were mainly vacation houses and they were unoccupied at the time of the earthquake.

An interesting feature of the area was the expulsion, together with sand, of occasional pieces of pumice, ranging from small gravel to cobble sizes in some of the mounds formed around the sand boils. The pumice particles were of very light weight so that they were readily carried up with the liquefied

sand through the vents and cracks through which water moved upwards to the ground surface. Areas of sand boils in the zone of moderate liquefaction are shown in Fig. 4.

In contrast to the extensive damage due to liquefaction in the La Playa area, damage to houses in nearby towns was slight. Even a cement-brick house located near an area of intense sand boils and land spreading at La Playa was virtually undamaged (4), and the shaking intensity in the area, based on this lack of damage, was assessed as VI on the modified Mercalli scale.

In view of the scarcity of well-documented cases of soil liquefaction it was considered important to determine the soil conditions within and immediately adjacent to the liquefied zone in order to supplement the available empirical data base used for liquefaction evaluations of other sites. At the same time,

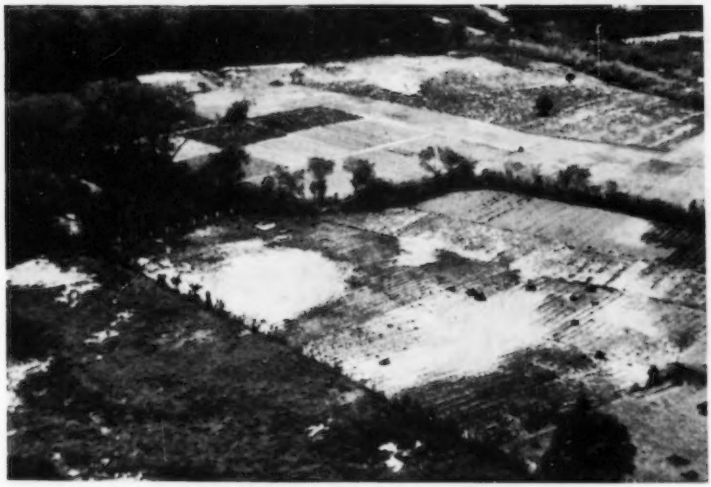

FIG. 4.—Sand Boils at Ground Surface in Zone of Moderate Liquefaction

it was considered useful to investigate whether the liquefaction that occurred at La Playa might have been anticipated through the use of currently used analyses and laboratory test procedures.

Guatemala Earthquake of February 4, 1976

The February 4, 1976 Guatemala earthquake occurred on the Motagua Fault and has been assigned a Richter magnitude of 7.5. Its epicenter (see Fig. 5) was located about 170 km northeast of Lake Amatitlan, but surface ruptures along the fault were mapped over a length of at least 240 km and the western end of the major east-west fault break was only about 40 km due north of the lake. In addition, some short length north-south offset faults were mapped in and around Guatemala City about 20 km north of the site. The distribution

of modified Mercalli intensities in the strong motion area of the earthquake, as assigned by the United States Geological Survey (USGS) (1), is shown in Fig. 6. Lake Amatitlan is located in Intensity Zone VI but very close to the isoseismal for Intensity VII. Based on the correlation of intensities with peak ground acceleration developed by Trifunac and Brady (9), this would indicate

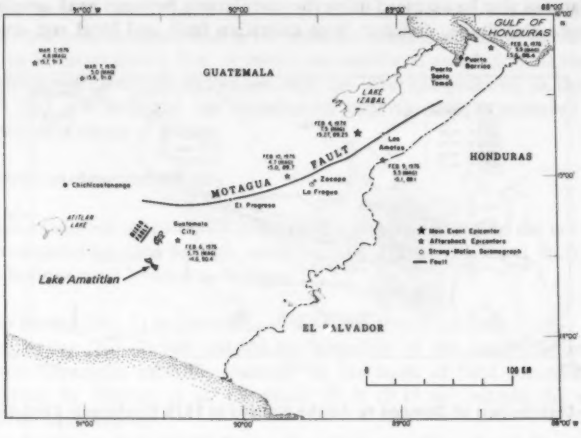

FIG. 5.—Location of Lake Amatitlan in Relation to Motagua Fault (after Espinosa)

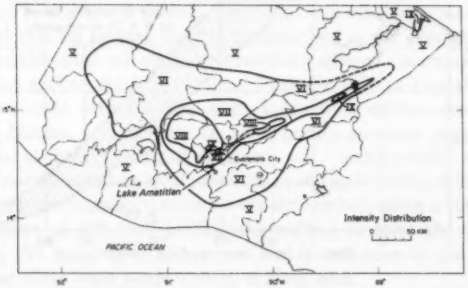

FIG. 6.—Distribution of Modified Mercalli Intensities from 1976 Guatemala Earthquake (1)

a peak ground acceleration in the vicinity of Lake Amatitlan of the order of 0.12 *g*.

Data on the damage to adobe houses during the earthquake has also been assembled by the USGS (1) and presented in the form of a damage distribution map shown in Fig. 7. The Amatitlan area lies near the boundary between Zone 0 (0%–25% damage) and Zone 1 (25%–50% damage). Observations of housing

damage at La Playa would seem to confirm this assessment and suggest that the peak ground accelerations were nearer the Trifunac and Brady mean value of 0.12 *g* rather than a significantly higher value which might be indicated by probability considerations within the available intensity versus peak acceleration data base.

Peak ground accelerations generated by the magnitude 7.5 earthquake at Lake Amatitlan can also be assessed using the correlations between peak acceleration, earthquake magnitude, distance from causative fault and local soil conditions

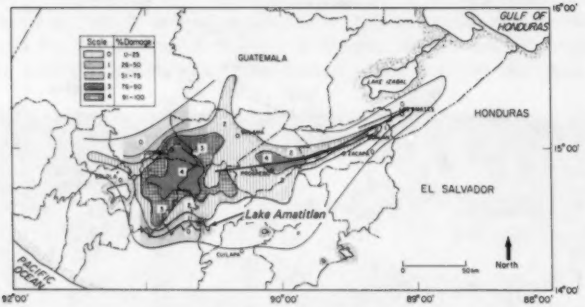

FIG. 7.—Distribution of Damage to Adobe Houses in 1976 Guatemala Earthquake (1)

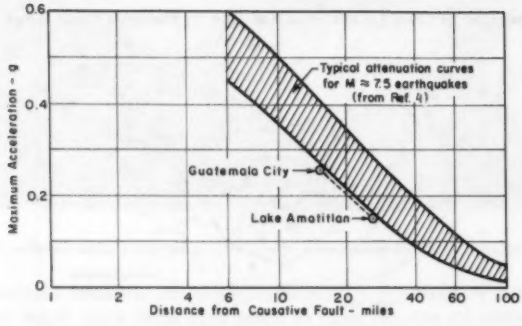

FIG. 8.—Use of Attenuation Laws to Estimate Peak Acceleration at Lake Amatitlan

proposed in Refs. 5 and 8. The correlations would indicate a peak acceleration in rock near Lake Amatitlan of the order of 0.21 *g*, but for the softer soil conditions near the lake this value would be expected to be reduced to about 0.16 *g*. A similar value is indicated by the correlations presented by Idriss (3).

Unfortunately, there were no records of the ground motions induced by the earthquake near Lake Amatitlan. However seismoscope records were obtained in Guatemala City (about 25 km from the causative fault), and an interpretation

of these by the USGS (1) indicates that the peak ground surface acceleration in this area was probably of the order of 0.25 *g*. At the increased distance (40 km) to Lake Amatitlan, the use of attenuation laws (see, e.g., Fig. 8) would indicate a peak ground surface acceleration in the vicinity of Lake Amatitlan of the order of 0.15 *g*.

The lack of damage to adobe houses in the vicinity of the lake would seem to indicate that the actual peak acceleration in this area was nearer the lower bound of the aforementioned values, but since the range indicated by the different procedures is compratively low, it seems reasonable to conclude that the peak ground surface acceleration developed near the lake was probably in the range of about 0.12 *g*–0.15 *g* and the liquefaction behavior can be assessed based on this probable range of values.

Soil Conditions in Liquefaction Area

The soil conditions in the area where liquefaction occurred (and did not occur) were investigated by four borings, each made to a depth of about 70 ft (21.35 m). The borings were located as follows:

1. One boring (No. 1) in the midst of the highly liquefied zone.
2. One boring (No. 2) just outside the boundary of the liquefied zone; this boring was especially carefully located, on the basis of field reconnaissance and mapping by Hoose, et al. (2) about 30 ft (9.15 m) outside the nearest evidence of liquefaction.
3. Two borings well inside in the nonliquefied zone (Nos. 3 and 4).

The locations of the borings are shown in Fig. 2. It would clearly have been desirable to have boring data in the liquefied zone before the earthquake. However, it was reasoned that by making borings as described in the preceding, it should be possible to establish the soil conditions representative of a marginal liquefaction condition for the ground motions resulting from the 1976 earthquake.

Borings were made with a hollow-stem auger using drilling mud to stabilize the sides and bottom of the hole. In each boring standard penetration tests were performed at intervals of 5 ft (1.53 m), and "undisturbed" samples were extracted in thin-wall seamless steel tubes for cyclic load testing in the laboratory. Standard penetration resistance values were determined using a rope and pulley system (two turns of old rope around the pulley) to raise the 140-lb weight and measuring the number of blows per foot penetration at the bottom of a drill hole whose sides were supported by drilling mud.

In addition, two test pits were dug to a depth of about 5 ft (1.53 m) on the level ground about 40 ft (12 m) from the beach. These showed the upper 4 ft (1.2 m) of soil to be pumice sand underlain by a thin layer of dense fibrous peats and organic silt. The soil exposed on the walls of the pits was a stratified brown fine sand with some silt. One pit was dug across four cracks with a total width of 25 cm; the ground surface showed several centimeters of vertical subsidence towards the lake. The same vertical differential movement could be seen in the walls of the pit and increased with depth. The second pit was dug across a 10-cm wide crack showing no vertical differential subsidence but the crack was partially filled with sand which had been forced up from below,

and had intersected the horizontal stratifications. Two field density tests in the pumice sand which constituted the upper four feet showed that it had a wet density of 55.5 lb/cu ft–61.5 lb/cu ft, a water content of about 56% and a dry density of 35.5 lb/cu ft–39.4 lb/cu ft. These tests were taken in the

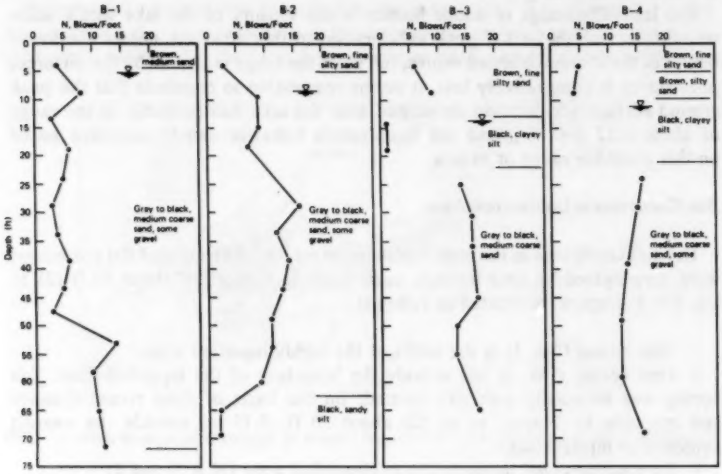

FIG. 9.—Boring Logs at La Playa Site

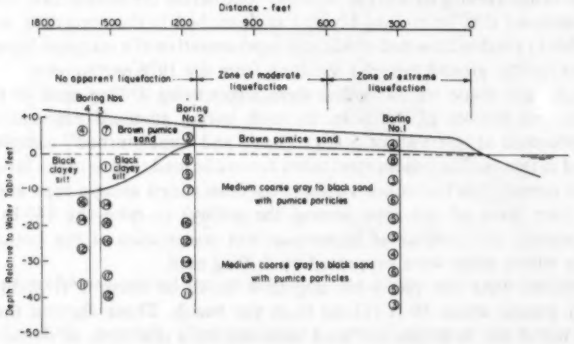
Distance - feet
No apparent liquefaction
Zone of moderate liquefaction
Zone of extreme liquefaction
Boring Nos. 4 3
Boring No. 2
Boring No. 1
Brown pumice sand
Black clayey silt
Medium coarse gray to black sand with pumice particles
Depth Relative to Water Table - feet

FIG. 10.—Schematic Soil Profile Through La Playa Area

moist soil above the water table. It may be noted that pumice sands were also present south of the La Playa area and there were other small areas of liquefaction but these were not investigated in the present study.

The soil profile to a depth of about 70 ft (22 m) is shown by the logs of

the borings in Fig. 9, which also show values of the standard penetration resistance. Based on these results, a schematic and highly simplified soil profile along a section extending from the shoreline to a distance about 1,600 ft (488 m) inland is shown in Fig. 10.

It may be seen that the entire area is covered by a surficial layer of brown pumice sand varying in depth from about 5 ft–10 ft (1.5 m–3 m) underlain in the zone of liquefaction by medium coarse sand containing some pumice fragments and in the nonliquefied zone by an intermediate layer of black clayey silt above the same type of sand with pumice particles. The water table varies in depth from about 4 ft–5 ft (≃1.5 m) near the shoreline to about 12 ft (≃4 m) depth in the area where no liquefaction was observed. It is interesting to

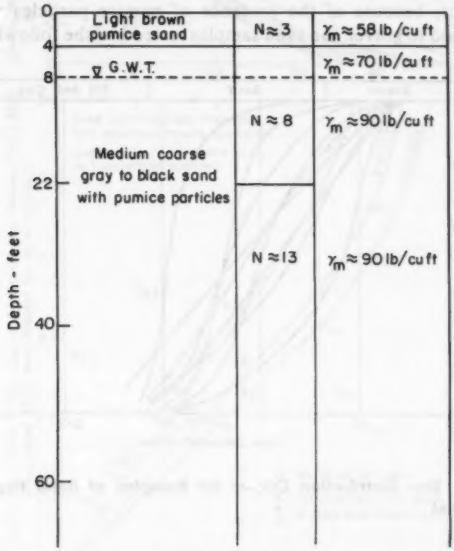

FIG. 11.—General Soil Characteristics at Boundary of Liquefaction Zone

note that the very lightweight pumice sand at all boring locations was located above the water table and thus was not itself the zone in which liquefaction occurred. The source of liquefaction was presumably in the saturated sand containing pumice particles below depths of 6 ft–10 ft (≃2 m–3 m). In the heavily liquefied zone this material had a penetration resistance value, N, of only about 5 ft (≃1.5 m) to a depth of 50 ft (≃15 m) but presumably this value is representative of the liquefied and restabilized sand. There is no way of establishing the penetration resistance of this material before the earthquake.

For this reason, the remaining borings were made in the nonliquefied zone, one very close to the boundary (Boring No. 2), and two well behind the liquefaction zone. With increasing distance from the shoreline, the average penetration

resistance increased and the depth of the water table increased, both factors which would tend to reduce the possibility of liquefaction of the sand deposit.

An examination of the soil profile in Fig. 10 indicates that the conditions at Boring No. 2 are probably representative of the limiting conditions at which liquefaction would just occur or just not occur for the ground motions and soil conditions in the La Playa area and this profile has therefore been used for a more detailed study. The general soil characteristics are shown more clearly in Figs. 11 and 12. The latter two figures show the grain size distribution curves for nine samples taken from depths between 30 ft and 45 ft (9 m and 14 m) in Borings No. 3 and 4. Similar soil types were found below the water table in Borings 1 and 2 where liquefaction occurred. It may be seen that the sand ranges from fine to coarse, though most of the samples are medium coarse sand. However, because of the presence of pumice particles ranging in size from coarse sand to gravel, the sand samples tested had the following characteris-

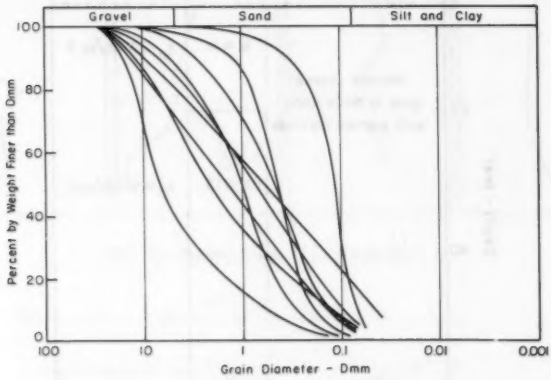

FIG. 12.—Grain Size Distribution Curves for Samples of Sand Representative of Liquefied Material

tics: average dry density of sand ≈58 pcf (0.93 g/cc); average specified gravity of solid particles ≈2.1; average water content of sand ≈60%; and average density of wet sand ≈92.5 pcf (1.48 g/cc). For the generalized soil profile shown in Fig. 11, the saturated density was simplified to a rounded value of 90 pcf (1.45 g/cc).

Liquefaction Analysis Based on Empirical Data

One of the methods currently used to assess the liquefaction potential of a sand deposit is a procedure based on an empirical correlation between the cyclic stress ratio induced by the earthquake and the standard penetration resistance corrected to an effective overburden pressure of 1 ton/sq ft (or 1 kg/cm^2) (6). The proposed empirical curves, based on analyses of other sites, which separate areas where liquefaction has occurred in previous earth-

quakes from those which have not are shown in Fig. 13. Correction factors for determining the standard penetration resistance, N_1, at an overburden pressure of 1 ton/sq ft are shown in Fig. 14. The data for the Lake Amatitlan site may be used to check the position of the curve for magnitude 7-1/2 earthquakes on Fig. 13.

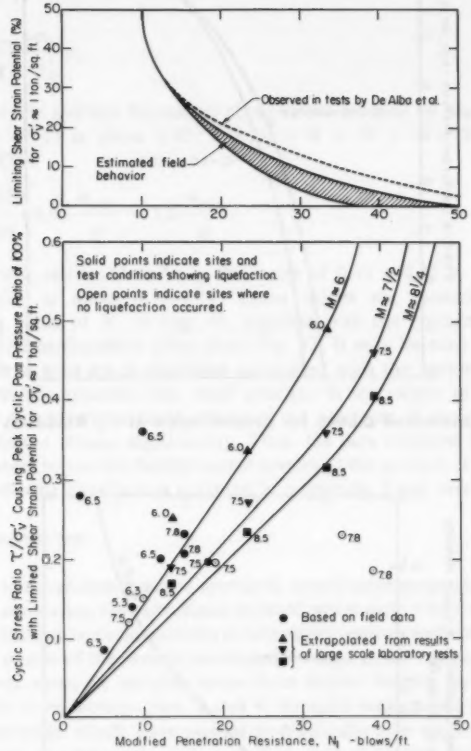
Limiting Shear Strain Potential (%) for $\sigma'_v \approx 1$ ton/sq ft
Observed in tests by De Alba et al.
Estimated field behavior
Cyclic Stress Ratio τ/σ'_v Causing Peak Cyclic Pore Pressure Ratio of 100% with Limited Shear Strain Potential for $\sigma'_v \approx 1$ ton/sq ft
Solid points indicate sites and test conditions showing liquefaction.
Open points indicate sites where no liquefaction occurred.
M = 6
M = 7 1/2
M = 8 1/4
Based on field data
Extrapolated from results of large scale laboratory tests
Modified Penetration Resistance, N_1 - blows/ft

FIG. 13.—Correlation Between Field Liquefaction Behavior of Sands for Level Ground Conditions and Penetration Resistance (Supplemented by Data from Large-Scale Tests) (6)

For borderline conditions of liquefaction and no liquefaction at La Playa, the soil conditions are shown in Fig. 11. From this it may be seen that liquefaction is most likely to have developed in the lower blow count zone, $N \simeq 8$, extending from about 8 ft–22 ft (2.44 m–6.71 m) below the ground surface.

At this depth, computations of the effective overburden pressure show

$$\sigma'_0 \simeq 4 \times 58 + 4 \times 70 + 7(90 - 62.4) \simeq 704 \text{ psf (or } 0.35 \text{ kg/cm}^2) \quad \ldots\ldots (1)$$

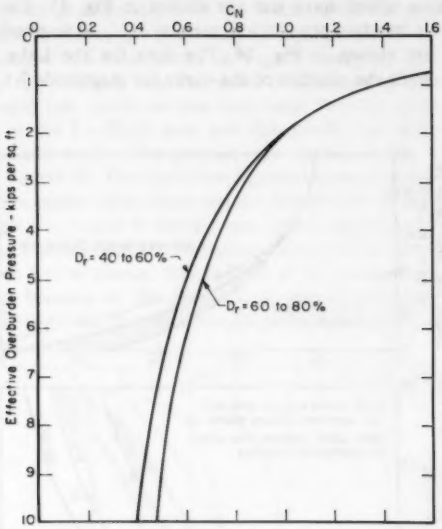

FIG. 14.—Recommended Curves for Determination of C_N Based on Averages for WES Tests

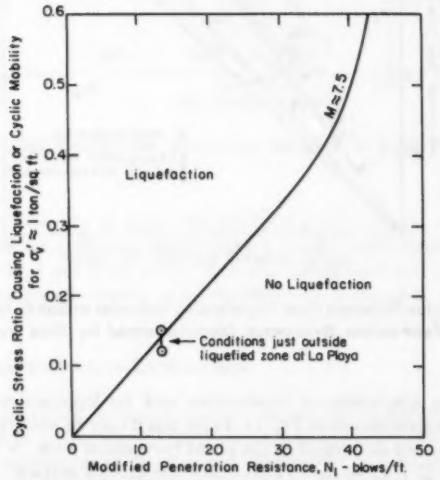

FIG. 15.—Empirical Relation Between Stress Ratios Causing Liquefaction and Modified Penetration Resistance (6)

The value $N_1 = C_N \times N$, in which C_N = a function of the effective overburden pressure. For $\sigma_0' = 704$ psf (0.35 kg/cm^2), the value of $C_N \simeq 1.6$, and thus

$$N_1 \simeq 1.6 \times 8 \simeq 13 \quad \ldots\ldots\ldots\ldots\ldots\ldots\ldots\ldots\ldots\ldots\ldots\ldots\ldots\ldots\ldots\ldots (2)$$

The cyclic stress ratio induced by the earthquake may be estimated from the equation (Ref. 7)

$$\frac{\tau_{av}}{\sigma_0'} \simeq 0.65 \frac{a_{max}}{g} \frac{\sigma_0}{\sigma_0'} r_d \quad \ldots\ldots\ldots\ldots\ldots\ldots\ldots\ldots\ldots\ldots\ldots\ldots\ldots\ldots\ldots\ldots (3)$$

in which τ_{av} = the average horizontal shear stress induced by the earthquake; r_d at a depth of 15 is about 0.95; and $\sigma_0 \simeq 4 \times 58 + 4 \times 70 + 7 \times 90 \simeq 1{,}150$ psf. Thus

$$\frac{\tau_{av}}{\sigma_0'} \simeq 0.65 \frac{1{,}150}{704} 0.95 \frac{a_{max}}{g} \simeq 1.0 \frac{a_{max}}{g} \quad \ldots\ldots\ldots\ldots\ldots\ldots\ldots\ldots\ldots\ldots\ldots\ldots\ldots\ldots\ldots\ldots (4)$$

Since a_{max} was estimated to be in the range of 0.12 g–0.15 g, the probable value of τ_{av}/σ_0' is about 0.12–0.15. These values are plotted against the corresponding value of N_1 in Fig. 15, together with the boundary curve for magnitude 7-1/2 earthquakes taken from Fig. 13. It may be seen that the data for the La Playa area are in excellent agreement with the proposed empirical curve. It is readily apparent that small changes in the values of unit weights used in these computations could influence the positions of the plotted points but they would not change significantly. Thus, the data obtained from the field study would seem to provide further corroboration of the position of the empirical curve for predicting liquefaction potential in magnitude 7-1/2 earthquakes.

Laboratory Investigation

In addition to the aforementioned approach, liquefaction potential is sometimes evaluated by comparing the earthquake-induced stress ratio with that determined to cause liquefaction or cyclic mobility in laboratory tests on undisturbed samples.

During the course of the present investigation, eight cyclic triaxial compression tests were performed on samples taken from depths ranging from 30 ft–45 ft (9.15 m–13.73 m) in Borings Nos. 3 and 4. Samples were obtained in thin-wall seamless steel tubes which were pushed hydraulically into the soil at the base of the hole. In the laboratory, the samples were saturated prior to testing. In these zones the standard penetration resistance was about 13 to 16, corresponding to an N_1 value of about 18, so these samples are likely to show somewhat higher resistance to liquefaction than the soil in the depth range of 8 ft–20 ft (2.44 m–6.1 m) in Boring No. 2.

The results of these tests, showing the number of cycles required to produce a residual pore pressure ratio of 100% are plotted in Fig. 16. The scatter is due to the natural variability of the samples, both in characteristics and density, but it does not appear to show any significant relationship to either. A reasonable average curve has therefore been drawn through the entire set of data. Beyond the point in the test where the pore pressure reached a value of 100%, large deformations developed rapidly so the data in Fig. 16 may be considered

representative of the stress conditions in triaxial compression tests producing a liquefied condition.

For a magnitude 7-1/2 earthquake, the number of equivalent uniform stress cycles is likely to be of the order of 15 and the field stress ratio, τ_{av}/σ'_0, likely to cause liquefaction is about 0.57 times the stress ratio in cyclic triaxial tests (6). Thus, from this test data, the stress ratio required to cause liquefaction would apparently be about:

$$\left(\frac{\tau_{av}}{\sigma'_0}\right)_l \simeq 0.57 \times 0.32 \simeq 0.185 \quad \ldots \ldots \ldots

Analysis of Highly Liquefied Zone

Since it is impossible to determine the pre-earthquake properties of the sand in the zone of extensive liquefaction near the shoreline, it is not possible to make a detailed analysis of its potential behavior either by empirical methods or by analytical-experimental methods. However, some indication of its liquefaction potential may be obtained if it is assumed that the liquefaction characteristics of the sand in this zone were no better than those of the sand in Boring No. 2, just outside the zone of liquefaction. Conditions near the shoreline would be expected to be more conducive to liquefaction due to the shallower depth of the water table in this zone.

In the zone of extensive liquefaction, the water table was at an average depth of about 5 ft (1.53 m) below the ground surface. At a depth of 15 ft (4.58 m), the effective overburden pressure would then be only

$$\sigma_0' \simeq 4 \times 58 + 1 \times 70 + 10(90 - 62.4) \approx 578 \text{ psf} \quad \ldots\ldots\ldots\ldots\ldots\ldots (6)$$

while the total overburden pressure would be

$$\sigma_0 \simeq 4 \times 58 + 1 \times 70 + 10 \times 90 \approx 1{,}202 \quad \ldots\ldots\ldots\ldots\ldots\ldots\ldots\ldots (7)$$

Thus, the stress ratio induced by the earthquake would be about

$$\frac{\tau_{av}}{\sigma_0'} \simeq 0.65 \frac{a_{max}}{g} \frac{\sigma_0}{\sigma_0'} r_d$$

$$\frac{\tau_{av}}{\sigma_0'} \simeq 0.65 \frac{a_{max}}{g} \frac{1{,}202}{578} 0.95$$

$$\frac{\tau_{av}}{\sigma_0'} \simeq 1.28 \frac{a_{max}}{g} \quad \ldots\ldots\ldots\ldots\ldots\ldots\ldots\ldots\ldots\ldots\ldots\ldots\ldots\ldots (8)$$

For values of a_{max} ranging from 0.12 g–0.15 g this leads to values of cyclic stress ratios developed of about 0.155–0.19.

If the sand at a depth of 15 ft (4.58 m) had the same penetration resistance as the sand in Boring No. 2, then the cyclic stress ratio required to induce liquefaction would be of the order of 0.12–0.15, thus indicating a factor of safety against liquefaction in the near-shore area of only about 0.63–0.97. Under these conditions the extensive liquefaction which actually developed should not be considered surprising. In fact, if the density or penetration resistance of the sand in this zone were also somewhat lower than that further away from the shore (near Borings 2, 3, and 4), the situation would be even more unfavorable.

An alternative approach to assessing the resistance to liquefaction of the sand in the near-shore area is to use the laboratory test results in conjunction with the penetration test data to assess the stress ratio causing liquefaction for the sand in Boring No. 2. Up to values of N_1 of about 30 or 35, the resistance to liquefaction of a sand seems to be essentially directly proportion to N_1 (see Fig. 13). Thus, since the stress ratio causing liquefaction in the laboratory tests corresponds roughly to sand for which $N_1 \simeq 18$ while the value of N_1 at a depth of 15 ft (4.58 m) in Boring No. 2 is about 13, the laboratory test data would indicate a liquefaction resistance for this sand

corresponding to a cyclic stress ratio of

$$\left(\frac{\tau_{av}}{\sigma_0'}\right)_l \simeq 0.185 \frac{13}{18} \simeq 0.135 \quad \ldots\ldots\ldots\ldots\ldots\ldots\ldots\ldots\ldots\ldots (9)$$

Again it may be seen that this value, if it applied to the sand near the shoreline, would be much less than the earthquake-induced stress ratios estimated to range between 0.155 and 0.19. In fact, it would indicate a factor of safety in the range of 0.71–0.87. Again, if the sand nearer the shoreline were of somewhat poorer characteristics, the situation would be even less favorable than that indicated by the preceding figures.

On the basis of these evaluations, it should not be considered surprising that liquefaction near the shoreline was so extensive and dramatic in its effects.

Effects of Pumiceous Nature of Sand

The low unit weight of the pumiceous sands at the La Playa site would appear to have been a significant factor in producing the liquefaction that occurred. The primary reason for this is the very low effective stresses produced by this sand at significant depths below the water table.

Consider, e.g., the conditions that would have developed at La Playa if the sand had been a typical quartz sand with the same resistance to liquefaction as the actual sand containing pumice, i.e., requiring an induced stress ratio of 0.12–0.15 to induce liquefaction.

For the quartz sand, the unit weight of the moist sand might have been about 105 lb/cu ft (168.1 g/cc), and the total unit weight about 115 lb/cu ft (184.1 g/cc). For a water table at a depth of 5 ft (1.53 m), as existed in the highly liquefied zone, the effective pressure at a depth of 15 ft (4.58 m) would have been

$$\sigma_0' \simeq 5 \times 105 + 10\,(115 - 62.4) \simeq 1{,}051 \text{ psf} \quad \ldots\ldots\ldots\ldots\ldots\ldots (10)$$

while the total overburden pressure would be

$$\sigma_0 \simeq 5 \times 105 + 10 \times 115 \simeq 1{,}675 \text{ psf} \quad \ldots\ldots\ldots\ldots\ldots\ldots\ldots (11)$$

Thus, the stress ratio induced by the earthquake would be about

$$\frac{\tau_{av}}{\sigma_0'} \simeq 0.65 \frac{a_{max}}{g} \frac{\sigma_0}{\sigma_0'} r_d$$

$$\frac{\tau_{av}}{\sigma_0'} \simeq 0.65 \frac{a_{max}}{g} \frac{1{,}675}{1{,}051} 0.95$$

$$\frac{\tau_{av}}{\sigma_0'} \simeq 0.98 \frac{a_{max}}{g} \quad \ldots\ldots\ldots\ldots\ldots\ldots\ldots\ldots\ldots\ldots\ldots\ldots (12)$$

For values of a_{max} ranging from 0.12 g–0.15 g, this leads to values of cyclic stress ratios developed of about 0.12–0.15, and corresponding computed factors of safety against liquefaction ranging from 0.83–1.3.

Thus, depending on the acceleration developed, there is a very good chance that a normal type of quartz sand would not have liquefied at all, in contrast

to the much lower factors of safety indicated for the pumiceous sand (0.63–0.97), and the evident high degree of liquefaction of the area.

It may be concluded that very lightweight saturated cohesionless soils are much more vulnerable to earthquake-induced liquefaction than typical quartz sands and should be treated with special caution in seismically active regions.

Conclusions

The foregoing presents the results of a field and laboratory investigation of the extensive area of liquefaction which occurred at La Playa on the shore of Lake Amatitlan in the Guatemala earthquake of 1976. The investigation leads to the following conclusions:

1. The soil in which liquefaction occurred was a layer of sand containing particles of pumice which occurred between depths of about 5 ft–70 ft (1.5 m–22 m) or more below the ground surface. It was covered by a surficial layer of lightweight pumice sand and because of the pumice particles in the liquefied layer, its total unit weight had the relatively low value of about 90 lb/cu ft (1.45 g/cc).
2. In spite of the fact that the sand is somewhat lighter in weight than sand deposits which have liquefied in other earthquakes, its liquefaction characteristics are apparently influenced by the same factors as other sand deposits and its overall behavior is consistent with that exhibited by other sands.
3. The penetration resistance of the sand at the boundary between liquefied and nonliquefied zones is in good accord with previously developed empirical correlations between liquefaction potential and the standardized penetration resistance (N_1) at which liquefaction can just be expected to occur.
4. The behavior of the sand in the liquefaction and nonliquefied zones was consistent with experimental-analytical predictions of liquefaction potential based on the averaged results of cyclic loading triaxial compression tests performed on undisturbed samples to evaluate the liquefaction characteristics of the sand and conventional procedures used in conjunction with this type of test data to evaluate liquefaction potential.
5. The high degree of liquefaction at the La Playa site was probably due in large measure to the lightweight nature of the pumiceous sands. A typical quartz sand at the same site with the same cyclic load characteristics as the sand containing pumice might well have remained stable in spite of the earthquake shaking. Consequently, lightweight cohesionless soils should be treated with special caution with regard to their liquefaction potential in seismically active regions.
6. The results of the investigation provide an extremely useful case history in which field data on soil characteristics in an earthquake-liquefied zone and a nonliquefied zone can be correlated with field performance, thereby supplementing the limited number of available case studies of this type which can be used as a basis for predicting probable behavior at other sites. The results also tend to corroborate currently used procedures for evaluating liquefaction potential although in the case of the laboratory test data, this clearly depends on the degree to which the in-situ properties of the soil are represented by the "undisturbed" samples extracted from the deposit.

In spite of the inevitable limitations of any study of this type it is hoped that the results of the investigation, used with appropriate judgment, will contribute to the available data base relating to earthquake-induced liquefaction and thereby to an improved predictive capability of this type of behavior in seismically active regions.

Acknowledgments

The entire investigation was supported by a grant for the Nuclear Regulatory Commission. This support together with the assistance of Kenneth L. Lee in providing field data on the damage and soil conditions, A. Lopez in facilitating the field boring program, T. S. Hirschmann in providing the drilling equipment and crew under difficult conditions, L. Mejia in conducting part of the soil testing program, L. S. Cluff in providing photographs of the damage area, and Seena N. Hoose of the USGS for several enlightening and informative conversations are gratefully acknowledged.

Appendix.—References

1. Espinosa, A. F., "The Guatemala Earthquake of February 4, 1976, A Preliminary Report," *Geological Survey Paper 1002*, United States Government Printing Office, Washington, D.C., 1976.
2. Hoose, S. N., Wilson, R. C., and Rosenfeld, J. H., "Liquefaction-Caused Ground Failure during the February 4, 1976, Guatemala Earthquake," *Proceedings of the International Symposium on the February 4th, 1976, Guatemalan Earthquake and the Reconstruction Process*, Vol. 2, 1978.
3. Idriss, I. M., "Characteristics of Earthquake Ground Motions," *Earthquake Engineering and Soil Dynamics*, Vol. 3, ASCE, 1978, pp. 1151–1267.
4. Krinitzsky, E. L., and Bonis, S. B., "Notes on Earthquake Shaking in Soils, Guatemala Earthquake of 4 February, 1976, Informal Report," United States Army, Washington, D.C., Aug., 1976, 32 p.
5. Schnabel, P. B., and Seed, H. B., "Accelerations in Rock for Earthquakes in the Western United States," *Bulletin of the Seismological Society of America*, Vol. 63, No. 2, Apr., 1973, pp. 501–516.
6. Seed, H. B., "Soil Liquefaction and Cyclic Mobility Evaluation for Level Ground During Earthquakes," *Journal of the Geotechnical Engineering Division*, ASCE, Vol. 105, No. GT2, Proc. Paper 14380, Feb., 1979, pp. 201–255.
7. Seed, H. B., and Idriss, I. M., "Simplified Procedure for Evaluating Soil Liquefaction Potential," *Journal of the Soil Mechanics and Foundations Division*, ASCE, Vol. 97, No. SM9, Proc. Paper 8371, Sept., 1971, pp. 1249–1273.
8. Seed, H. B., Murarka, R., Lysmer, J., and Idriss, I. M., "Relationships of Maximum Accelerations, Maximum Velocity, Distance from Source and Local Site Conditions for Moderately Strong Earthquakes," *Bulletin of the Seismological Society of America*, Vol. 66, No. 4, Aug., 1976, pp. 1323–1342.
9. Trifunac, M. D., and Brady, A. G., "Correlation of Peak Acceleration, Velocity and Displacement with Earthquake Magnitude, Distance and Site Conditions," *International Journal of Earthquake Engineering and Structural Dynamics*, Vol. 4, No. 5, July-Sept., 1976, pp. 455–472.

JOURNAL OF THE GEOTECHNICAL ENGINEERING DIVISION

TECHNICAL NOTES

Note.—Discussion open until September 1, 1981. To extend the closing date one month, a written request must be filed with the Manager of Technical and Professional Publications, ASCE. This paper is part of the Journal of the Geotechnical Engineering Division, Proceedings of the American Society of Civil Engineers, ©ASCE, Vol. 107, No. GT4, April, 1981.

Technical Notes

To provide a place within ASCE for publication of technical ideas that have not advanced, as yet, to the point where they warrant publication as a Proceedings paper in a *Journal*, the publication of Technical Notes was authorized by the Board of Direction on October 16–18, 1967, under the following guidelines:

1. An original manuscript and two copies are to be submitted to the Manager of Technical and Professional Publications, ASCE, 345 East 47th Street, New York, N.Y., 10017, along with a request by the author that it be considered as a Technical Note.
2. The two copies will be sent to an appropriate Technical Division or Council for review.
3. If the Division or Council approves the contribution for publication, it shall be returned to Society Headquarters with appropriate comments.
4. The technical publications staff will prepare the material for use in the earliest possible issue of the *Journal*, after proper coordination with the author.
5. Each Technical Note is not to exceed 4 pages in the *Journal*. As an approximation, each full manuscript page of text, tables, or figures is the equivalent of one-half a *Journal* page.
6. The Technical Notes will be grouped in a special section of each *Journal*.
7. Information retrieval abstracts and key words will be unnecessary for Technical Notes.
8. The final date on which a Discussion should reach the Society is given as a footnote with each Technical Note.
9. Technical Notes will not be included in *Transactions*.
10. Technical Notes will be included in ASCE's annual and cumulative subject and author indexes.

The manuscripts for Technical Notes must meet the following requirements:

1. Titles must have a length not exceeding 50 characters and spaces.
2. The author's full name, Society membership grade, and a footnote reference stating present employment must appear on the first page of the manuscript. Authors need not be Society members.
3. The manuscript is to be submitted as an original copy (with two duplicates) that is typed double-spaced on one side of 8-1/2-in. (220-mm) by 11-in. (280-mm) white bond paper.
4. All mathematics must be typewritten and special symbols must be properly identified. The letter symbols used must be defined where they first appear, in figures or text, and arranged alphabetically in an Appendix.—Notation.
5. Standard definitions and symbols must be used. Reference must be made to the lists published by the American National Standards Institute and to the *Authors' Guide to the Publications of ASCE*.
6. Tables must be typed double-spaced (an original ribbon copy and two duplicate copies) on one side of 8-1/2-in. (220-mm) by 11-in. (280-mm) paper. An explanation of each table must appear in the text.
7. Figures must be drawn in black ink on one side of 8-1/2-in. (220-mm) by 11-in. (280-mm) paper. Because figures will be reproduced with a width of between 3 in. (76 mm) to 4-1/2 in. (110 mm), the lettering must be large enough to be legible at this width. Photographs must be submitted as glossy prints. Explanations and descriptions must be made within the text for each figure.
8. References cited in text must be typed at the end of the Technical Note in alphabetical order in an Appendix.—References.
9. Dual units, i.e., U.S. Customary followed by SI (International System) units in parentheses, should be used throughout the paper.

Acoustic Emission Monitoring of Seepage

By Robert M. Koerner,[1] M. ASCE, W. Martin McCabe,[2] and Luis F. Baldivieso[3]

Introduction

In a series of previously published papers (1,2,3), the acoustic emission (AE) method for monitoring soil stability was described. Briefly, the technique is based on monitoring nonequilibrium conditions within a soil mass by using a pickup transducer (i.e., accelerometer, hydrophone, or high frequency AE sensor), which is connected to an AE device. This device amplifies, filters, and then counts the number of threshold crossings that the incoming AE pulses create. These counts are directly related to the instability of the material producing them; e.g., high counts are indicative of major instability, low counts indicate minor instability, and zero counts indicate stability. The technique has been used for earth dam stability monitoring and is being investigated for a number of other applications, one of which is the monitoring of water flowing through earth masses, e.g., seepage in earth dams.

This technical note is presented with the goal in mind of showing the technical feasibility of the method and of quantifying certain aspects of AE monitoring of seepage of water through soil. The work is a laboratory study in which both clear water and turbid water were passed through a column of soil at various flow velocities. Flow rates and AE rates from these laboratory tests are then compared to a previously-conducted field study at the site of reservoir leakage beneath a small earth dam.

Test Setup and Monitoring Scheme

The test apparatus consisted of a plastic cylinder 20 cm in diameter and 43 cm high. Water flows into the base of the cylinder, then upward through a perforated base plate, and then through the soil column. After passing through the soil, the water is collected in a reservoir, and under steady-state seepage conditions, a flow rate is determined. Fig. 1(*a*) shows the experimental details

[1]Prof., Dept. of Civ. Engrg., Drexel Univ., Philadelphia, Pa. 19104.
[2]Research Assoc., Dept. of Civ. Engrg., Drexel Univ., Philadelphia, Pa. 19104.
[3]Grad. Student, Dept. of Civ. Engrg., Drexel Univ., Philadelphia, Pa. 19104.

Note.—Discussion open until September 1, 1981. To extend the closing date one month, a written request must be filed with the Manager of Technical and Professional Publications, ASCE. Manuscript was submitted for review for possible publication on June 24, 1980. This paper is part of the Journal of the Geotechnical Engineering Division, Proceedings of the American Society of Civil Engineers, ©ASCE, Vol. 107, No. GT4, April, 1981. ISSN 0093-6405/81/0004-0521/$01.00.

for the case of clear water seepage. For the turbid water tests, a separate reservoir containing a soil/water suspension was passed through the test soil. This turbidity was caused by the introduction of approx 38 g of clayey silt soil per liter of water. The experimental setup for this case is shown in Fig. 1(*b*). The soil through which the water (both clear and turbid cases) passed was a poorly-graded, angular, medium-sized gravel. It was placed in a medium dense state with a resulting dry density of 1.5 g/cm^3. This type of coarse-grained soil was selected due to its high permeability which allowed for a wide range of flow rates to be tested. AE monitoring was performed by embedding a waterproof hydrophone at the midpoint of the soil during its placement. The hydrophone, which is most sensitive perpendicular to its longitudinal axis, was placed as shown in the sketches of Fig. 1. The cable from the hydrophone was then brought out of the test cylinder to the AE monitoring device. The system used has a voltage sensitivity of 10.5 V/psi and was used with high-pass and low-pass filters set at 200 Hz and 50 kHz, respectively. The threshold voltage was adjusted so as to screen out the entrance water valve noise at

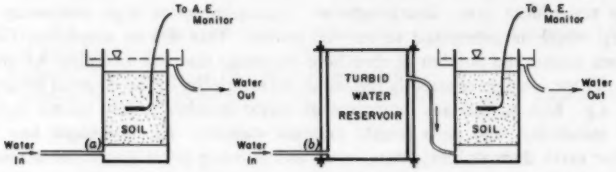

FIG. 1.—Experimental Setup for Seepage Tests Using AE Monitoring Method for: (*a*) Clear Water Seepage; (*b*) Turbid Water Seepage

the highest flow rate, and was used at this value for all tests. Thus, all equipment settings remained constant throughout, which hopefully allows for relative comparisons to be made between test results.

Clear Water Seepage Tests

After complete saturation of the test soil, clear (tap) water was passed through the column of soil at a constant velocity with AE data being accumulated over varying time periods up to 30 min. The AE data was taken at 10-sec intervals which allowed for an AE rate to be plotted against time from the start of the test. Fig. 2 presents this information for flow rates from 38 ml/s–120 ml/s. For this and the two curves to follow, no data points are shown due to a relatively high degree of scatter; thus the curves represent average trends. The significant region of these curves is the terminal long-term value of the AE rate under constant flow. These values are seen to gradually increase with increasing flow rates. Additional tests were conducted up to flow rates of 200 ml/s where the trend continued (see Fig. 3). Also of significance is the minimum value of flow which is detectable using this test setup and monitoring equipment. In Fig. 2 this value is seen to be 45 ml/s. While the lower flow rate of 38 ml/s did give an initial AE response, it decayed to lower than threshold value after about 5 min. The reason for the curves to show an initial pulse is not

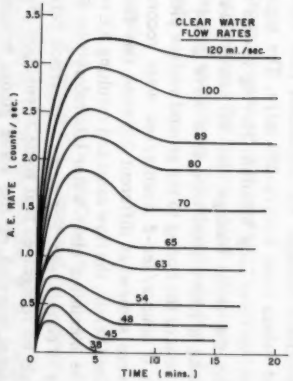

FIG. 2.—AE Response Curves for Lower Flow Rates with Clear Water Seepage

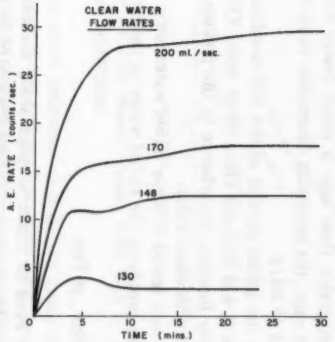

FIG. 3.—AE Response Curves for High Flow Rates with Clear Water Seepage

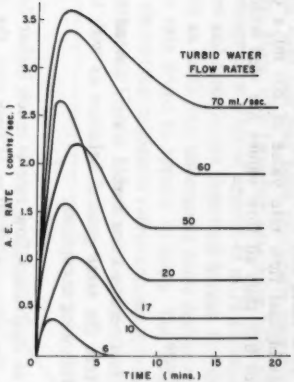

FIG. 4.—AE Response Curves for Low Flow Rates with Turbid Water Seepage

known but could have come from an initial movement of the embedded pickup hydrophone as it, and its adjacent soil, adjusted to a new equilibrium position under each increasing flow rate. It should be noted that this AE pulse gradually decreases with higher flow rates and is entirely absent at the maximum flow rate of 200 ml/s. This highest flow rate value of 200 ml/s corresponds to a Reynold's Number of 0.2; thus all flow values are well within the laminar range.

Turbid Water Seepage Tests

The parallel set of test results using turbid water, instead of clear water, is shown in Fig. 4. Here the same general behavior as with the clear water tests is seen with the following exceptions:

1. The AE rate at an equivalent flow rate is much higher for turbid water than with clear water. For example, at 70 ml/s flow rate, the clear water AE rate is 1.5 counts/sec whereas the turbid water AE rate is 2.6 counts/sec.
2. The minimum detectable flow rate is much lower for turbid water than for clear water. In this case, the minimum detectable value is 10 ml/s, whereas with clear water it was 45 ml/s.
3. The AE pulse at the initial portion of the test is relatively larger in these turbid water tests than it was with the clear water tests. This seems to indicate that a somewhat greater location disturbance to the pickup hydrophone occurs with turbid water than with clear water.
4. The highest flow rate tested in these turbid water tests was 70 ml/s, which exhausted the reservoir supplying the turbid water to the test cylinder.

Correlation with Field Seepage Test

AE monitoring was used to locate seepage along the axis of an earth dam, which was leaking with what appeared to be clear water (4,5). Under consideration was a 300-m section along the dam axis in which the owner located 11 randomly-spaced, open-ended borings. He conducted flow rate tests in these borings with measured values from 0 ml/s–250 ml/s. The higher values were concentrated in a specific 62-m long location. Having access to the location of seepage from within the cased borings, the AE activity was monitored at the same locations using a heavy steel wire as a wave guide to transmit the emissions from the bottom of the boring to the ground surface pickup transducer. AE count rates from 0 counts/sec–8 counts/sec were recorded. While the monitoring systems were somewhat different between this field test and the laboratory tests described herein, the flow rates and resulting AE rates do compare within reason. (For the maximum clear water laboratory test flow rate of 200 ml/s, the AE rate was 29 counts/sec. For direct comparison between laboratory and field tests, it should be recognized that some attenuation probably occurred in the field as the signal traveled up the wave guide, bringing the two AE count rates to a reasonable comparison.) Perhaps of the greatest significance was the fact that the field prediction of maximum seepage location was verified by both flow rate and AE monitoring.

Conclusion

In examining the AE method for earth dam stability monitoring, the question often arises as to the possibility of using the method for seepage monitoring. While a modest field test had been previously completed, a more controlled feasibility study, along with base-line data have been presented in this paper. Clear water seepage flow rates of approx 45 ml/s are required for AE detection using equipment and sensitivities described herein. For the case of turbid water seepage (as with an earth dam undergoing some degree of piping), the minimum detectable flow rate drops to approx 10 ml/s. The behavior of AE rates for flow velocities above these minimum values appears to behave as an exponentially increasing function (see Fig. 5). Here it can be seen that high flow rates produce

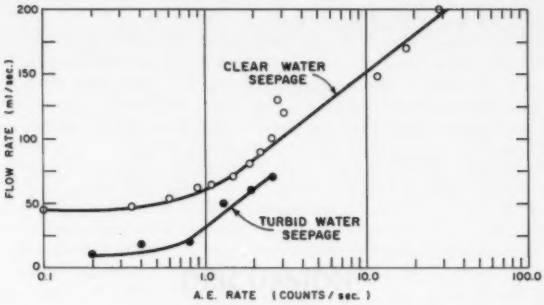

FIG. 5.—Summary of AE Test Result Values from Figs. 2, 3, and 4 for Clear and Turbid Water Seepage Conditions

proportionately many more emissions than do the lower flow rates. A modified experimental setup to test still higher flow rates would be necessary to evaluate AE generation throughout the laminar flow range into the turbulent regime.

Acknowledgment

The AE monitoring system used to perform these tests is on loan from Weston Geophysical Corporation of Westboro, Mass. We acknowledge this cooperation and in particular the enthusiasm for implementation of the AE technique by Vincent J. Murphy.

Appendix.—References

1. Koerner, R. M., Lord, A. E., Jr., McCabe, W. M., and Curran, J. W., "Acoustic Emission Behavior of Granular Soils," *Journal of the Geotechnical Engineering Division*, ASCE, Vol. 102, No. GT7, Proc. Paper 12239, July, 1976, pp. 761–773.
2. Koerner, R. M., Lord, A. E., Jr., and McCabe, W. M., "Acoustic Emission Behavior of Cohesive Soils," *Journal of the Geotechnical Engineering Division*, ASCE, Vol. 103, No. GT8, Proc. Paper 13129, Aug., 1977, pp. 837–850.
3. Koerner, R. M., Lord, A. E., Jr., and McCabe, W. M., "Acoustic Emission Monitoring of Soil Stability," *Journal of the Geotechnical Engineering Division*, ASCE, Vol. 104,

No. GT5, Proc. Paper 13753, May, 1978, pp. 571–582.
4. Koerner, R. M., Lord, A. E., Jr., and McCabe, W. M., "Acoustic Emission (Microseismic) Monitoring of Earth Dams," *Proceedings*, Conference on Evaluation of Dam Safety, Nov. 28–Dec. 3, 1976, pp. 274–291.
5. Koerner, R. M., Reif, J. S., and Burlingame, M. J., "Detection Methods for Location of Subsurface Water and Seepage," *Journal of the Geotechnical Engineering Division*, ASCE, Vol. 105, No. GT11, Proc. Paper 14989, Nov., 1979, pp. 1301–1316.

JOURNAL OF THE
GEOTECHNICAL
ENGINEERING DIVISION

DISCUSSION

Note.—This paper is part of the Journal of the Geotechnical Engineering Division, Proceedings of the American Society of Civil Engineers, ©ASCE, Vol. 107, No. GT4, April, 1981. ISSN 0093-6405/81/0004-0529/$01.00.

Discussions

Discussions may be submitted on any Proceedings paper or technical note published in any *Journal* or on any paper presented at any Specialty Conference or other meeting, the *Proceedings* of which have been published by ASCE. Discussion of a paper/technical note is open to anyone who has significant comments or questions regarding the content of the paper/technical note. Discussions are accepted for a period of 4 months following the date of publication of a paper/technical note and they should be sent to the Manager of Technical and Professional Publications, ASCE, 345 East 47th Street, New York, N.Y. 10017. The discussion period may be extended by a written request from a discusser.

The original and three copies of the Discussion should be submitted on 8-1/2-in. (220-mm) by 11-in. (280-mm) white bond paper, typed double-spaced with wide margins. The length of a Discussion is restricted to two *Journal* pages (about four typewritten double-spaced pages of manuscript including figures and tables); the editors will delete matter extraneous to the subject under discussion. If a Discussion is over two pages long it will be returned for shortening. All Discussions will be reviewed by the editors and the Division's or Council's Publications Committees. In some cases, Discussions will be returned to discussers for rewriting, or they may be encouraged to submit a paper or technical note rather than a Discussion.

Standards for Discussions are the same as those for Proceedings Papers. A Discussion is subject to rejection if it contains matter readily found elsewhere, advocates special interests, is carelessly prepared, controverts established fact, is purely speculative, introduces personalities, or is foreign to the purposes of the Society. All Discussions should be written in the third person, and the discusser should use the term "the writer" when referring to himself. The author of the original paper/technical note is referred to as "the author."

Discussions have a specific format. The title of the original paper/technical note appears at the top of the first page with a superscript that corresponds to a footnote indicating the month, year, author(s), and number of the original paper/technical note. The discusser's full name should be indicated below the title (see Discussions herein as an example) together with his ASCE membership grade (if applicable).

The discusser's title, company affiliation, and business address should appear on the first page of the manuscript, along with the *Proceedings* paper number of the original paper/technical note, the date and name of the *Journal* in which it appeared, and the original author's name.

Note that the discusser's identification footnote should follow consecutively from the original paper/technical note. If the paper/technical note under discussion contained footnote numbers 1 and 2, the first Discussion would begin with footnote 3, and subsequent Discussions would continue in sequence.

Figures supplied by the discusser should be designated by letters, starting with A. This also applies separately to tables and references. In referring to a figure, table, or reference that appeared in the original paper/technical note use the same number used in the original.

It is suggested that potential discussers request a copy of the *ASCE Authors' Guide to the Publications of ASCE* for more detailed information on preparation and submission of manuscripts.

Dam Failure in Benefit/Cost Analyses[a]

Discussion by Francis G. McLean,[4] M. ASCE

The authors have proposed a thought provoking course of action. Their presentation addresses both the economics and safety of a proposed project without, in the opinion of the writer, a proper separation of the two topics. A separation of the topics, in light of the actual planning, engineering/design, construction and operation/maintenance sequence which results in a completed, functioning dam, follows.

Safety

The true safety of a project results from the quality of the engineering/design (13,14,15) and construction sequence and is not impacted by the economic evaluation. Continued safety of a project depends on operation and maintenance procedures, including performance surveillance and continued technical assessments of criteria. A project could, for example, have the costs of a hypothetical probability of failure included in the benefit/cost analysis (BCR), show benefits adequate to warrant construction, and still be grossly unsafe if designed, constructed, operated, or maintained inadequately. In fact, if the costs associated with safe design, construction and operation are unconservatively (under) estimated during planning, the BCR would appear more attractive. The real costs directly associated with achieving a safe project are currently incorporated into the economic evaluation process in each of the areas delineated in the following sections:

Site Investigations.—A thorough understanding of the site conditions, both hydrologic and geologic, are necessary to achieving a safe project. Experienced personnel and consultants, coupled with adequately planned and executed site investigations and evaluations, are requisite to attain this understanding. The more difficult (less favorable) the site conditions, the larger the costs included in BCR calculations during the planning stage to accommodate a more extensive program of investigation and testing. In addition, more effort may be expended in these areas earlier in the process in order to better define potential costs and achieve more realistic BCR results.

Design.—Builders of major dams are generally aware of the hazard potential and usually lean toward conservative choices in the design process, which may lead to more expensive designs. For example, dams may be assumed to crack (from a variety of causes) and defensive measures provided through wider, more plastic cores and provisions for specially processed filter and drainage zones; or, potential for liquefication may be determined to exist, resulting in

[a]January, 1980, by Gregory Baecher, Marie-Elisabeth Paté, and Richard De Neufville (Proc. Paper 15100).

[4]Chf., Geotechnical & Materials Branch, U.S. Army Corps of Engrs. SPD, San Francisco, Calif.

poor foundation materials being removed or insitu densities being improved. In each instance project costs may be increased and probability of failure reduced. Engineering of these projects is continued through the construction stage in order to safely adapt the design to conditions actually uncovered at the site.

Construction.—During this phase the precise lines of the designer's plans are turned into reality through the efforts of the contractor and owner's representative, who supervises and inspects construction to assure safe adaption of the design to the site. The experience and integrity of the contractor and inspection personnel account for the actual safety of the project, providing that original design concepts were adequately formulated for the site. Attention to details, such as the techniques of foundation treatment and compaction of the core zone at the rock contact, hold the key to construction of a safe dam, and rigorous inspection to assure that proper materials and methods are employed is necessary. These costs are reflected in the estimates. The safe adaption of a design to actual conditions often results in cost overruns, to the betterment of safety and detriment of the BCR.

Operations and Maintenance.—The profession is cognizant of the record of failures during the early phase of a project life. Therefore, close monitoring of first fillings and project performance for the first 5 yr–10 yr is the usual practice on projects. Instrumentation is provided to aid in this monitoring. Regular inspections and evaluations of instrumentation data are required, and timely maintenance of the project necessary, to assure a continued understanding of project performance and safety. The associated costs are included in the estimates of annual operation costs in the BCR.

Economics

The BCR is the yardstick which is used to measure project "profitability" to determine whether a project should be built, or to select between alternatives. During planning site specific project feasibility and associated costs are established so that realistic BCRs can be estimated for purposes of decision making. This BCR reflects the cost of project safety as indicated previously, and is the dependent variable in the safety/BCR relationship.

Summary

Based on the foregoing it is not apparent that the inclusion of a discounted cost of failure in BCR calculations is ". . . more appropriate for the protection of the public than an implicit zero probability of failure" as stated by the authors. The only apparent protection offered to the public would be the significant reduction of the BCR calculated for all projects, whether marginal or much needed, without an actual site specific assessment of safety. To the writer's knowledge no recent dam failure, or near failure, (Baldwin Hills, Walter Bouldin, Teton, Lower San Fernando, Kelly Barnes) would have been prevented, or the public better protected, by the author's proposed course of action. In addition, if this approach is to be taken, a uniformity of application would require that the cost of failure due to earthquakes, hurricanes, tornadoes, etc., be included for all major construction projects which pose a public hazard, i.e., buildings, liquified natural gas (LNG) facilities, refineries, etc.

The writer has avoided discussion of the data presented by the authors in an attempt to provide separation and perspective of the topics of safety and

economics. Probability methods would better be applied to the technology of dam design and construction to improve safety; or, a site specific design could be completed and assessed for the probability of failure to see if the resulting risk is acceptable to the public interest. However, beneficial or extensive applications in these areas appear to be somewhere in the future.

Acknowledgments

The discussion offered herein is based on the experience and professional associations of the writer and is not offered as, nor constitute, the position of the Corps of Engineers. A debt of gratitude is due to the many professionals who have engaged in the design and construction of safe dams through the years, the fruits of whose technical and beneficial legacy we all share.

Appendix.—References

13. *Embankment—Dam Engineering, Casagrande Volume*, R. Hirschfeld and S. Poulos, ed., John Wiley and Sons, New York, N.Y., 1973.
14. Peck, R. B., "Let's Get It Straight About Those Dams," *The Military Engineer*, SAME, Jan.–Feb., 1978.
15. "Federal Guidelines for Dam Safety," Federal Coordinating Council for Science, Engineering and Technology, June, 1979.

Discussion by Ralph B. Peck,[5] Hon. M., ASCE

The studies summarized in this brief note represent a substantial step forward. It would be difficult to disagree that BCR should include recognition of the probability of failure, or that the suggested default value of 10^{-4}/dam yr is presently reasonable. Moreover, it is logical to infer that the value 10^{-4} represents the frequency of unexpected causes.

The authors indicate that reduction of this default value, or elimination of the need for relying on such a value, will depend on the success of research leading to analytically derived probabilities of failure. Although not intended by the authors, this might be construed to suggest that reduction of the default value by probabilistic analysis could somehow increase the safety of dams. Such a view would be untenable, as the safety of a dam is determined by physical factors, not probabilistic assessments.

The failure of Teton Dam dispelled any complacency regarding the inherent safety of major dams designed by experienced organizations. This failure would presumably be assigned by the authors to "unexpected causes," but both investigative panels concluded that the failure should not have been unexpected and that the design was deficient in a number of respects. These deficiencies could have been lumped together as a failure to provide defenses in depth against possible weaknesses in the first line of defense (the impervious core and the grout curtain). The knowledge required to cope with the conditions existed; it was not used.

Whether we like it or not, there are aspects of dam design, particularly earth

[5]Prof. of Foundation Engrg., Emeritus, Univ. of Illinois at Urbana-Champaign, Urbana, Ill.; also, Consulting Engr., Albuquerque, N.M.

dam design, that are not now and may never be susceptible to quantitative analytical procedures. Most of these (except for overtopping, seldom a problem in recently designed dams because of present conservatism in spillway requirements) appear in the foundation or at the interface between foundation and embankment. Most, like those at Teton, would yield to the provision of several lines of defense against qualitatively assessed weaknesses. Most, in other words, would be susceptible to experienced judgment.

If we discount judgment and the potential for its application in providing defenses in depth, we may discourage the use of judgment and may never decrease the default value below 10^{-4}/dam yr. If we encourage it and consciously apply it in developing defenses in depth, the historical record within a few decades may justify a lower default value. This may be a more promising approach than awaiting the development of analytically derived probabilities of failure. At best, these analytically derived probabilities could only improve the reliability of estimating the risk of failure; they would be powerless to alter that risk by creating safer dams.

Closure by Gregory Baecher,[6] A. M. ASCE, Marie-Elisabeth Paté,[7] and Richard de Neufville,[8] M. ASCE

That the failure of Teton Dam, as Peck remarks, should dispel complacency regarding the inherent safety of major dams is a point to be emphasized. The fact that nearly all major dams prove safe, a truly remarkable achievement, must not obscure the complementary fact that some dams fail catastrophically.

It should be stressed in this connection that analytical estimates of the probabilities of these failures are difficult or impossible to obtain. As a practical matter, civil engineers go to great lengths to guard against every potential cause of failure they can identify. The risks remaining thus principally come from sources not analyzed. These may be due to poor physical understanding, simple omission, or gross error. For purposes of analysis of the planning decisions, the result is the same, however: the identification of these risks is beyond the reach of analysis.

We thus entirely concur with Peck's suggestions that it may be best to justify lowering the default value for the probability of failure upon the more favorable historical record that may eventually develop, if and when this improvement occurs.

When planning dam projects, it is our responsibility to incorporate into the evaluation the real possibility that any dam might fail. We do not know in advance which dams will fail and how these failures will occur. If we did, we would defend against these eventualities or not build the project. Consequently, we must assume that every dam could fail. This means that in comparing dam

[6]Asst. Prof., Dept. of Civ. Engrg., Massachusetts Inst. of Tech., Cambridge, Mass. 02139.

[7]Asst. Prof., Dept. of Civ. Engrg., Massachusetts Inst. of Tech., Cambridge, Mass. 02139.

[8]Prof. of Civ. Engrg. and Chmn., Tech. and Policy Program, Massachusetts Inst. of Tech., Cambridge, Mass. 02139.

projects, those posing larger hazards to life and property must have their benefits reduced accordingly.

As Peck and Mclean remark, analysis of probabilities will not in itself increase the safety of dams. This safety ultimately depends on the experienced judgement of the designers and the care taken to "provide defense in depth." The inclusion of failure risks in BCR is not immediately aimed at decreasing failure rates, but at better allocating limited resources among public investments. Yet in the longer run, the resulting tendency to avoid dam projects posing higher risks to the public might enhance safety.

Cracking, Leakage, and Erosion of Earth Dam Materials[a]

Discussion by Marvin R. Pyles,[3] A. M. ASCE

The authors have taken a long step in a much needed direction. Erosion of soil particles through a continuous medium such as a filter zone in an earth dam has been studied extensively, but erosion of soil particles through a crack has not. Producing a crack by tensile deformation while applying a hydraulic gradient should be a good technique for studying this behavior, but caution is advised.

The apparent erodibility of any soil is a function of: (1) The characteristics of the soil; and (2) the environment in which the erosion takes place. Of particular note in the authors' test apparatus is the size of the opening (δ) between the top and bottom halves of the cylinder. In the test series on both soil A (moraine) and soil B (silty-clayey fine sand), the maximum size opening reached, as indicated by Figs. 7, 8, 9, and 10, ranged between 2.7 mm and 5.8 mm. Since the method of measurement employed by the authors identifies an eroded soil particle as one which passes through the opening between the top and bottom halves of the cylinder, it is important to consider the size of that opening.

The probability of one of many soil particles passing through an opening of given dimension would look something like the relationship shown in Fig. 14 as a function of the ratio of opening size to particle size. The reason that all particles smaller than the opening do not have a probability equal to one of passing through the opening is that there are many particles in the population, and they can interact, bridging across the opening and preventing erosion. In the authors' test results, the ratio of maximum opening size to maximum particle size for soil A ranges from 0.88 to 1.46. For soil B, the ratio ranges from 13.3 to 39.3, an order of magnitude greater than that of soil A. It is easy to see from the schematic probability plot in Fig. 14 that soil B is much more

[a]February, 1980, by Erik I. Hjeldnes, and Bhagwat V. K. Lavania (Proc. Paper 15220).
[3]Research Asst., Univ. of California, Berkeley, Calif.

likely to erode through the opening between the top and bottom cylinders than is soil A, giving soil A the appearance of being "self-healing." In the authors' tests, it is not a property of the soil, but a constraint imposed by the test apparatus that has been illustrated. To compare the soils properly, they should be tested in a manner such that both are equally affected by the constraints of the apparatus.

The authors do not make it clear in the description of the testing technique whether the samples were saturated after compaction and before testing, or were tested at the compaction water content. If the samples were tested at the compaction water content, then capillary stresses could have played an important role in the tensile behavior of the soil, and thus the results of the erosion tests. The condition in the field that is of concern is cracking in the core of an embankment, and subsequent leakage. Depending on where and

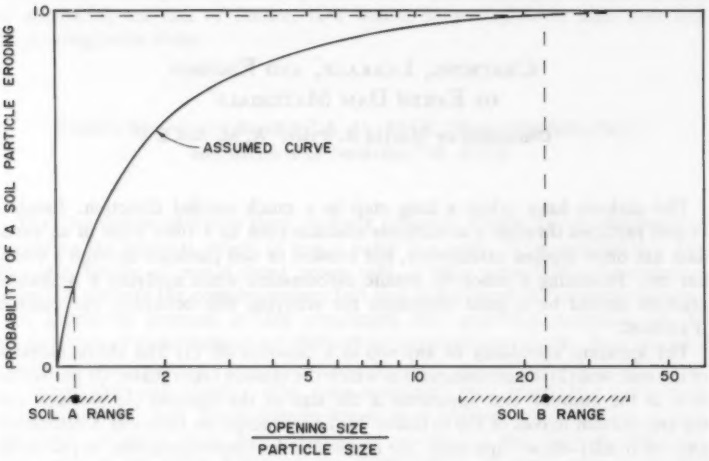

FIG. 14.—Schematic Erosion Probability Relationship

when cracking occurs in an embankment, the core could be saturated or not, so both conditions may be of interest, and show significantly different behavior.

The tensile stress field applied by the apparatus used by the authors is surely nonuniform. The roughened sides of the cylinders should limit if not completely restrict tensile deformation of the sample adjacent to the sides, while allowing deformation at the center of the sample. This will produce a tensile stress distribution like that shown in Fig. 15 obtained from a linear elastic finite element analysis of the test apparatus. The magnitude of the stress in the soil immediately adjacent to the division between the top and bottom halves of the cylinder is on the order of 10 times the mean tensile stress on the cross section. Since soil is not elastic, the actual stress concentration will no doubt be something less than this, but still significant. The presence of stress concentrations does not necessarily invalidate test results for comparing one soil to another, but

tensile stress concentrations could have initiated cracking and subsequent leakage at a mean stress and deformation level that would not have otherwise produced these effects.

In addition to the physical considerations of the test apparatus and test procedure, there is a need to consider soil and water chemistry, and their effects on the erosion potential of soil particles adjacent to a crack in the core of a dam. This is apparently beyond the scope of the authors' present study, but cannot be ignored in the long run.

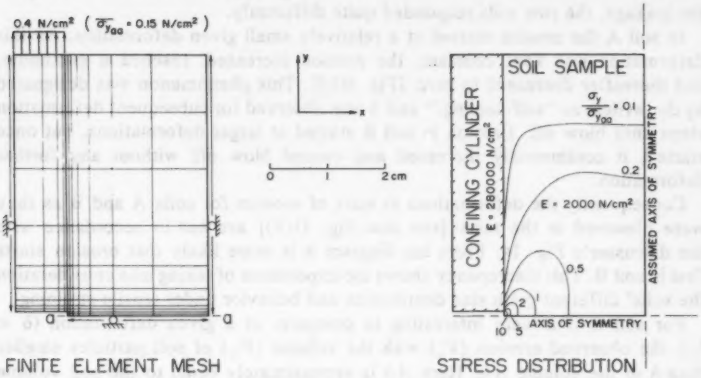

FIG. 15.—Stress Analysis Results for Approximate Maximum Mean Tensile Stress Observed for Soil A and Soil B

The technique presented by the authors may have promise for the comparative indexing of soils for use in earth and rockfill dams, but much study needs to be done to answer the questions presented here.

Closure by Erik I. Hjeldnes[4] and Bhagwat V. K. Lavania[5]

The writers would like to thank Pyles for his interest in our paper. His comments give us an opportunity to explain more thoroughly the testing technique and the results achieved. The following sections address specific points raised by Pyles. To some extent the closure also bears evidence of a valuable personal communication with G. A. Leonards.

Laboratory Approach.—Apparatus and testing technique are very simple and have of course many limitations. However, they served the main purpose of

[4]Assoc. Prof., Univ. of Trondheim, The Norwegian Inst. of Tech., N-7034 Trondheim-Nth, Norway.

[5]Executive Engrg., Tehri Dam Designs, Roorkee, State of U.P.; formerly, Grad. Student, Univ. of Trondheim, The Norwegian Inst. of Tech., Norway.

these tests, i.e., to study the behavior of compacted soils with respect to leakage and erosion under simultaneously acting tensile strain and hydraulic gradient. In our opinion this is a very important requirement of the testing conditions. It was not our intention to study only one part of the problem, namely erosion through a previously constructed crack.

Erosion Properties of Soils A and B.—The writers are of the opinion that the opening (δ in Fig. 2) through which the leakage has to pass does not seriously affect our conclusions concerning the erosion behavior of soils A and B. As can be seen from the measurements of leakage (q_m) and soil content (V_s) in the leakage, the two soils responded quite differently.

In soil A the erosion started at a relatively small given deformation. As this deformation was kept constant, the erosion increased, reached a maximum, and thereafter decreased to zero [Fig. 4(*b*)]. This phenomenon was designated by the writers as "self-healing," and it was observed for subsequent deformation steps until blow off. Erosion in soil B started at larger deformations, but once started, it continuously increased and caused blow off without any further deformation.

Consequently the deformations at start of erosion for soils A and B as they were observed in the tests [see also Fig. 11(*b*)] are not in accordance with the discusser's Fig. 14. From his diagram it is more likely that erosion starts first in soil B. This discrepancy shows the importance of taking into consideration the soils' different grain size distribution and behavior under tensile straining.

For soil A it is very interesting to compare, at a given deformation ($\delta < \delta_f$), the observed erosion (V_s) with the volume (V_{st}) of soil particles smaller than δ in the volume $A\,\delta$. Here $A\,\delta$ is approximately equal to the soil volume affected by the hydraulic gradient, and therefore V_{st} should be the upper limit for the erosion. Simple calculations show that $V_s << V_{st}$, a result that confirms the "self-healing" effect and shows that the outlet size is not the only restriction.

Saturation of Samples.—The curves in Figs. 7–10 show that leakage (q_m) started for deformations (δ) much smaller than deformation at blow off. It is therefore evident, because of the water flow through the sample, that the soil close to the fracture plane was highly saturated, and that the capillary forces had no significant influence on the observed behavior.

Stresses on Fracture Plane.—It is obvious that the stresses on the fracture plane are not uniform, and that there probably exist stress concentrations. The discusser has shown this (Fig. 15) for an elastic material in tension. It is, however, appropriate to mention that for all tests with hydraulic gradient (Figs. 7–10) the total force (P) on the fracture plane is a compressive force, except for a possible small tension at the very start in some few of the tests. Hence the average total stress $\sigma = P/A$ is a compressive stress. (Tensile deformation does not necessarily imply tensile stress.)

The total force can be divided into a resultant pore pressure (U) and a resultant effective stress (P'), i.e., $P = P' + U$. The results observed indicate that in these tests U is predominant and consequently P' is small. In further and more advanced tests of this kind one should try to measure the distribution and magnitude of stresses on the fracture plane, at least the pore pressures.

Chemical Effects.—As mentioned by the discusser, soil and water chemistry could have some influence on the erosion behavior. Primarily one would expect such effects in fine-grained soils. The writers are of the opinion that in most

cases this will be of minor importance, but research aiming to clarify the question will be most welcomed.

The writers hope these remarks have clarified the points raised in the discussion. Obviously there is a need for more research to investigate the cracking, leakage, and erosion behavior of soils. Emphasis should preferentially be placed on large-scale experiments, as "prototype-like" as possible. The scope must be to improve the design criteria and the guidelines for choosing the most suitable materials for earth and rockfill dams.

Technical Papers

Original papers should be submitted in triplicate to the Manager of Technical and Professional Publications, ASCE, 345 East 47th Street, New York, N.Y. 10017. Authors must indicate the Technical Division or Council, Technical Committee, Subcommittee, and Task Committee (if any) to which the paper should be referred. Those who are planning to submit material will expedite the review and publication procedures by complying with the following basic requirements:

1. Titles must have a length not exceeding 50 characters and spaces.

2. The manuscript (an original ribbon copy and two duplicate copies) should be double-spaced on one side of 8-1/2-in. (220-mm) by 11-in. (280-mm) paper. Three copies of all figures and tables must be included.

3. Generally, the maximum length of a paper is 10,000 word-equivalents. As an *approximation*, each full manuscript page of text, tables or figures is the equivalent of 300 words. If a particular subject cannot be adequately presented within the 10,000-word limit, the paper should be accompanied by a rationale for the overlength. This will permit rapid review and approval by the Division or Council Publications and Executive Committees and the Society's Committee on Publications. Valuable contributions to the Society's publications are not intended to be discouraged by this procedure.

4. The author's full name, Society membership grade, and a footnote stating present employment must appear on the first page of the paper. Authors need not be Society members.

5. All mathematics must be typewritten and special symbols must be identified properly. The letter symbols used should be defined where they first appear, in figures, tables, or text, and arranged alphabetically in an appendix at the end of the paper titled Appendix.—Notation.

6. Standard definitions and symbols should be used. Reference should be made to the lists published by the American National Standards Institute and to the *Authors' Guide to the Publications of ASCE*.

7. Figures should be drawn in black ink, at a size that, with a 50% reduction, would have a published width in the *Journals* of from 3 in. (76 mm) to 4-1/2 in. (110 mm). The lettering must be legible at the reduced size. Photographs should be submitted as glossy prints. Explanations and descriptions must be placed in text rather than within the figure.

8. Tables should be typed (an original ribbon copy and two duplicates) on one side of 8-1/2-in. (220-mm) by 11-in. (280-mm) paper. An explanation of each table must appear in the text.

9. References cited in text should be arranged in alphabetical order in an appendix at the end of the paper, or preceding the Appendix.—Notation, as an Appendix.—References.

10. A list of key words and an information retrieval abstract of 175 words should be provided with each paper.

11. A summary of approximately 40 words must accompany the paper.

12. A set of conclusions must end the paper.

13. Dual units, i.e., U.S. Customary followed by SI (International System) units in parentheses, should be used throughout the paper.

14. A practical applications section should be included also, if appropriate.